On the Stability of Selected Hydrogen-bonded Semiconductors in Organic Electronic Devices§

Mihai Irimia-Vladu[1,2]*, Yasin Kanbur[2,3], Fausta Camaioni[1,4], Elisabetta Coppola[1,4], Cigdem Yumusak[2], Cristian-Vlad Irimia[5,1], Angela Vlad[6], Alessandra Operamolla[7], Gianluca M. Farinola[7], Gian-Paolo Suranna[8], Natalia González[9], María Carmen Molina[9], L. Fernando Bautista[10], Heinz Langhals[11,2], Barbara Stadlober[1], Eric Daniel Głowacki[12,2], Niyazi Serdar Sariciftci[2]

[1] Joanneum Research Forschungsgesellschaft mbH, Franz-Pichler Str. Nr. 30, 8160 Weiz, Austria

[2] Linz Institute for Organic Solar Cells (LIOS), Physical Chemistry, Johannes Kepler University Linz, Altenberger Str. Nr. 69, 4040 Linz, Austria

[3] Department of Metallurgical and Materials Engineering, Karabuk University, Baliklarkayasi Mevkii, 78050Karabük, Turkey

[4] School of Industrial and Information Engineering, Politecnico di Milano, Via Raffaele Lambruschini, 15, 20156 Milano MI, Italy

[5] Bundesreal Gymnasium Seebacher, Seebachergasse 11, 8010 Graz, Austria

[6] National Institute for Laser, Plasma and Radiation Physics (INFLPR), Atomistilor Street, No. 409, Magurele, Ilfov, 077125, Bucharest, Romania

[7] Dipartimento di Chimica, Università degli Studi di Bari Aldo Moro, Via E. Orabona 4, I -70126 Bari, Italy

[8] Department of Civil, Environmental and Chemical Engineering (DICATECh), Politecnico di Bari, Via Orabona 4, 70125 Bari, Italy

[9] Department of Biology and Geology, Physics and Inorganic Chemistry, Rey Juan Carlos University, Calle Tulipán s/n. 28933 Móstoles (Madrid), Spain

[10] Department of Chemical and Environmental Technology, Rey Juan Carlos University, Calle Tulipán s/n. 28933 Móstoles (Madrid), Spain

[11] Department Department of Chemistry, Ludwig-Maximilians University München, Butenandtstr. 13, D-81377 München, Germany

[12] Linköping University, Department of Science and Technology, Laboratory of Organic Electronics, Bredgatan 33, Norrköping 60221, Sweden

KEYWORDS: Organic Electronics; Hydrogen Bonded Pigments, Measurement Stability

CORRESPONDING AUTHOR: Mihai Irimia-Vladu: mihai.irimiavladu@gmail.com

§: This article is dedicated to Professor Dr. Jean-Luc Brédas, an honorable friend and colleague, whose work illuminated many of us in the field of Organic Electronics.

ABSTRACT: The electronics era is flourishing and morphing itself into Internet of Everything, IoE. At the same time questions arise on the issue of electronic materials employed: especially their natural availability and low cost fabrication, their functional stability in devices, and finally their desired biodegradation at the end of the life cycle. Hydrogen bonded pigments and natural dyes like Indigo, Anthraquinone and Acridone have robustness in functionality and versatility in designing electronics and sensors components, and are bio-origin and biodegradable. With this Perspective Article, we intend to coalesce all the scattered reports on the above mentioned classes of Hydrogen bonded semiconductors, spanning across several disciplines and many active research groups. The article will comprise both published and unpublished results, on stability during aging, upon electrical, chemical and thermal stress, and will finish with an outlook

section related to biological degradation and biological stability of selected hydrogen bonded molecules employed as semiconductors in organic electronic devices. We demonstrate that when the purity, the long range order and the strength of chemical bond, are considered, then the Hydrogen-bonded organic semiconductors are the privileged class of materials having the potential to compete with inorganic semiconductors. As an experimental historical study of stability, we fabricated and characterized organic transistors from a material batch synthesized in 1932 and compared the results to fresh material batch.

INTRODUCTION

Smart electronic appliances became ubiquitous in our daily life and are responsible for the impressive advancement of the human society during the past 50 years passed. Inorganic semiconductors such as silicon or gallium arsenide are the key, indispensable components of the ongoing surge of smart appliances. Nevertheless, despite their apparent robustness and high performance, inorganic based electronics suffer from the limited availability of key elements (*e.g.* Indium, Lithium, Gallium), as well as the high energy demand for their fabrication that pose a real threat to the development of our "low carbon foot-print" based society. With this respect it was demonstrated that the so-called "process embodied energy", or electrical energy per kilogram of material processed is on average 3 orders of magnitude higher in semiconductor processing than in high throughput plastic processing such as injection molding, and can even reach extraordinary values for specific processes like oxidation of dielectric layers that are up to 8 orders of magnitude higher in energy demand than the energy expended for metal manufacturing through melting or evaporation [1, 2, 3]. The already mentioned energy request of inorganic electronics manufacturing will only augment progressively because of the: (i) fast paced technological advancement, (ii) incessant market demand for new products and functionalities, as well as (iii) manufacturer strategy of constantly increasing its sales, with all these factors leading to a situation where the electronics and smart appliances are deliberately designed to become obsolete within few years of their fabrication. The colossal demand of such products is leading to a series of unfortunate and undesirable consequences: (a) a massive amount of waste from electrical and electronic equipment (WEEE) and (b) a rapid exhaustion of already scarce natural elements [4].

Organic semiconductors on the other hand offer great promises through their ease of synthesis in a multitude of derivatives, their low temperature processability as well as their amenability for fabrication of flexible, stretchable, conformable, even imperceptibly thin devices [5, 6, 7, 8, 9, 10, 11]. Synthetic organic semiconductors are the core element of organic electronic devices (field effect transistors-OFETs, light emitting diodes-OLEDs, organic solar cells-OPVs, photodetectors, *etc.*). Importantly, organic electronics field succeeded to fulfill the full level of commercial expectation already as components of organic light emitting diodes (OLEDs). A possible reason for not being used in other fields of application, could be attributed to their low charge carrier mobility and limited operational/air stability when compared to their inorganic counterparts [12, 13, 14]. A conceivable explanation of this lower performance could be the inner arrangement of the core elements of the synthetic organic semiconductors, where either the small molecules or polymer chains are linked to one another through weak van der Waals forces. This type of bonding is at least to some extent responsible for their rather modest air stability and low charge carrier transport as compared to covalently bonded inorganic semiconductors like silicon. In all the past 25 years, synthetic chemistry field enthusiastically delivered vast libraries of van der Waals bonded organic semiconductors featuring the coveted π-π conjugated core [12, 13, 15, 16, 17, 18, 19, 20, 21, 22]. However despite the tremendous scientific and financial effort, the highest ever field effect mobility is around the value of 10 cm^2/Vs in functional devices [12], while an operational frequency in simple circuits design (3 and 5 stages ring oscillators) of 40 MHz [23] was only recently achieved. Both values exemplified above fall at least 3 orders of magnitude below the ones recorded by their inorganic counterparts that remain key, indispensable elements of high speed, high performance and high reliability smart appliances. Nevertheless, it should be pointed out that question of high speed is not always posed for daily use household electronics, and there might be a high demand for low speed electronics too. Nevertheless, the low mobility remains an important issue in the development of organic electronics devices.

Nature, on the other hand, synthesizes air stable organic molecules either lacking at all, or featuring minimal intra-molecular π-conjugation, molecules that are coupled to one another through much stronger intra-molecular as well as inter-molecular hydrogen bond forces, as is the case for DNA or cellulose (the most abundant biopolymer on Earth), many flower and animal pigments, *etc.* In fact, nature offers a plethora of organic materials with electrical properties ranging from insulators to conductors; many of them were recently studied and reported for various organic electronics applications [24, 25, 26, 27]. The fact is that the scientific community centers its attention always for long range π–π conjugation as prerequisite for the identification and design of organic semiconductors [18,28,29], and therefore molecules featuring naturally occurring cores are in general overlooked.

The preliminary results of our team showed that many Hydrogen-bonded semiconductors are air-stable materials which are easily processible into thin films characterized by a long range order resembling one of their covalently bonded, inorganic counterparts [30, 31, 32, 33, 34, 35]. Despite having limited intramolecular π-conjugation, such mole-

cules form an extensive intermolecular π-conjugated network, with excellent charge carrier transport and resistance to degradation [36, 37, 38, 39, 40, 41]. This extended class of hydrogen-bonded pigments and dyes show at their core functionalities groups like diketo pyrrolo pyrrole (DPP), anthraquinone, acridone, indigo, naphthoquinone, etc., bonded with N-H---O type hydrogen bridge to the next units. We will analyze in this Perspective Article the chemical, thermal, electrical and operational stability, and their attitude to sustain surface covalent modification of their aggregates and thin films without loss of performances. We will survey the family of Indigo dyes (Indigo, Tyrian purple, di-chlorinated and di-fluorinated Indigo, Epindolidione, di-fluorinated and di-chlorinated Epindolidione respectively), Acridone pigments (Quinacridone, di-methylated Quinacridone and di-chlorinated Quinacridone) as well as Indanthrene Blue as one representative example of a molecule belonging to the impressive library of Anthraquinone dyes. The chemical structure of the molecules exemplified in this article is displayed in **Figure 1.**

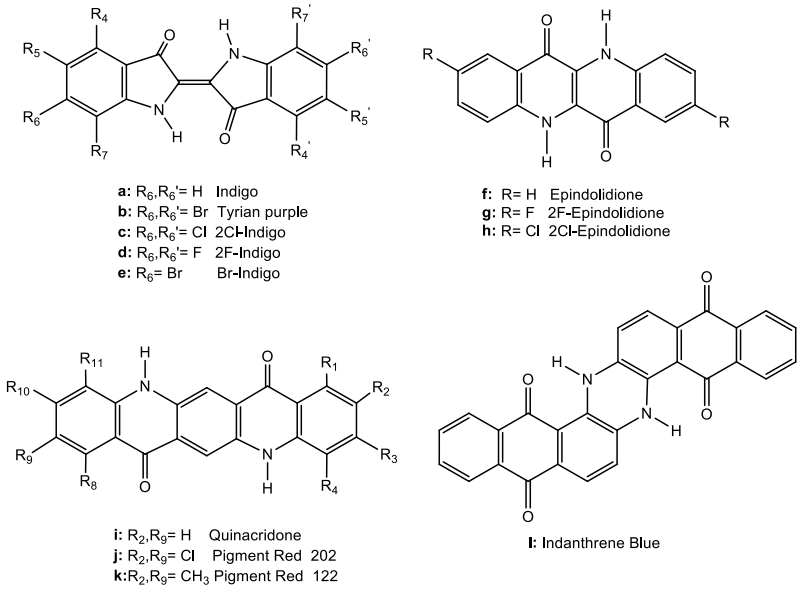

Figure 1*: Hydrogen bonded small molecules semiconductors reviewed in this work for their stability in functional devices: a) Indigo, b) Tyrian Purple, c) 2Cl-Indigo, d) 2F-Indigo, e) Br-Indigo, f) Epindolidione, g) 2F-Epindolidione, h) 2Cl-Epindolidione, g) Quinacridone, j) Pigment Red 202, k) Pigment Red 122, l) Indanthrene Blue.*

This Perspective article comprises both published and unpublished data on the stability characteristics of the above mentioned H-bonded molecules, and is divided in 5 main sections (chapters), each of them offering the reader a complementary view (a slightly different perspective of stability): electrical, thermal, chemical and operational. The reader may find therefore obvious that not all the described sets of experiments was carried out for all the molecules presented here, otherwise the set of experimental data would have become astronomically large. Nevertheless, this shortcoming leaves wide open the door for the research community to identify and bring to light all the missing pieces of the stability lego of hydrogen bonded semiconductors. We use throughout this Perspective Article the organic field effect transistor characteristics as the explicit tool of comparison among the exemplified molecules, and decided to offer the reader the possibility to compare the respective performance of these materials by simple visual inspection of the graphs; with this respect we refrain from producing extensive tables of explicit values, or plotting graphs of various figures of merit. By presenting the transistor characteristics for all the highlighted hydrogen bonded semiconductors, the reader has unequivocally the possibility to asses in full the performance of the respective materials, without missing key pieces of information, like for example the degree of hysteresis, the OFF and ON level values, occurrence of threshold voltage, etc.

Chapter 1. Short notes on Natural Occurrence, Extraction and Synthesis of H-bonded Molecules Analyzed in this Study

Before going into a brief excursion on the organic chemistry of H-bonded pigments, a fundamental concept should be clarified, that is the difference between pigments and dyes. The pigments are coloured compounds, either of an organic or inorganic nature, insoluble in the binder in which they are dispersed, and with a different index of refraction than the one of the binder. If the pigment had in fact the same index of refraction of the binder, there would be no phenomenon of dispersion of light and the system would be perfectly transparent. On the other hand, organic dyes are sub-

stances, generally soluble, that confer their colour to certain substrates. They are applied by solution and are permanently bonded with the substances to be coloured, usually textile fibbers or plastics, thanks to real chemical bonds. A pigment is more stable than a dye, since the dye particles are solvated, and are therefore more easily attacked by atmospheric agents such as air oxygen or solar radiation [42]. Unlike their inorganic counterparts, organic pigments show a decidedly better colouring and opacity, as well as extremely bright and clean tones. The molecules of organic pigments are generally characterized by planar conjugated chromophores, and were therefore investigated in the field of organic electronics as suitable candidates for semiconductor materials [13, 29]. The colour properties and the resistance to degradation are significantly influenced by the characteristics of the pigment in the solid state, such as crystallinity, particle size and aggregation state. Due to their structural characteristics, pigment molecules in general, and hydrogen bonded molecules in special, tend to be assembled in very ordered crystalline structures [37, 38, 39]. The main driving forces of the crystal formation process of the latter ones are the intra- and inter-molecular hydrogen bonds, the π-π stacking interactions between adjacent planar molecules and the weak van der Waals interactions between chains of molecules. The overall effect of the aforementioned interactions generally leads to stabilization of the crystal lattice by lowering the energy of the system. Many organic pigments are even polymorphic, each with its characteristic colour, and obviously having different electronic and optical transport properties. Based on the diversity of chemical structure and technical performance, organic pigments are conventionally classified into "classic pigments" on the one hand, and High-Performance Pigments (HPP) on the other. Compared to "classic pigments", HPPs have more recent origins and excellent resistance properties; they are more expensive and are used in highly specialized applications where exceptional resistance to light, climatic conditions and heat is required [43]. Among the most important, recently reported high-performance pigments relevant for organic electronics are hydrogen-bonded heterocyclic compounds, in the indigo, anthraquinone and acridone families; some of these molecules will be presented in this study.

Short History of Indigo, Tyrian Purple, Quinacridone and Indanthrene Blue

Indigo (**1**) and Alizarin (**2**) were natural origin, highly prized dyes in the past eras, since there was a lack of stable and brilliant textile dyes in the preindustrial time of the mankind, in contrast to the much larger variety of colouring compounds (dyes and pigments) available nowadays. Pigments proved to be less problematic than dyes concerning their photo stability because they contained comparable large amount of coloured material in the compact crystallite, and a slight photo-decomposition caused only little effect on their de-coloration.

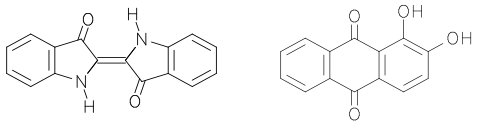

1 **2**

Textile dyes were much more problematic because monomolecular material was spread over a large surface or only of a few layers for aggregated dyes. Thus, the majority of coloured natural materials such as the ones extracted from flowers like anthocyanes for example were not photo stable. A further restriction was the mass availability because large amounts of dyes were required for textile dying. Thus, textile dying was concentrated to very few natural products where indigo and alizarin retained their special position for extensive periods of time. There are still consequences seen today, for example the strikingly identical hue in the national flags of many countries where only blue textiles stained with indigo, red textiles stained with alizarin and uncoloured white material could be used at times, and the respective tints remained characteristics even today; examples are the French, British, Russian, Austrian, Czech, Romanian, U.S.A. flags and many more.

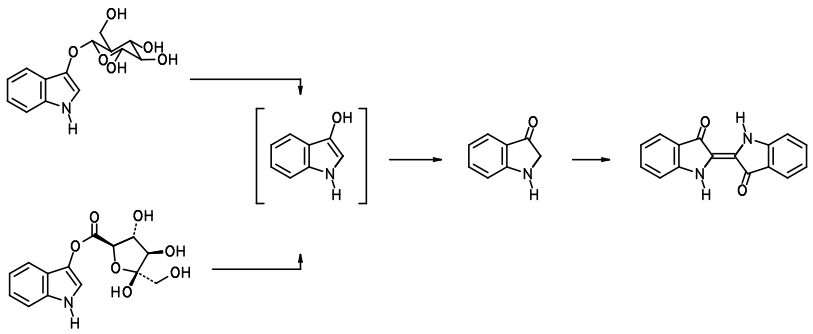

Scheme 1: *Preparation of Indigo from natural products. Upper path shows the dyer's woad (Isatis tinctoria) and lower path the true indigo (Indigofera tinctoria) as the source where enzymatic cleavage to 3-hydroxyindole, tautomerism to indoxyl and oxydation with atmospheric oxygen forms indigo.*

The hardly soluble Indigo was applied as a vat dye, *i.e.* it was solubilized in alkaline medium and thus reduced to its colourless bis-anion form, leucoindigo. A re-oxydation by means of atmospheric oxygen caused a precipitation and adsorption to the surface of the fibre. As a consequence, the dying with Indigo was not as rub-fast as with Alizarin (details in **Supplementary Information**, where also impression of colorations with Indigo and Alizarin are described). Precursors of Indigo are widely found in many plants, however, generally with rather low content. An agricultural production in Europe was based on the plant dyer's woad (*Isatis tinctoria*) with a very complicated process of isolation including enzymatic steps. The importance of the dye was estimated so high that an official quality control was established in the European places where Indigo was produced. Later-on true Indigo (*Indigofera tinctoria*) containing a higher amount of the precursor of Indigo was grown in India. The precursor of Indigo is the aglucon 3-hydroxyindole and is obtained by means of enzymatic removing of the carbohydrate followed by tautomerisation and oxidation to the insoluble Indigo (**1**); see **Scheme 1**.

3

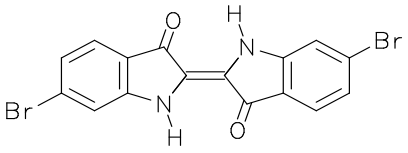

Figure S1 in the **Supplementary Information** file presents the rainbow spectrum (lower coloured ribbon) and the complementary spectrum obtained for a single absorption band in the visible and white light. The upper coloration in **Figure S1** indicates a gap for historic textile dying between red and blue where the colour purple (magenta) is close to the maximum of both the sensitivity of the human eye and the radiation maximum of the sun; the targeting of this spectral region allows pronounced optical effects. The absorption of the historical Tyrenian purple closes this gap and favoured the estimation of the very high value of such coloration being reserved for very important persons such as kings or emperors. Moreover, the production of this dyestuff as a natural product was very elaborate and costly because the source of a precursor was a maritime snail where compound **3** is formed in a photochemical reaction from a precursor existing in the snail body; the exact function of the precursor of 3 in the snail body is not clear yet, but is thought to be a component of defence. The Austrian chemist Paul Friedländer isolated around the year 1900, 1.5 g of compound **3** from 12000 Mediterranean Sea snails. The effort of extraction is considerable, and the sustainability of natural production of Tyrian purple questionable, considering that about 10000 snails seem to be necessary for the economic dying of 1 kg of wool. In Asia Minor the precursor of purple was isolated from dead animals whereas it was extracted from living animals in Central America and the Caribbean.

The substitution of the positions 6 and 6' of compound **1** with bromine atoms to obtain compound **3** causes a spectral shift of the absorption to shorter wavelengths (hypsochromic shift) and consequences of this event are described in Supplementary Information file (**Figure S2**). Tyrian purple, both the natural product and synthetic material, is nowadays applied in textile dying only for special cases because the technical synthesis is comparably expensive, the stability limited and there are other well available and more stable synthetic dyes for similar colorations.

The scope of dying changed fundamentally with the production of dyestuff by the chemical industry. Picric acid (RN 88-89-1) was the first synthetic dyestuff developed by Peter Woulfe in 1771 and is nowadays replaced by the similar chromophore 2,4 dinitro-1-naphthol (RN 605-69-6, Martius' yellow) for less problematic handling. Finally, William Henry Perkin's mauveine (RN 6373-22-4) synthesised in 1856 was one of the most prominent early synthetic dye. The still highly appreciated Indigo and Alizarin became targets of chemical research where the structures and the first syntheses were established by Adolf von Baeyer and Carl Graebe, respectively. The fast and sustained success of these natural-identical products was not only based on their lower price, but also on the higher purity of the chemically prepared materials, because by-products of the natural materials broaden their absorption spectra to a more dull shade, whereas the pure dyes allowed a more brilliant coloration of textiles.

Second Heumanns's synthesis for the first large scale technical synthesis of Indigo (**1**) in 1897 is presented in **Scheme 2**. The key step for this synthesis as well as for Heumann's first synthesis and others is the base-induced ring closure under rough basic conditions such as melt NaOH or KOH at about 200°C. Insight into the structure-property relationships of Indigo and its functional derivatives has been provided by P.A. Troshin and co-workers [45]. The disubstitut-

ed indigoids reported in **Scheme 3** have been synthesised according to a two-step method published by Voss and Gerlach [44] starting from the 5-halogeno-2-nitrobenzaldehyde yielding, after reaction with nitromethane and sodium methanoate, followed by reduction with sodium dithionite, the relevant 5,5'-dihalogeno indigoids or, in turn, starting from the 4-halogeno-2-nitrobenzaldehyde to obtain the corresponding 6,6'-dihalogeno indigoids. The authors showed how chemical derivatization significantly influences optical and electronic properties of these materials, with 6,6' dihalogeno derivatives outperforming their positional isomers in terms of figures of merit when employed as p-type and n-type semiconductors in OFET devices.

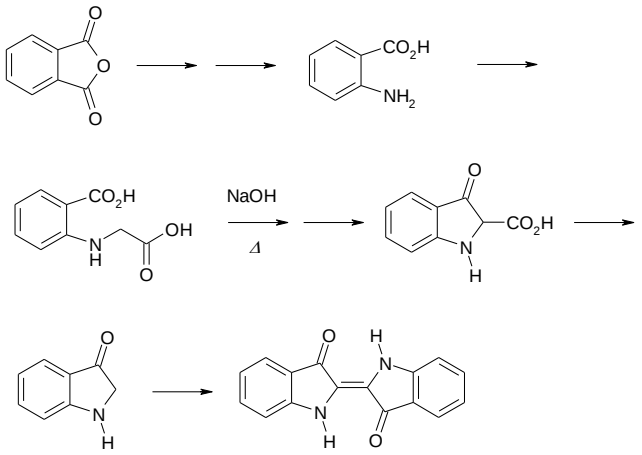

1

Scheme 2: *Second Heumann's synthesis of Indigo (1) starting with the well-accessible phthalic anhydride, reaction with ammonia, Hofmann degradation to anthranilic acid, base-supported substitution with chloroacetic acid and ring closure by melt with sodiumhydroxide (initially). The decarboxylation of the resulting β-ketocarboxylic acid proceeds spontaneously under mild conditions and atmospheric oxygen is sufficient for the oxydation of indoxyl to Indigo (1).*

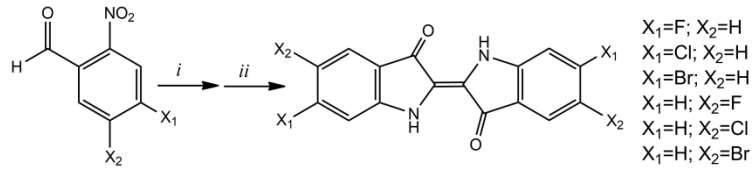

Scheme 3: *Preparation of 5,5'- and 6,6'-substituted dihalogeno substituted indigoids (adapted from reference* [45] *and references therein). Reaction conditions: i) nitromethane, CH_3ONa/ CH_3OH; ii) $Na_2S_2O_4$, NaOH/H_2O.*

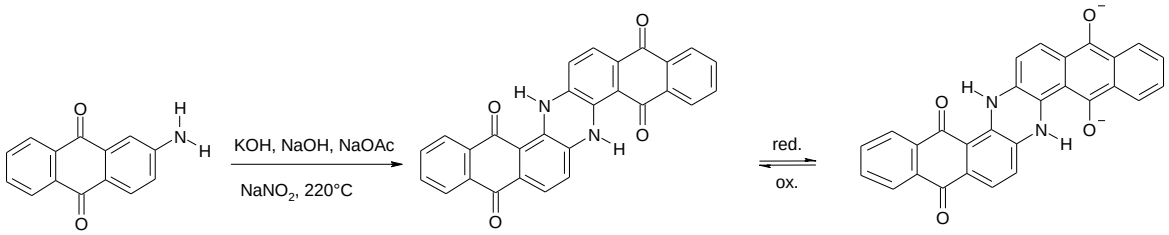

4 vat

Scheme 4: *Synthesis of Indanthrene blue RS (4) by alkali melt of 2-anminoanthraquinone and reduction to the blue vat.*

The concept of the reaction of aromatic amines with melt alkali for the anellation of aromatic systems to generate dyestuff prompted René Bohn in 1903 to the reaction of 2-aminoanthraquinone with such a melt and obtained the blue dyestuff (**4**), see **Scheme 4**. The latter could be applied in vat dying to obtain shades similar to Indigo (**1**) where he named (**4**) Indigo from Anthracene and shortened it as Indanthrene. The reaction seems to be a Tschitschibabin reaction of the deprotonated amine with a second molecule in position 1 under the rough reaction conditions. The dying with the new material gave surprisingly good results because of its extraordinary high stability compared with the one of Indigo. There are no problems with rub-fastness such as with Indigo; this may be a consequence of stronger intermolecular hy-

drogen bonds in (**4**), whereas the hydrogen bonds in (**1**) are partially intra-molecular. Meanwhile the most stable known textile dyes despite of their chemical structures are named Indanthrene dyes as a trade mark and (**4**) got the name Indanthrene Blue RS; we will refer to it as Indanthrene Blue in this study. The stability of (**4**) concerning hypochlorite as bleach is much higher than that of Indigo, however, a further improvement became attractive as is briefly detailed in the **Supplementary Information** file.

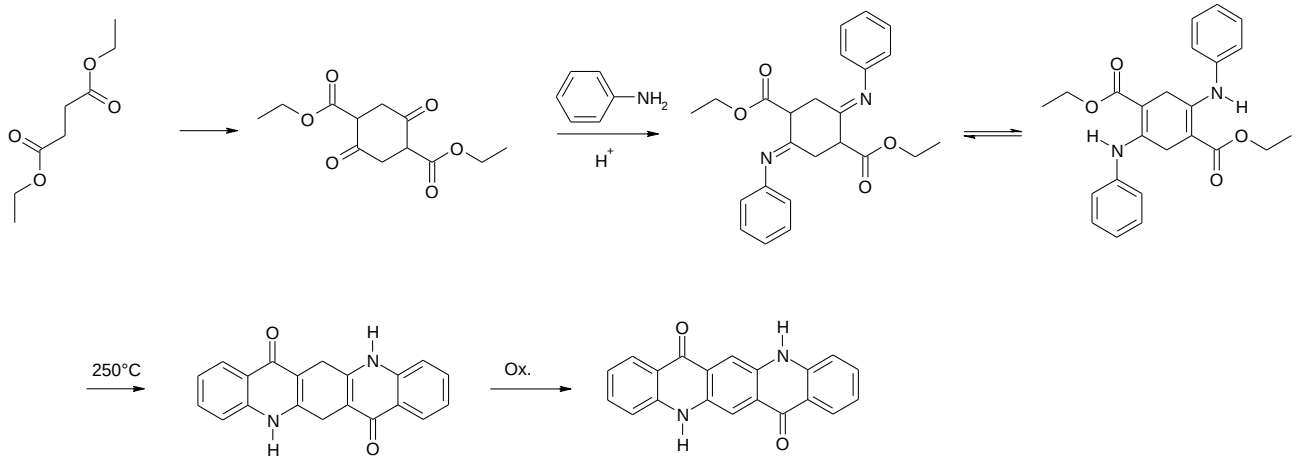

5

Scheme 5: *Synthesis of Quiancridone (**5**) starting with succinic ester, base-induced self-condensation with ring closure, condensation with aniline to the bis-ketimine, tautomerism to a donor-acceptor-substituted double olefins, electrophilic ring closure under rough reaction conditions and finally full aromatisation (5).*

The intermolecular hydrogen bonds still weak in (**1**) and stronger in (**4**) allow both the generation of increasingly rub-fast colorations of textiles and the preparation of pigments of very low solubility. Quinacridone, (**5**) is a further example with strong intermolecular hydrogen bonds. These are formed between the NH group of one molecule with the carbonyl group of the neighboring molecule, resulting in a quasi-polymeric structure in the crystalline state with low solubility. Quinacridone (**5**) was prepared as soon as 1935 by Carl Liebermann; however, the high industrial potential of the material was not realised before the 1960s at DuPont. The technical synthesis starts with succinic ester and its very efficient base-induced self-condensation to form a six-membered ring where the carbonyl groups were condensed with aniline with the formation of a bis-ketimine as depicted in **Scheme 5.** The reaction pathway has an amazing yield approaching 100% for well executed schemes [46, 47], a fact that renders the extremely low production price and high quantity of Quinacridone available at chemical suppliers (more insight on this issue will be offered in this article).

Synthesis of Epindolidione and Epindolidione derivatives

The Epindolidiones (with chemical structure displayed in **Scheme 6**), although technically considered isomers of Indigo, can be numbered among the Quinacridone-based pigments as they are structurally related to the Quinacridone.

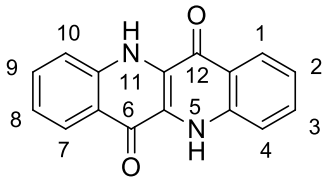

Scheme 6: *The Epindolidione structure and its carbon atom numbering. Its IUPAC name: dibenzo[b,g][1,5]naphthyridine-6,12(5H,11H)-dione.*

The first investigation aimed at describing a substituted Epindolidione dates back to a 1934 publication by Ainley and Robinson, who were intrigued by the fact that this class of materials and in particular the epindolidione parent molecule could be "*not only be isomeric with indigotin* (Indigo) *but might well be a congener of that pigment in many of its processes of preparation"*. The name Epindolidione, first indicated by these authors, was derived from the name assigned to the Ep-

indoline base, the dihydroxy-derivative of which was subject to a prototropic equilibrium, the keto form of which was given the name of Epindolidione [48]. Unfortunately, application of the synthetic scheme proposed by Ainley and Robinson to the preparation of Epindolidione, led to low yields [49] and could not practically be extended to the preparation of other substituted Epindolidiones. The isomerization from Indigo directly to Epindolidione has also been carried out thermally and studied theoretically by Haucke and Graness [50, 51] while heating Indigo at 460°C in gas phase and vacuum. Although functional, this method is not practical for the preparation of functionalised Epindolidiones for research relevant purposes.

However, the interest in the Epindolidione raised in the 1960s following the commercial success of the Quinacridone pigments for various colouring purposes [46, 47]. In 1967, by extending a synthetic method used for Quinacridone, DuPont researchers reported in a patent [52] the first synthesis of high yield (66.5%) Epindolidione, which was later published in the open literature [53]. From then on, Epindolidione synthesis was the subject of numerous patents [54, 55]. In a 1988 study by researchers of Kodak laboratories it was reported that thin films of the Epindolidione gave rise to photoconductivity and a hole mobility of about 0.01 cm^2/Vs could be measured [56]. Since the amine and carbonyl functional groups in the Epindolidione strongly perturb conjugation, the Epindolidiones as themselves cannot be regarded as having the same conjugation extension of acenes [18, 57]. Sharing some peculiarities with parent Indigo (*n.a.* details over unusual optical properties of Indigo are briefly presented in the **Supplementary Information** file), the colourless Epindolidione molecule in solution has also characteristic a dramatic change induced by the strong aggregation in solid state. This latter event leads to pigment particle formation with unusual optical properties. Lately, innovative and more efficient approaches to the synthesis of the Epindolidione and some of its halogenated derivatives (displayed in **Scheme 7**) were investigated [35, 58]. Moreover, their optical, electrochemical, and electrical properties have been studied in detail, and for the first time the crystalline structure of Epindolidione has been resolved [59].

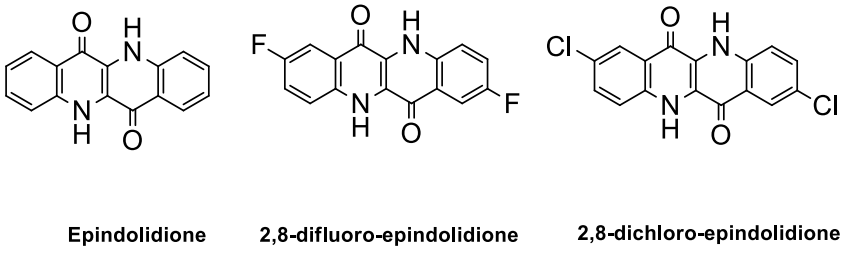

Scheme 7: *The structure of Epindolidione and two of its 2,8-halogenated analogues*

The syntheses of dihalogeno derivatives of Epindolidione can be carried out as reported in **Scheme 8**. The scheme constitutes, nowadays, the most practical route for the obtainment of a wide range of Epindolidiones, and is here exemplified for Epindolidione as well as two of its 2,8-substituted derivatives. In practice, it mainly takes into account the contributions from Jaffe [53, 60] as well as some optimization proposed later on [61]. The intriguing challenge of synthesising Epindolidione polymers has motivated also research focused on the obtainment of 2,8- dibromo epindolidione. Wang, Pei and co-workers have succeeded in this task [62]. The key is the use, in the last ring closure, of an $AlCl_3$/NaCl mixture at 160 °C.

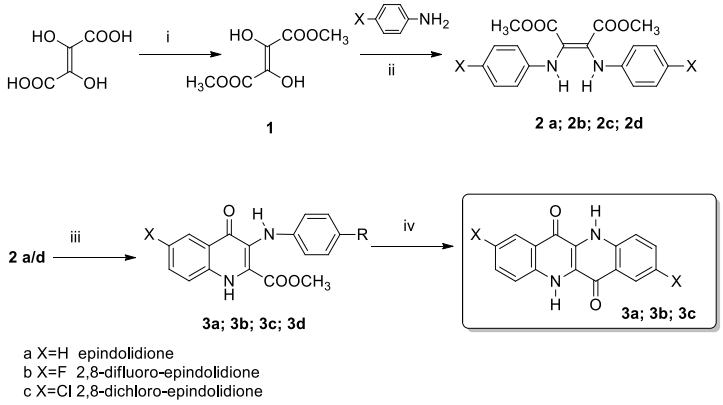

Scheme 8: *Synthesis of dihalogeno Epindolidione, adapted from references [58] and [62] i: $CH_3OH/SOCl_2$, 0°C-RT; ii: aniline (a) or 4-halogeno-aniline (b,c,d), HCl (cat)/CH_3OH (reflux); iii DOWTHERM™ A (reflux); iv polyphosphoric acid ($H_{2+n}P_nO_{3n+1}$) 150°C.*

Chapter 2. H-bonded Semiconductors Operational (Electrical) Stability in OFET Devices and Circuits under the Influence of: Aging, Measurement Cycling, Air Exposure, Bias-stress, Chemical and Thermal Instabilities

2.1 Key Observations Assisting or Leading to Stability of Hydrogen-bonded Pigments

With the discovery of conductivity in polymers by Bolto, McNeill and Weiss in polypyrrole [63] and one decade later by Heeger, Shirikawa and MacDiarmid in polyacetylene [64], organic electronics era started and promised along its development the establishment of cost-conscious science, where easily affordable organic materials would be integrated in electronic devices via low cost lab processes that could be easily expanded and adapted to industry relevant, high throughput fabrication. Thirty years fast forward into the research and development efforts of organic electronics, and the field has produced (except for niche applications of course), one sole market candidate, i.e. the organic light emitting diode (OLED) that can be nowadays identified in mass produced electronics worldwide, like flat screen television sets, desktops or laptops, or even mobile phone devices. The other two important members of the organic devices family, *i.e.* the organic field effect transistors (OFETs) and circuits as well as organic photovoltaics (OPVs) lag significantly behind OLEDs in development, performance and market acquisition, in spite of a tremendous investment and effort made by scientific community and industry. If pure organic materials based photovoltaics inherit highly insurmountable limitation barriers in their development, mainly due to the photophysics and charge separation / transport mechanisms in organic layers [65, 66], organic field effect transistors show performance limitations of their own due to a combined series of physical, electrical and mostly technological factors [14, 67]. Whether the rules limiting the performance of van der Waals bonded organic semiconductors in OFET devices described in the latter reference (*i.e.* contact resistance, charge transport mechanism, short channel effect, area of electrodes overlap, *etc.*) are applicable in whole or in part to hydrogen bonded semiconductors, it is still a subject which is not fully understood. This uncertainty stems from the inner mechanism of operation of a hydrogen bonded semiconductors, where it was demonstrated that the "highly conjugated core" (the sought-after prerequisite for the design of van der Waals bonded semiconductors), does not play a crucial role, but other factors like molecular conformation, the growth mechanism or polarity of the underlying surface are of more critical importance [31, 32, 45, 68].

Organic field effect transistors definitely lag behind their inorganic counterparts where cycle stability, speed of operation and endurance are certain accolades that trigger the aggressive expansion of electronics worldwide. We argue that these fashionable benefits of inorganic semiconductors can be reduced to three major characteristics of these materials: their high purity, their extensive order and their coupling through very strong (covalent) bonds. All these features are missing for the classic (van der Waals bonded) organic semiconductors, where levels of purity of 99%, 98% and even lower are considered acceptable for the fabrication purposes of organic electronic devices (pertinent to this publication theme is the example of Indigo that is commercially available at Sigma-Aldrich with a dye content, *i.e.* a purity of 95%; Quinacridone available at TCI Europe with a purity of 93% for a lower price or greater than 99% for a higher price/gram; or Indanthrene Blue available also at TCI Europe with an uncertain purity that is estimated to be around 97%). The inorganic semiconductors feature extensive order at the atomic level that can reach levels of perfection for the entire device, where impurity levels of 0.00001% play a crucial role in defining the n- or p- type characteristic of the respective semiconductor. Hydrogen bonded, organic semiconductors can mitigate the gap that exist between the van der Waals and covalently-bonded semiconductor materials through their improved level of order at the molecular level [36, 37], that is a direct characteristic of the stronger intermolecular bonds. But if the bond strength and the afferent degree of order are two material properties (*n.a.* the degree of order can be manipulated via specific deposition techniques), it rests only in our power to control the third important prerequisite (*i.e.* the level of purity) of such semiconductor materials. In this work, we demonstrated the importance of this latter aspect by pursuing careful purification via train sublimation for all the investigated organic semiconductors; therefore all the materials subjected to this study were exposed to at least 3 rounds of purification in vacuum that guaranteed a purity level in excess of 99%, although the exact quantification of this level was not of immediate interest. This chapter is dedicated to disparagingly assess the electrical performance of OFET and simple circuits featuring selected hydrogen bonded semiconductors in terms of the electrical measurement instabilities generated by aging, cycling, air exposure, bias-stress, chemical and thermal factors. Importantly, this chapter demonstrates the significance of OFET design as a valuable tool of assessing the performance of organic semiconductors and the functionality of organic field effect transistors.

The device geometry used for OFETs fabrication in this work involved a staggered bottom gate top contact electrodes on glass substrates, aluminum electrode as gate contact, electrochemically grown AlOx layer capped by a vacuum processed aliphatic dielectric (either tetratetracontane, $C_{44}H_{90}$; pentacontane, $C_{50}H_{102}$ or polyethylene) as dielectric layer, vacuum processed organic semiconductor and top contact electrodes. A schematic of such device geometry is presented in **Figure 2** .

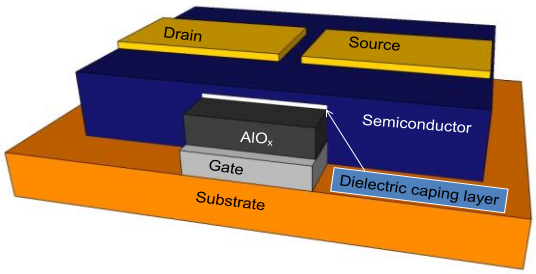

Figure 2: *Schematic of the OFET design employed exclusively in this work*

The influence of the purity of the organic semiconductor to the performance of the OFET device is clear from the comparison of the transfer characteristics of three samples fabricated with Indigo having various levels of purity: an original (as received) material from Aldrich, a one-time purified and a three times purified compound, presented in the same plot in **Figure 3a)**. Although the respective devices were fabricated with identical instrumentation, in identical configuration (layer thicknesses), by the same person, and using identical recipe for the development of all the active layers (bottom gate, dielectric, semiconductor and top contact electrodes), the device fabricated without prior purification of the Indigo semiconductor showed (not at all surprisingly) the poorest performance among all in terms of charge mobility and hysteresis. One single round of sublimation was enough to clearly improve the hysteresis and the charge mobility of both channels, but more distinctly of the hole channel by one order of magnitude. Performing three successive rounds of purification of the Indigo material resulted in a further improvement of both hysteresis and mobility of the two channels (electron and hole) by an additional one order of magnitude. The **Figures 3b)** and **S3 a)** in the **Supplementary Information** file display the stability to measurement in air of two OFETs with Indigo semiconductors that were not encapsulated. In **Figure 3b)**, the device was initially never exposed to ambient atmosphere, it was measured in glove box under nitrogen as baseline measurement after its fabrication (black line), and re-measured after 7 days of storage in glove box (red line). After the respective measurement, the device was exposed to ambient atmosphere for one day, and then introduced in glove box and re-measured (green line). A final measurement in ambient air followed (blue line). What can be immediately understood from inspecting **Figure 3b) and S3 a)** is that Indigo, due to its high LUMO level of -3.8 eV definitely cannot be air-stable with respect to its electron channel (*i.e.* at positive V_{gs} values). Surprisingly, even levels of oxygen as low as 2 ppm that were displayed by the glove box monitor, seemed to be enough to generate a visible decay of the electron channel (red line in **Figure 2b)** compared to original black line), while as expected bore no influence on the performance of the hole channel (*i.e.* visible at negative V_{gs} values in **Figure 2b)**). Interestingly, a simple storage of the Indigo device outside glove box, without measurement can produce a significant degradation of the electron channel of about one order of magnitude mobility, even when the device is re-introduced and measured inside glove box under inert atmosphere (**Figure 3b),** green line). Finally, a direct measurement of the OFET in air produced a major degradation of the electron channel in excess of two orders of magnitude mobility, with the appearance of a significant hysteresis of the transfer curve, mostly predominant in the electron channel (**Figure 3b),** blue line). **Figure S3 a)** shows the behavior of a device that was aged for significantly longer times compared to the one in **Figure 3b)**. After one month and respectively 10 weeks storage inside glove box, the sample showed progressive decay of the electron channel, in line with the observation of the sample described in **Figure 3b)**, meaning that even minuscule amount of oxygen are enough to induce degradation of the electron channel; however the hole channel fluctuated, in the sense that it showed an initial decay, followed by a recovery. We consider that this behavior can be accounted to the presence of other potential instabilities, and does not represent a trend. Nevertheless, when the sample was stored for 12 days outside glove box and then re-introduced and measured inside glove box, the decay of the electron channel was more pronounced as the one displayed by the sample analyzed in **Figure 3b)** to which one day only of exposure to oxygen was allowed. Nevertheless, both cases show that the oxidation of the Indigo is faster at the beginning of the time of exposure to oxygen but later on it levels out to a stable value. Interestingly, one single measurement outside glove box induces a major decay of the electron channel of Indigo to a level not achieved after 12 days exposure to oxygen but without measurement.

The **Figure S3 b) and S3 c)** in the **Supplementary Information** file present the stability of Indigo based OFET devices when protected by encapsulation. In **Figure S3 b),** a 1.5 μm layer of Parylene C was deposited on the top of gold contacts, covering entirely the channel and the underlying layer of Indigo semiconductor, including its sides. Different than the behavior of Indigo presented in **Figure 3** relative to the decay of electron channel, in this case the device operated in ambient air without any visible form of degradation for at least 8 days allocated to the completion of this experiment. If parylene C deposition requires special attention regarding the handling of the OFET and is time consuming in the sense of deposition time required for parylene C, then the encapsulation of an OFET inside the glove box by simply

covering the channel with a sticky Kapton tape (commercially available poly imide tape) represented a much faster approach that required only 5 seconds of time, mostly dedicated to uniformly pressing the tape onto the OFET sample. The respective sample was removed from glove box and measured in ambient air, showing an absolutely minimal degradation of the hole channel (possibly due to the effect of pressure over the contact electrodes), and a minimal decay of the electron channel transport. The **Figure S3 c)** displays under the horizontal axis the levels of threshold voltage shifts for the two channels. We observe that the level of degradation of the electron channel after Kapton tape encapsulation is similar to the one observed for the sample in **Figure 3b)** after storage for 7 days in glove box when an oxygen level of 2 parts per million was present. In a separate experiment we wanted to assess the influence of light and dark conditions over the transfer characteristics of Indigo. We measured one OFET in complete darkness inside the glove box within a closed measurement box, and compared the measurement result with another one when the sample was exposed to full light inside the glove box and was placed in the same time on the top a solar simulator (also inside glove box) at its full operational power of 100 mW/cm^2 light intensity. We observed a minimal change in the transfer curve, in the sense that a small decay of electron channel was observed, while a minimal improvement of the hole channel occurred. Nevertheless, we cannot conclude unequivocally that the presence of light induced such small drifts, considering that these changes (or at least the one visible for the electron channel) may be generated by the cycling of the sample as presented in **Figure S3 d).**

Tyrian purple (6,6'-Br-Indigo) is a relative of Indigo molecule that due to the closer packing and more co-facial orientation of two adjacent molecules in the chain, affords higher degree of charge transport compared to Indigo [69]. Nevertheless, as it is the case for all hydrogen bonded molecules, the maximum level of mobility can be achieved only when the molecule is deposited on highly non-polar, aliphatic (*i.e.* hydrophobic) dielectrics [31, 34, 45, 68] that render a stand-up conformation of the molecules and the subsequent horizontal delocalization of charges and their ensuing favorable transport between the pair of top contact electrodes**. Figure 3c)** shows the undesired case when a hydrogen bonded semiconductor (Tyrian purple in this case) is deposited on highly polar dielectrics; the dielectric to semiconductor interface offers in this case no possibility for channel formation and subsequent charge transport. We found intriguing that on polar dielectrics (*e.g.* poly vinyl alcohol, poly vinyl triazol, CuI, polyaniline, shellac, benzocyclobutene, guanine, adenine, melamine, glucose, *etc.*) the transfer characteristic of Tyrian purple represented the shape of an almost horizontal line, and the transistor did not produce the characteristic transfer curve regardless of the electric field applied to the dielectric (the **Figure S4** in the **Supplementary Information** file).

What we also observed during the deposition of the hydrogen-bonded semiconductors layers, was that slow evaporation (*i.e.* deposition rate between 0.05 to 0.1 nm/sec) of top contact electrodes (Au in case of Tyrian purple) resulted in devices displaying a pronounced lower performance of the electron channel compared not only to the hole channel itself (**Figure S5** panel **a)**) but to the electron channel of devices where a fast Au deposition was performed (*i.e.* deposition rate between 1 nm/sec and 1.5 nm/sec), as displayed in the device shown in **Figure S5** panels **b)** and **c)**. In the case of the latter device, a nearly ideal balance of electron and hole channels were obtained for a fast deposition of top contacts, regardless of the measurement condition in the positive quadrant (*i.e.* positive V_{ds}, **Figure S5 b)**) or negative quadrant (negative V_{ds}, **Figure S5 c**), and respective mobility values are displayed on each graph.

As in the case of Indigo, we evaluated the stability to measurement in air for Tyrian purple. Different than Indigo, Tyrian purple has characteristic a LUMO level of -4.0 eV which lies right at the border of insensitivity to oxygen induced oxidation [69, 70]. It is therefore not surprising that compared to Indigo, Tyrian purple displays a much higher resistance to degradation during the measurement in air. **Figure S6 d)** presents the case of a device with Tyrian purple semiconductor that was measured inside glove box (black curve) then exposed for 3 weeks to ambient atmosphere and immediately re-introduce in glove box and re-measured (green curve). The device showed no degradation in the sense of mobility of the hole channel (identical absolute values of sqrt(Ids) for both before and after the air exposure), but displayed a shift of ~ 1 V of both threshold values (*i.e.* $V_{th\text{-}e}$ and $V_{th\text{-}h}$) towards more positive values, that could be traced to the slight degradation or contamination of the contact electrodes due to extensive exposure to oxygen. Regarding the electron channel degradation, the device showed minimal decay of the electron mobility, visible by the slightly decreased absolute value of the Sqrt(I_{ds}) curve, on the right axis of **Figure S5 d)**. **Figure 3d)** presents the case of another device with Tyrian purple channel that was measured inside glove box (baseline measurement, black line), immediately measured outside glove box (pink line) without any longer exposure to ambient air stretching beyond the measurement time, and finally introduced immediately back into the glove box and re-measured (blue line). The conclusion of the two separate experiments is that Tyrian purple displays a much higher resistance to degradation under operation in air than Indigo (see **Figure 3**) where it was shown that Indigo degradation occurred even by simply exposing the Indigo to ambient air without measurement (**Figure 3b)** and **Figure S3a)).** In the case of Tyrian purple, the OFET performance with respect to electron channel decays only when measured in air, albeit displaying a more limited degradation than Indigo (see for comparison **Figures 2b)** and **2d)** for the case of the measurements completed outside the inert atmosphere of the glove box). Nevertheless it should be pointed out that both Indigo and Tyrian purple are similarly resistant to degradation of the hole channel when the semiconductor was exposed to, or alternatively, even measured in air.

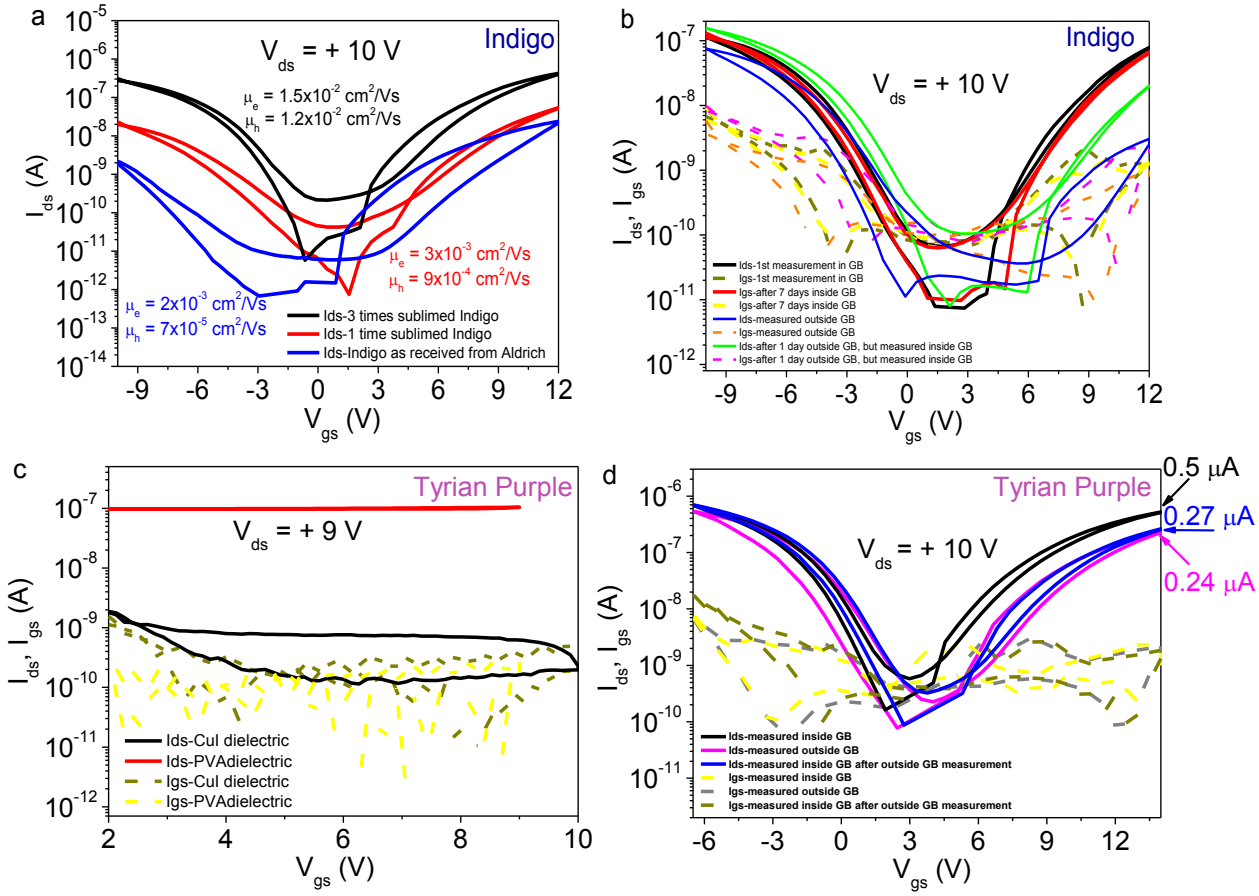

Figure 3: *Transfer characteristics of OFETs with Indigo semiconductor on Al gate, AlOx-Tetratetracontane dielectric, and Au source and drain electrodes.* ***a)*** *OFETs with Indigo semiconductor deposited on identical dielectric layers: as received from Sigma-Aldrich, one time purified and respectively three times purified by train sublimation;* ***b)*** *Investigation of stability to air exposure for Indigo-based OFETs: first measurement in glove box for a sample never exposed to air (black line), measurement in glove box after 7 days of storage (red line), measurement in glove box after exposing one day the sample to ambient air (green line) and measurement outside glove box (blue line); Transfer characteristics of OFETs with Tyrian purple (6,6'-Br-Indigo) semiconductor on Al gate, AlOx-Tetratetracontane dielectric, and Au source and drain electrodes.* ***c)*** *Proof that the transistor characteristics of hydrogen bonded semiconductors are hardly obtained [25] on polar dielectrics: thin CuI (red curve) and thin poly vinyl alcohol (PVA, black curve);* ***d)*** *Transfer characteristics of OFETs with Tyrian purple semiconductor on Al gate, AlOx-Tetratetracontane dielectric, and Au source and drain electrodes. The sample was measured in glove box (initial measurement, black line), measured outside glove box, in air (pink line) and measured inside glove box, after the outside glove box measurement (blue line), showing a full recovery of the hole channel and a slight recovery of electron channel.*

Concluding from the experience gained through the electrical measurements of Indigo and Tyrian purple based OFETs, we can assess that both semiconductors are stable semiconductors material for ambient air operation if appropriate encapsulation is provided. Alternatively, operation in inert atmosphere is more desirable. Indigo performance is not affected by the level of illumination. Nevertheless there are many more influential factors that could affect the performance of indigo as an organic semiconductor layer, like for example exposure to various chemical vapors, or subjecting the fully fabricated OFET sample to variations in temperature, UV radiation, among others.

When "perfect balance" conditions of the electron and hole channels are fulfilled for two OFET devices, as shown in **Figure S5 b-c)**, then the two respective OFETs can be connected to form a simple inverter circuit having a common gate electrode as presented in reference [34] and coined as "*complementary-like inverter*" [70]. **Figure 4** displays the curves of such inverter measured at an external voltage of 20 V in the positive quadrant and -20 V in the negative quadrant, while varying the frequency of measurement (increment time of data points collection). We performed the experiment with increments of 10 fold from 10 Hz to 1 MHz, and observed very good stability both with respect to hysteresis occurrence, which remained insensitive to the speed of the measurement, and to the level of voltage gain of the inverter. The great advantage of a complementary-like inverter is the ease of its fabrication, that requires no special attention in

adjusting the difference in the semiconductors mobility (*i.e.* the mobility of the n-channel semiconductor and the p-channel semiconductor) via geometric adjustment of the channel length and width [71]. Nevertheless, the fact that the same semiconductor operates as n-channel at one gate voltage and p-channel at another gate voltage during the same sweep, makes difficult to fully switch off the semiconductor to its OFF level. As a consequence, the ambipolar semiconductors offer in general a relatively high OFF level in the transfer curves of the OFETs [72], as it is obvious in the case of Tyrian purple where the OFF level of the drain currents lie in general in the level of 1 to 10 nA (see **Figures 3** and **S5**). This undesired characteristic of the ambipolar semiconductor is translated in a drawback of a complementary-like inverter, as it is visible in the **Figure 4a)** and **4c)** by the imperfect "Z" shape, where the horizontal levels are both tiled, upwards and downwards respectively. This type of behavior is called "imperfect rail-to-rail operation" of the inverter was observed elsewhere for complementary-like inverters [72, 73] and can preclude the utilization of complementary-like inverters for the establishment of more advanced circuits like ring oscillators and logic gates. In the latter designs, a specific number of inverters have to be connected in series and offer complementary or even feeding functions to one another.

This "imperfect rail-to-rail" behavior is visible also in the **Figure S6** (**Supplementary Info** file) where inverter transfer curves are provided for various levels of supply voltage (V_{DD}), from 12 V to 20 V in the positive quadrant and from -12 V to -20 V in the negative quadrant of the inverter respectively. All the characteristics were measured at 1 MHz frequency and showed minimal hysteresis behavior; in addition, the excellent balance of the two semiconducting channels of every individual OFET, and the exceptional reproducibility of charge transport mobility for both electrons and holes for the two OFETs resulted in a nearly perfectly balanced inverter with maximum gain values of 116 in the negative quadrant and 118 in the positive quadrant for ± 20 V external voltage of the inverter (see **Figure S6 b) and S6 d)**), however with no rail-to-rail operation, as detailed above (**Figures 4a)** and **4c)**). Nevertheless it should be highlighted that complementary-like inverters fabricated with vacuum processible hydrogen bonded semiconductors (already referred in the above sections were the cases of Indigo and Tyrian purple, but will be also shown in the next sections similar inverters with Quinacridone channel) do not require high temperature post fabrication annealing treatment for the establishment of their high performance characteristic, as it is the case with solution processed semiconductors described elsewhere, where OFETs post fabrication annealing temperatures, sometimes in the range of 200°C to 300°C or even higher are required [72, 74, 75, 76].

In the course of investigation of Indigo derivatives, we came across three such closely related molecules to parent Indigo: monobromo-Indigo, dichloro- and respectively difluoro-Indigo. We built only simple OFET devices with each of the three above-mentioned materials and looked at the balance of the two channels when operated in glove box (**Figure S7** in **the Supplementary Information** file). Although fabricated in the same configuration and the same recipe of deposition of the constituent layers, we noticed that the monobromo Indigo displays a much less developed electron channel compared to the hole channel performance (**Figure S7 a)** and **S7 b)**). This event repeated for both types of measurements performed, *i.e.* with positive and negative drain voltages. The difference in mobility of the two channels is significant, *i.e.* 0.1 cm^2/Vs for the hole channel and 6×10^{-3} cm^2/vs for the electron channel. Interestingly, the device showed no hysteresis in the hole channel active region, but a small hysteresis in the electron channel active region. In our already published work [77] we showed that 6,6'-Cl-Indigo can be engineered after significant effort to function as relatively well balanced ambipolar semiconductor (**Figure S7 c)** and **S7 d)**). Nevertheless, different than monobromo-Indigo, dichloro-Indigo showed persistently higher performance for the electron channel compared to the hole channel. Two such OFET devices were connected and a transfer characteristics of a complementary-like inverter was measured [77]. Nevertheless, the performance of the inverter was significantly lower than the one of parent Indigo [31], or Tyrian purple (**Figure 4 and S6**). 6,6'-F-Indigo showed a much better balance of the two semiconducting channels than 6,6'-Cl-Indigo, with a small advantage of the hole channel compared to the electron channel with respect to charge mobility; however both channels showed similar hysteresis level, in contrast to monobromo-Indigo (see **Figure S7 e)** compared to **S7** panels **a)** and **b)**). **Figure S7 f)** in the **Supplementary Info** file presents the output characteristics of the 6,6'-F-Indigo OFET, where the superlinear increase, *i.e.* the clear print of ambipolar semiconductor is visible at low gate voltages, (*i.e.* -6 V, -3.8 V, -1.6 V respectively), due to injection of majority charge carriers in a channel instantaneously dominated by minority carriers. We did not pursue the investigation of difluoro-Indigo into the field of simple electrical circuits (inverters), however we believe that well balanced inverter characteristics and gains can be obtained after optimization of fabrication procedure to render well balanced performance of two adjacent OFETs.

Epindolidione is not a derivative, but an isomer of Indigo itself, that can be derived directly from Indigo while heating the latter material in vacuum at a temperature of 460°C [50, 51]. Alternative routes of synthesis exist also, as described in the Chapter 1, of this Perspective article dealing with Chemical Synthesis of H-bonded Semiconductors. We analyzed Epindolidione in comparison with its better known counterpart, Tetracene, and observed a net superiority of Epindolidione in terms of charge transport (hole only in both materials' cases) and stability to operation in air with both OFET devices un-encapsulated, stored in air and operated in air as shown in reference [35]. In this work we want to present other facets of the stability and characteristics of Epindolidione (see **Figure 5a**).

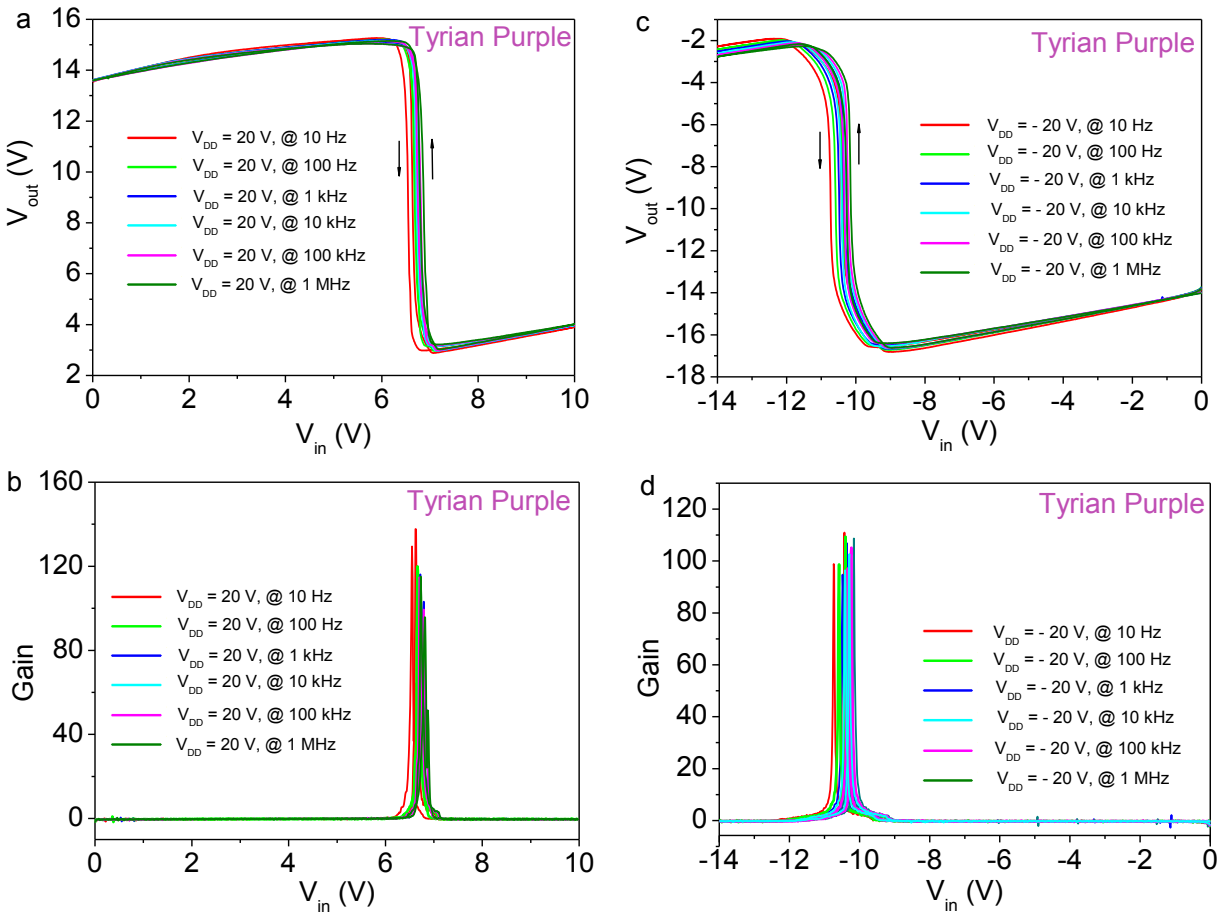

Figure 4: *Complementary-like inverters with Tyrian purple semiconductor obtained by connecting two OFETs featuring a common gate electrode.* ***a)*** *Inverter transfer characteristic at V_{dd} = 20 V in the positive quadrant, measured at frequencies spanning the interval 10 Hz to 1 MHz;* ***b)*** *the respective inverter gains of the characteristics displayed in a), in the positive quadrant;* ***c)*** *Inverter transfer characteristic at V_{dd} = - 20 V in the negative quadrant, measured at frequencies spanning the interval 10 Hz to 1 MHz;* ***d)*** *the respective inverter gains of the characteristics displayed in c), in the negative quadrant.*

Although the energetic levels (HOMO = -5.6 eV and LUMO = -2.9 eV) makes one believe that it is difficult to obtain electron channel transport when contacted by gold, this event is in fact possible when slow thermal evaporation of gold contact is performed (**Figure 5a)**). In a similar control experiment, we noticed that even Pentacene can be rendered ambipolar when gold is slowly thermally evaporated (*e.g.* at a constant rate of 0.01 nm/sec, see the **Figure S8 a-b)**), rather than depositing gold fast, as was observed to be ideal for hydrogen bonded semiconductors (*i.e.* deposition rates between 1 and 1.5 nm/ sec, see **Figure S5 a)-c)** and the explanations in text referring to the importance of evaporation rate). Surprisingly though, despite the clear ambipolar (*i.e.* V-shape) of the transfer characteristic of Epindolidione, that cannot be accounted to the leakage current (the latter being in excess of 3 orders of magnitude lower than the drain current), we did not record any superlinear increase in current at low applied gate voltages in output characteristics (see the **Figure S8 c) in the Supplementary Information file**), possibly due to the high imbalance of the two channels, with the hole channel being overwhelmingly superior to the electron channel. A similar observation was recorded for pentacene (**Figure S8 b)**). However, it is still possible to obtain higher values of the electron channel by performing derivatization of Epindolidione to adjust the respective LUMO level of the derivative molecule(s) to the work function of electron injecting electrodes like aluminum. We accomplished this event by synthesizing two derivatives of Epindolidione, *i.e.* difluoro- and dichloro-Epindolidione, by simple derivatization of the Epindolidione core, as described in Chapter 1. OFETs were fabricated with the two derivatives of Epindolidione, on a composite gate dielectric consisting of anodically grown 32 nm of AlO_x and 10 nm tetratetracontane (TTC) passivation layer and they showed only n-type behavior with the electron mobility of 0,1 cm^2/Vs and 8×10^{-3} cm^2/Vs, respectively, as shown in **Figure S9** of **Supplementary Information** file.

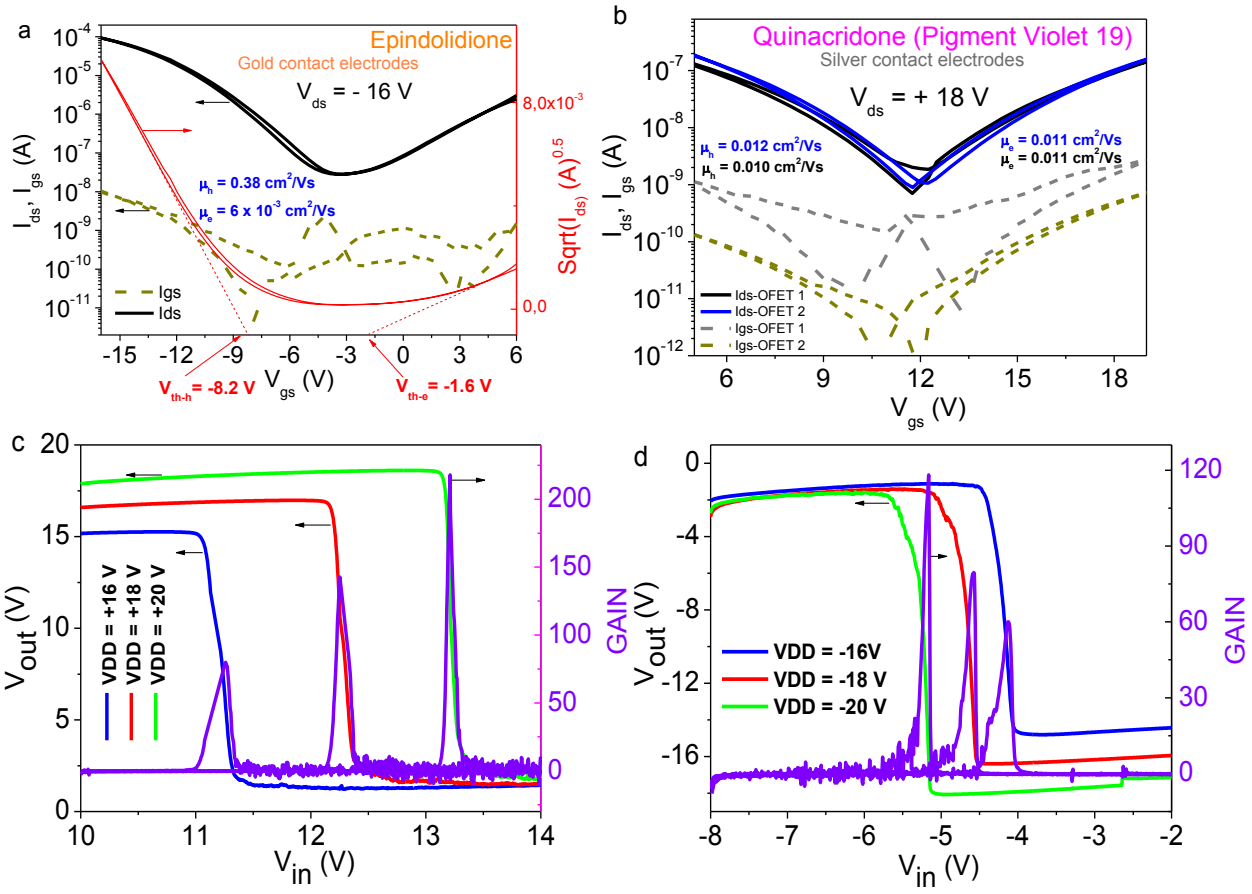

Figure 5: *OFETs with Epindolidione and Quinacridone semiconductors on Al gate and AlOx-Tetratetracontane dielectric. Au was used for source and drain electrodes in panels a), c), and d), while Ag for S-D electrodes of panel b).* ***a)*** *Ambipolar characteristics of Epindolidione that can be obtained only for slow deposition of top Au electrodes (rate lower than 0.01 nm/sec;* ***b)*** *Ambipolar characteristics of two transistors with Quinacridone semiconductors and Ag as source and drain electrodes, showing nearly perfect balance of the electron and hole channels and excellent reproducibility in fabrication;* ***c)*** *and* ***d)*** *Complementary-like inverter transfer characteristics of the two OFETs displayed in panel b) having a common gate electrode. Panel c) displays three measurements of various supply voltages (V_{dd}) in positive quadrant, while panel d) similar measurements for negative V_{dd} in negative quadrant. The inverter gain is displayed on the right side of c) and d) panels.*

Quinacridone and many of its derivatives are commodity pigments utilized for ink jet printer formulation (developed by Xerox Corporation in the 1960s [47]), rugged paints for cars, outdoors and even textiles. We showed in our previous work that Quinacridone translates its high resistance to degradation into highly stable OFETs operated in air without encapsulation [35]; the respective OFETs were contacted by gold for the top contacts (source and drain electrodes) and afforded only the hole channel operation. However, when contacted by a metal that makes the semiconductor afford also electron injection, due to the better matching between the LUMO level of the semiconductor and the work function of the metal, Quinacridone shows not only the presence of the electron channel but displays in the same time ambipolarity. Such example is offered in the **Figure 5b)** where Quiancridone was contacted by silver as material for top source and drain electrodes. The figure displays two OFETs fabricated on the same slide, with a common gate electrode. The slight difference in performance (in other words the good fabrication reproducibility) of the transfer characteristics of the two OFETs recommend them for the assembly of complementary-like inverters by simply connecting two of the side terminals of two adjacent OFETs fabricated on a common gate electrode. The inverter transfer characteristics are presented in **Figure 4c)** and **4d)**, where inverter gains of 120 in the negative quadrant and 220 in the positive quadrant are recorded. The difference in gain between positive and negative quadrant is most likely due to the slight difference in mobility of the hole channel of the two initial OFET devices, shown in **Figure 5b)**. A very interesting observation can be obtained when comparing the **Figures S6 b)** and **S6 d)** in **Supplementary Info** file on one side and **Figures 5c)** and **5d)** on the other side, in other words the performance of the inverters in terms of their respective gain for Tyrian purple and

Quinacridone. Although the field effect mobility of Tyrian purple OFETs was higher by more than one order of magnitude than the respective values of the Quinacridone OFETs (see **Figure 5b)**), the performance of the inverters with Tyrian purple was not impressively higher even in the case of champion devices, which we reported in [69], (*i.e.* gains of 250 and 285 in the two quadrants). However, when the two channels of an ambipolar semiconductor are better balanced in terms of their field effect mobility (**Figure S5 b)** and **S5 c)**), as it was the case for Tyrian purple [also see Ref. 69], then the inverter gains in the two quadrants are also closely balanced.

Due to the presence of hydrogen bonds that exist both internally (intramolecular) as well as externally (intermolecular, *i.e.* from molecule to molecule), the Quinacridone displays excellent resistance to decomposition. We showed through a TGA analysis that the 5% weight loss for Quinacridone occurs at temperatures in excess of 500 °C [35]. What was interesting to pursue and to find out was if such resistance to degradation of Quinacridone material could be translated into a high resistance to degradation and performance retention of Quinacridone based OFETs when subjected to various temperature annealing steps. In **Figure S10 a), S10 b)** and **S10 c)** in the Supplementary Information file display our investigation with respect to resistance to either thermal or UV radiation alone, or to both combined events, for devices fabricated in identical geometry and showing initially highly comparable characteristics. **Figure S10 a)** shows the resistance to UV irradiation of a fully fabricated OFET with Quinacridone semiconductor. The inset displays the UV spectrum of the portable lamp employed in the test. It is visible that the exposure of the device to UV irradiation in glove box had negligible effects over the behavior of the OFET device. However, heating another device to 250°C on top of a hot plate inside the glove box for only 5 minutes had beneficial effects (see **Figure S 10 b)**), resulting in an increase of mobility of the semiconductor, albeit with a loss on the side of hysteresis, which became more pronounced after the completion of the annealing test. We infer that the heating event altered the interface to the cross linked polyethylene layer underneath, and resulted into a more coalesced quinacridone film and a possible reduction in the number of grain boundaries, that contributed favorably to the charge transport, but unfavorably to the smoothness of the interface that was the primary cause for the occurrence of hysteresis. A combined effect of heating and UV radiation performed both in the same time offers a picture that aligns well with the observations collected from **Figures S10 a)** and **S10 b)**. Concluding from the observations collected from the experiments carried out in **Figures S10 a), S10 b) and S10 c)**, we see that especially the thermal annealing of the fully fabricated device has a beneficial role for charge mobility improvement, but this improvement comes at the price of a more pronounced hysteresis. For the respective experiments we employed polyethylene as the capping layer for the electrochemically grown aluminum oxide dielectric, since polyethylene can be UV-cross linked by exposure for 30 minutes inside the glove box to the UV radiation of a portable lamp (as the one presented in the inset of **Figure S10 a)**) while heated in the same time to a temperature slightly above its melting point of ~ 105°C, *i.e.* at 110°C. We used for the crosslinking event the combination of UV irradiation and 110°C exposures for 30 minutes inside glove box; we observed a non-conclusive evidence over the improvement of the quality of the layer when the crosslinking event was performed in ambient air. The fact that Quinacridone shows a high robustness to temperature variation recommends the semiconductor for real-life applications beyond the realm of laboratory demonstrations. We were interested to see how Quinacridone would fare into a process of fabrication of conformable electronics that require a combined event of heating and pressure endurance. With this respect we fabricated OFET devices on polycarbonate foils, that were subsequently laminated and finally thermoformed to a conformal design to suit an industrially relevant need for fabrication of electronics meant to intersperse into household objects. The device shown in **Figure S10 d)** was measured both immediately after its fabrication (black line) as well as after the thermoforming process that consisted of an application of a temperature of 110°C for 3 seconds, while subjecting the sample at a pressure of 110 bar (brown curve in **Figure S10 d)**). It is interesting to note that the ON current remained unaltered by the thermoforming process, with the only change that induced a slight mobility decrease of the device from 1.2×10^{-2} cm²/Vs to 8.9×10^{-3} cm²/Vs being the increase of the OFF level of the device, an event that could be assigned to the alteration of the interface, or possibly to the small degradation of the contacts that carried with them a decrease in the insulating properties of the non-crosslinked polyethylene dielectric layer.

We conclude our journey into general overview of electrical stability of bio-based molecules by investigating one of the most unexpected candidates: Indanthrene Blue. A material with long history in the chemical industry, Indanthrene Blue displays a remarkable resistance to degradation, being acclaimed for its fastness and resistance to chemical attack (see the explanations in Chapter 1). Its inertness recommended it for food processing industry, and Indanthrene Blue still carries a food number (E 130), although it is not any more approved to be engaged for such applications in both EU and USA. We employed Indanthrene Blue for the fabrication of organic field effect transistors, in a geometry and configuration similar to all the other devices presented in this work, also considering that the critical step is the existence of thin aliphatic layer on which Indanthrene Blue was grown and on which it can deliver its semiconducting properties (see the explanation given in **Figure 3)**. As shown in the **Figure S11 a)**, Indanthrene Blue is an ambipolar organic semiconductor with relatively well balanced electron and hole conductivity channels, i.e. 7.5×10^{-3} cm²/Vs for the electron channel and 1×10^{-3} cm²/Vs for the hole channel respectively.

As we intended all throughout this article to highlight for each investigated material a different facet of OFET development, we point out here the importance of having available the right infrastructure in obtaining reproducible results. We fabricated for this experiment batches with OFETs with Indanthrene Blue by altering only one variable, namely the deposition of the respective semiconductor from two different distances between crucible (material source) and the holder of OFET substrates. We deposited the material with the aid of identical shadow masks, at identical vacuum of 2×10^{-7} mbar, and at identical deposition rates and ramps; moreover by the same operator, nevertheless on two different instruments: an evaporator that has as a favorable design characteristic with a distance of only 10 cm from the crucible to the sample holder, and one other instrument that has a distance of 30 cm between the two elements (crucible and sample holder). **Figure S11 a)** and **S11 b)** illustrate the difference that can result (both in terms of mobility and hysteresis, with the former values displayed on each of the two graphs) when only one variable in the process is altered, and may provide sufficient evidence why reproducing results reported by one research group is difficult to be achieved by another group elsewhere. This fact is true considering that many variables in the process are unknown and unaccounted for, *e.g.* (i) the material purity (whose importance was already exemplified in **Figure 3a**)); (ii) its deposition rate and its deposition ramp; (iii) the vacuum level during the deposition process; (iv) the distance separating the evaporator source to substrate holder; (v) the angle of deposition; (vi) the rotation or not of the substrate holder during deposition; (vii) the OEFT shadow mask geometry (i.e. channel dimensions, W/L and area of overlap between the S-D electrodes and the bottom gate electrode); (viii) the patterning of the semiconductor; (ix) and finally the skill and dedication of the personnel employed in the two fabrication processes. If these nine enumerated factors are not providing enough variability, then we consider appropriate to introduce the tenth variable, which no publication ever mentions about, *i.e.* the cross-contamination. We observed in our previous work [34, 69, 78, 79, 80, 81] that despite careful cleaning of the physical vapor deposition instrument, when changing from one material to another, the first set of results were highly inconsistent and showed large variations from sample to sample performance in the same fabricated batch; typically dedicating the instrument to the processing of one material only for extended periods of time surpassing one week resulted in improving the obtained results in terms of semiconductor mobility, ON-OFF ratio and even hysteresis level. **Figure S12 c)** and **S12 d)** prove unambiguously the existence of ambipolarity in the OFETs with Indanthrene Blue channel, via both the superlinear increase of drain current at low applied gate voltages, as well as via saturation of the drain current at high applied gate voltages, both events happening in the negative as well as the positive quadrants.

Finally, in **Figure 6a)-b)** we give a concrete proof of the remarkable stability of Indanthrene Blue, this time via organic field effect transistor demonstration, doubled by FTIR analysis (**Figure 6c**)). We fabricated in identical transistor geometry two OFETs with Indanthrene Blue synthesized at very different times, and purified via 3 sequences of train sublimation. One batch carries the signature of TCI Europe as vendor and was synthesized in the year 2010; the other one belongs to BASF, was synthesized in the year 1932 and was subsequently deposited at the Historical Dyestuff Collection in Dresden, Germany from which we obtained a gram amount only, courtesy of retired professors Gundula Voss of University Bayreuth, Germany and Horst Hartmann of Technical University Dresden, Germany. While both samples showed ambipolarity, it is fair to observe that the 86 years old synthesized material displayed a factor of 5 lower performance. Nevertheless, the OFET sample with historic vat dye was produced in a vacuum evaporator instrument having characteristics a distance of 30 cm between the crucible carrying the indanthrene powder and the sample holder, while the OFET with indanthrene synthesized at TCI Europe was produced in an instrument of 10 cm distance between crucible and sample holder. This critical difference may explain the lower performance of the historic indanthrene blue and keeps the question open whether the historic pigment really degraded in the 86 years passed from its synthesis to the OFET fabrication. In **Figure 6c)** we present the FTIR spectra of the two Indanthrene powders and point out that all the major peaks fall in the same position for the two materials, proving one more time the amazing resistance to degradation of Indanthrene Blue.

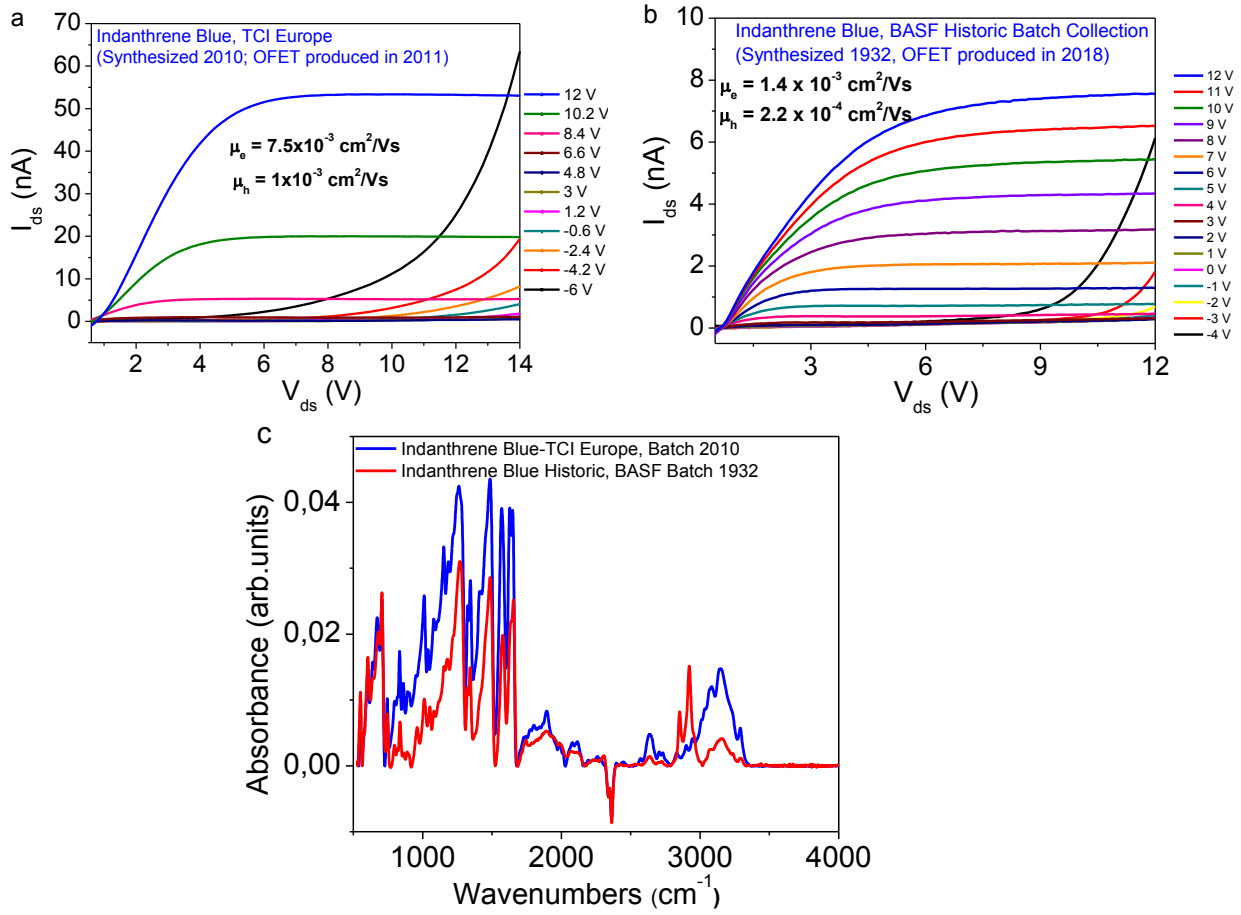

Figure 6: Output t*ransistor characteristics of OFETs with Indanthrene Blue (Vat Blue 4) semiconductor on Al gate, AlOx-tetratetracontane dielectric, and Au source and drain electrodes.* ***a)*** *Output characteristics of the device with transfer curve displayed in* ***Figure S11a)****. Indanthrene Blue was purchased from TCI Europe, from a batch synthesized in the year 2010. The OFET was produced in the year 2011;* ***b)*** *Output characteristics of an OFET with Indanthrene Blue obtained from the historic depository of dyes and pigments in Dresden, Germany. The batch belonged to BASF, synthesized in the year 1932, and the OFET was produced in the year 2018;* ***c)*** *FTIR spectra of the two indanthrene powders, showing the remarkable stability of Indanthrene Blue over 86 years passed from its synthesis. Both materials were purified 3 times by vacuum sublimation, and the same masks, dielectric layers and transistor geometry were employed in the two OFETs fabrication;* ***c)*** *FTIR spectra of the two precursor powders showing excellent correlation of the vibrational modes.*

A summary of the OFET performances of the semiconductor materials analyzed in this work is presented in **Table 1**. In this table we compiled the best results recorded by our group involving the analyzed hydrogen bonded organic semiconductors.

Table1: *Summary of OFET data for devices having the selected H-bonded semiconductors explored in this study.*

				Hole	Electron	Hole	Electron
Indigo	Sigma-Aldrich	AlOx+TTC (45+30)	2/75	1.5×10^{-2}	1.2×10^{-2}	3	3
Tyrian Purple	Our Synthesis	AlOx+TTC (45+30)	2/75	0.4	0.3	3	3
6,6'-Cl-Indigo	Our Synthesis	AlOx+TMSC (28+30)	2/25	9×10^{-3}	1.5×10^{-2}	2.5	3
6,6'-F-Indigo	Our Synthesis	AlOx+TTC (45+30)	2/75	4.4×10^{-2}	1.4×10^{-2}	3	3
Br-Indigo	Our Synthesis	AlOx+TTC (45+30)	2/75	0.1	7×10^{-2}	4	2
Epindolidione	Our Synthesis	AlOx+TTC (32+15)	5/40	1.5	6×10^{-3}	6.5	2
2,8-F-Epindolidione	Our Synthesis	AlOx+TTC (32+15)	2/60	-	0.1	-	5.5
2,8-Cl-Epindolidione	Our Synthesis	AlOx+TTC (32+15)	2/60	-	8×10^{-3}	-	3.5
Quinacridone	TCI Europe	AlOx+TTC (32+15)	5/40	0.28	1×10^{-2}	4.5	2.5
Pigment Red 202	CHEMOS GmbH	AlOx+Pentacontane (32+15)	2/35	1.8×10^{-2}	-	4	-
Pigment Red 122	CHEMOS GmbH	AlOx+Pentacontane (32+15)	2/35	1×10^{-2}	-	4	-
Indanthrene Blue	TCI Europe, 2010	AlOx+TTC (45+30)	2/75	1×10^{-3}	7.5×10^{-3}	2	2.5
Indanthrene Blue	BASF, 1932	AlOx+TTC (45+30)	2/75	2.2×10^{-4}	1.4×10^{-3}	1.5	2

2.2 Aging. Consecutive Measurements. Bias Stress. Thermal Stress.

Figure 7 a) shows the behavior of an Indigo based OFET that was measured inside glove box for 30 consecutive cycles. This shows that in the measurement cycling case, both channels decay equally constant and that indigo semiconductor is not a stable material for devices involving consecutive operation during their exploitation. **Figure 7 b)** shows the stability of an Indigo channel OFET employed as a "memory element". The design involved the presence of a staggered dual gate, in this case the bottom one being called "the active gate", as the one presented in **Figure 2** schematic of OFET employed throughout this work. The top gate is called "the floating gate". Both gates consisted of electrochemically grown aluminum oxide dielectric, capped each by a thin tetratetracontane (TTC) layer. Although the device design was similar to the one reported by Kaltenbrunner *et al.* in reference [82], our materials choice was different: we employed TTC for the capping layer for aluminum oxide dielectric and not SAM, and used Indigo as semiconductor channel instead of pentacene; nevertheless due to different thicknesses of the dielectric layers, our device worked at about 3 fold higher voltages albeit with a similar performance afforded by Indigo. We measured the device with a constant 8.5 V as drain voltage and then applied a pulse of +14.5 V as gate voltage for 1 second, while keeping drain voltage at a value of 0 V during this process. The presence of the floating gate induced a permanent change in the threshold voltage of the device, visible as the "write curve" in **Figure 7b)**. By repeating the process in the sense of applying -14.5 V as gate voltage while keeping drain voltage at 0 V level, a stable shift back to the original transfer curve was induced (the "erase curve" in **Figure 7b**). We repeated the cycle "write-erase" for 250 times each, and observed a mere 200 mV threshold voltage drift during this cycling, a value that fares favorably to the values reported by Kaltenbrunner *et al.* for a highly optimized memory element with self-assembled monolayers and pentacene channel [82]. Importantly, a stable memory window of 1.5 V between the threshold voltages of write and erase cycles was maintained during the 500 cycle testing of our OFET.

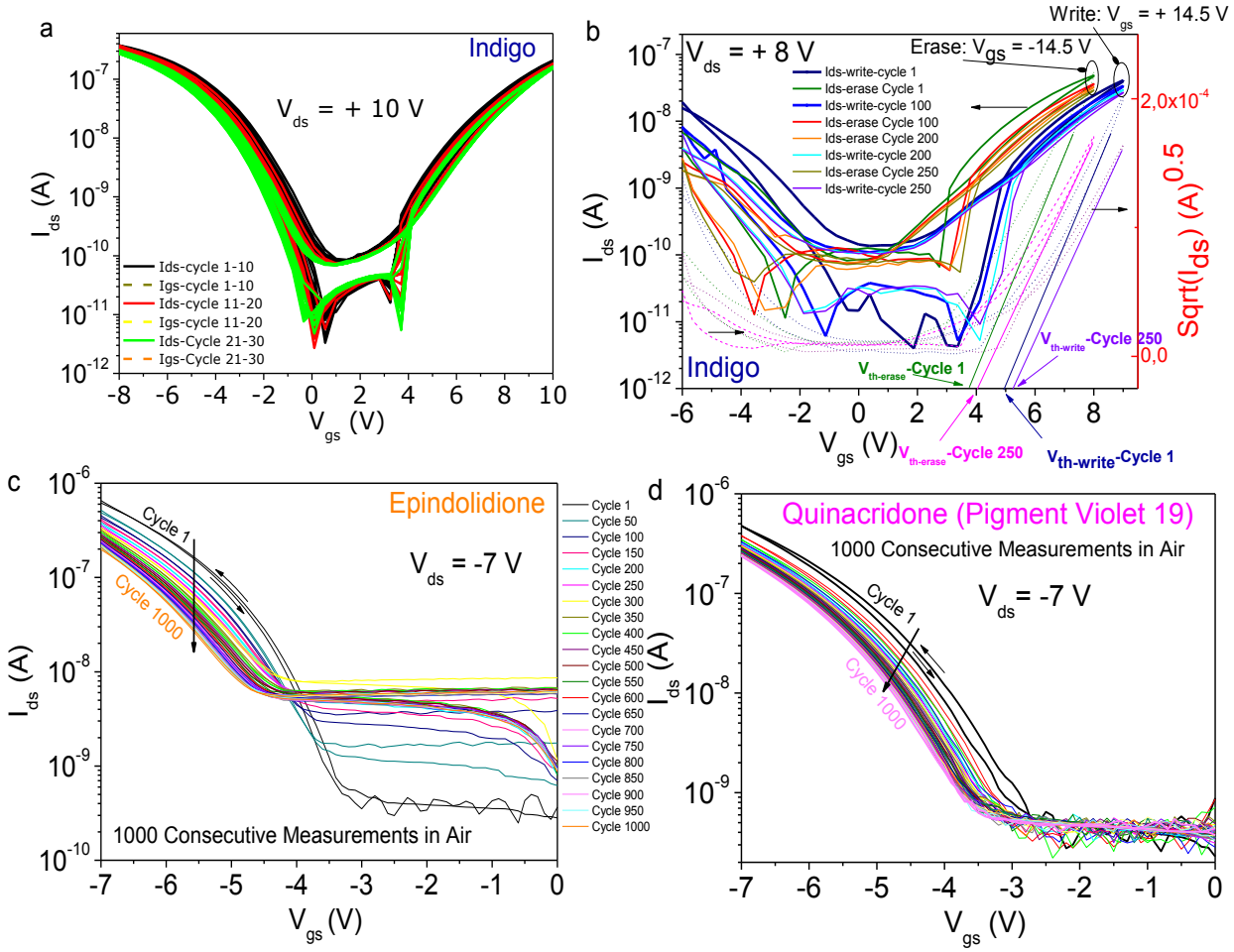

Figure 7: a) *Indigo-based OFET measured inside glove box for 30 successive cycles. The graph shows the transfer characteristics of cycles 1-10 (black lines), 10-20 (red lines) and 20-30 (green lines);* ***b)*** *Stability to a series of 500 "write-erase" cycles of 250 each using a gate voltage of 14.5 V to induce positive shift of the threshold voltage and -14.5 V to move the threshold voltage of the transfer characteristic back to the original position (erase cycle). A constant drain voltage of 8.5 V was employed for each transfer characteristic measurement. A stable write-erase window of ~ 1.5 V is produced and maintained after completion of the 250 write-erase combined cycles, although a small drift of 0.25 V to the more positive gate voltages is observed at the end of the testing.* ***c)*** *1000 consecutive measurements in air of an Epindolidione OFET, with initial characteristic (black type) and every successive characteristic with an increment of 50 being displayed;* ***d)*** *1000 consecutive measurements in air for Quinacridone OFET with initial characteristic (black type) and every successive characteristic with an increment of 50 being displayed. In a) and b) the OFET samples were fabricated on Al gate, AlOx-tetratetracontane dielectric, semiconductor, and Au source and drain electrodes. In c) and d) the OFET samples were fabricated on Al gate, AlOx-pentacontane dielectric, semiconductor, and Au source and drain electrodes.*

In a separate experiment, Epindolidione was deposited as an active semiconductor channel and the Epindolidione-channel OFET was cycled for 1000 consecutive measurements in air, without encapsulation (see **Figure 7c)**). With one minute time required for each transfer curve completion, the test was concluded in 16.5 hours. Starting from a hole channel mobility of 8.5×10^{-2} cm²/Vs, the device showed significant degradation after 1000 cycles, with a final mobility of 2×10^{-3} cm²/Vs. **Figure S12 a) in the Supplementary Information file** shows the square root of the drain current of the curves displayed in **Figure 7c)**, where a drift of approximately 1.5 V of the threshold voltage is produced as a result of the 1000 measurement cycles of an Epindolidione OFET in air. Quantifying this behavior of Epindolidione in the context of classic van der Waals semiconductors behavior on consecutive measurements in air (the devices being unprotected by encapsulation) is difficult due to the lack of the reported data for the latter class of materials. We should point out that this type of testing is not the same one as the classic bias-stress measurement where two steadily applied voltages are endured by the sample, *i.e.* both gate and drain voltages are applied continuously and concomitantly for a specific period of time. We did not finish yet the bias stress measurements for Epindolidione, but have accomplished it for other H-bonded semiconductors, and these results will be detailed in the sections to follow. Inspecting the frames **a)** and **c)** of **Figures 7** for the same type of experiment (*i.e.* consecutive cycling of devices), an emerging conclusion is that both Indigo and its isomer Epindolidione do not behave as outstanding candidates for this type of electrical stress. A device with a similar geometry and layer thicknesses to the one employed for Epindolidione in **Figure 7c)**, was also fabricated for Quinacridone and the respective not encapsulated OFET was subjected to a series of 1000 consecutive measurements in air that lasted also 16.5 hours (see **Figure 7d)** and **S12 b)** in the **Supplementary Information** file dealing with the decline of the maximum drain current during the 1000 cycles). Comparing the results of the two identical tests for Quinacridone and Epindolidione, we conclude that Quinacridone fares slightly better than Epindolidione with respect to cyclic measurement in air. The Quinacridone OFET was virtually insensitive to the cycling with respect to the OFF level, while the Epindolidione OFET showed a progressively higher OFF level during the advancement of the test. Moreover the ON level decrease for Quinacridone (*i.e.* from 4.8×10^{-6} A to 2.4×10^{-6} A) is slightly better than the decrease of the respective value for Epindolidione OFET (*i.e.* from 6×10^{-6}A to 2×10^{-6} A), basically a factor of 2 vs. a factor of 3 degradation.

In **Figure 8** we searched to complete the direct comparison between Epindolidione and Quinacridone, by assessing the stability to operation in air of several OFETs fabricated with the respective semiconductors [35]. In case of Epindolidione shown in **Figure 8a)**,the hole mobility values levelled off and did not decrease below about 50% of the initial mobility value even after extended times of storage and sporadic measurements in air summing up to 2 years (data not shown). The graph in **Figure 8a)** displays only few curves from the set of measurements, for the sake of avoiding cluttering the graph. In a similar experiment, several Quinacridone OFET samples were involved in the test, originating from different fabricated batches, and showed remarkably reproducible and consistent to one another results. The respective samples were measured inside glove box to obtain the base line without the presence of oxygen interference and then measured and stored in the lab room without encapsulation. The result of the aging measurement of one such OFET is displayed in **Figure 8b)**, where the longer testing of the Quinacridone-based device (*i.e.* 160 days, compared to 140 days for Epindolidione shown in **Figure 8a)**), was simply due to the fabrication of the Quinacridone batch of transistors at an earlier time. Different than Epindolidione, were a resistance to degradation in the sense of hole mobility retention of about 50% was observed after 140 days, Quinacridone OFETs showed significantly higher resistance to degradation, with a hole mobility retention in excess of 70% even after 160 days of aging. Combining the observations resulting from the analysis in **Figure 7c)-d)** relative to the consecutive cycling in air to the observations stemming from **Figure 8** relative to the stability to aging when one measurement per day was performed, we can conclude that Quinacridone is more robust than Epindolidione during aging and cycling in air. However, the highest hole mobility measure for a highly optimized OFET with Quinacridone fabricated in our laboratory and contacted by gold source and drain electrodes, was of only 0.28 cm²/Vs, which was about one order of magnitude lower than the respective value obtained for a champion device with Epindolidione, *i.e.* 1.5 cm²/Vs, a material for which mobilities in the range of 0.5 to 1 cm²/Vs were recorded in many of our OFET devices stemming from different batches. In our previous work [35] we argued that the tendency of Epindolidione to form higher grains might be a factor that leads to higher charge mobility than the one of Quinacridone. However we do not exclude other factors that may also play a role, like for example the more dense packing and co-faciality of Epindolidione molecules in adjacent chain. These issues are at this time not well understood and require further attention from the scientific community. If deposition techniques could be improved to render grains of Quinacridone as large or larger than the one obtained for Epindolidione in similar deposition conditions, then possibly mobility values of Quinacridone semiconductor could reach or even surpass the ones recorded for Epindolidione. When combining these advantages with the higher temperature resistance of Quinacridone (*n.a.* Epindolidione decomposes at a temperature lower by 125°C compared to Quinacridone [35]), then molecules featuring the Quinacridone core will show promises for the development of high performance organic electronics.

We went on expanding the stability study of Hydrogen-bonded molecules for organic electronic devices and investigated Quinacridone (Pigment Violet 19 in color index nomenclature), two of its close relatives, i.e. the 2,9-dichloro-Quinacridone (Pigment Red 202) and the 2,9-dimethyl-Quinacridone (Pigment Red 122) as well as Indanthrene Blue to

bias stress in glove box under nitrogen. All the curves are displayed for the three evaluated materials in **Figure 9**. We assessed both the maximum drain current (I_{ds}) retention characteristic with time passed during the 14.5 hours of bias stress (**Figure 9**), and also the behavior of the transfer characteristics for the four analyzed materials (**Figure 10**) after the completion of the bias stress (*i.e.* the process of recovery). The bias stress curves for the three evaluated Quinacridone pigments show all similar trend and shape, where a constant combined drain and gate voltage of -10 V for 14.5 hours induces a progressive degradation of the maximum drain current occurs for about 12 hours of bias stress. Interestingly, we observed that for all the Quinacridones investigated in this study (in all the fabricated batches), this degradation reversed after 12 hours of bias stress, in the sense that the maximum I_{ds} current started to recover. The reason behind this unexpected phenomenon is not immediately clear, and is currently the subject of investigation in our laboratory, and will be reported in one of our future publications. Interestingly, all the three investigated pigments showed remarkable resistance to bias stress, exemplified in the **Figure 9** by their retention of the initial maximum I_{ds} current after the completion of the stress: ~47% for Quinacridone, ~52% for Pigment Red 122 and ~ 40% for Pigment Red 202. These values are remarkable in the context of reported current retention of other investigated organic semiconductors (albeit all van der Waals bonded in the respective cases), where similar degradation were reported for some analyzed organic pigments, like DNTT or F16-Cu-Phthalocyanine [83]; although, in fairness, the bias stress for the most performing material was set as 150 hours in the respective publication.

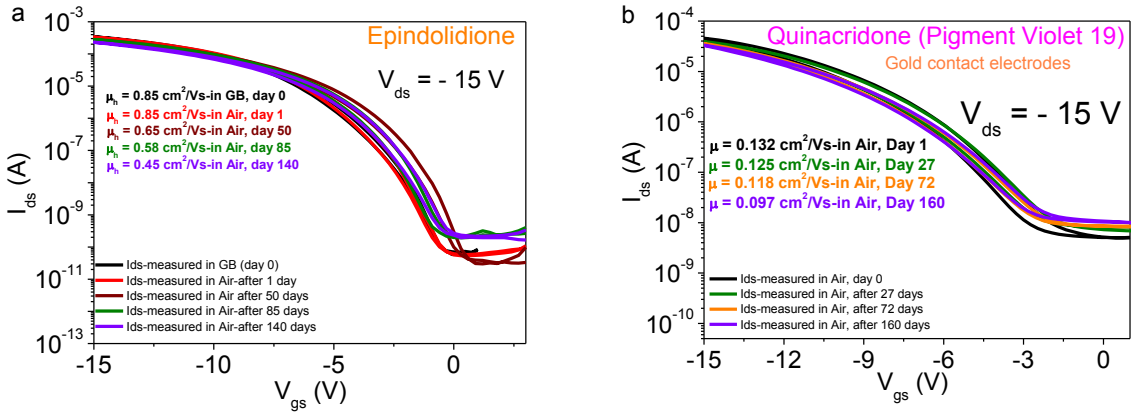

Figure 8: ***a)*** *Stability to measurements in air for an aging time of 140 days of the Epindolidione OFET, with baseline (black line) being the initial measurement in glove box under nitrogen. The decay in semiconductor mobility is displayed inside the graph. Only 4 measurements in air are displayed in order to avoid the cluttering of the graph. The sample had no encapsulation; it was stored and measured in air during the 140 days of test. The sample had Au as source and drain electrodes Al gate electrode and AlOx-Tetratetracontane as dielectric;* ***b)*** *Stability to measurements in air for an aging time of 160 days of the Quinacridone OFET, with baseline (black line) being the initial measurement in glove box under nitrogen. The decay in semiconductor mobility is displayed inside the graph. Only 4 measurements in air are displayed in order to avoid the cluttering of the graph. The sample had no encapsulation, was stored and measured in air during the 160 days of test. The sample had Au as source and drain electrodes Al gate electrode and AlOx-Tetratetracontane as dielectric.*

If Indanthrene Blue displays a remarkable resistance to degradation with time of storage, (**Figure 6**), not the same accolade can be drawn for its bias stress stability. **Figure 9d)** shows the behavior of an Indanthrene Blue OFET subjected to a constant bias of 11.5 V as drain and gate voltage for 14 hours and 15 minutes. Different than Quinacridone and the two derivatives of Quinacridone that showed retention currents in the range of 40% to 50% of original drain current, Indanthrene Blue fares more modestly in this respect, with a remnant drain current falling in the range of 3% of the original value before bias stress (**Figure 9d)**). Regarding the recovery event after the completion of the bias stress, we present in **Figure 9** the transfer curves for the three Quinacridone pigments and the Indanthrene Blue dye, recorded at various times passed after test, each of them compared to the initial measurement taken before bias stress. We considered a full recovery only the case when a nearly perfect match of the two transfer curves occurred, *i.e.* the one recorded before bias stress and the one after completion of bias stress. We observed a similar trend in behavior of all the three Quinacridones OFETs, namely the OFF levels of each semiconductor characteristic was the one most affected by the bias stress. The Quinacridones based OFETs recovered completely the initially recorded transfer curves before bias stress in times spanning the interval of 3 to 5 hours. We point out that these values are good for organic electronic devices, where recovery times ranging from minutes to hours, but even days are reported. Interestingly though, as it is visible in **Figure 10**, Pigment Red 202, the device that showed the lowest performance in terms of drain current retention was the one to recover the, in terms of both ON-OFF ratio, and threshold voltage value. If Indanthrene Blue recorded far more modest retention values of the drain current after bias stress, in a similar modest manner was also its performance with respect to recovery

of the original transfer characteristic after completion of the bias stress. With this respect, we could not recorded a perfect recovery even after 96 hours passed from completion of the electrical stress: the electron channel recovered within 75% of the initial value (*i.e.* 3.28×10^{-8} A from 4.5×10^{-8} A drain current value at +12 V applied gate voltage), the hole channel recovered within 65% of the initial value (*i.e.* 2.75×10^{-8} A from 4.35×10^{-8} A drain current value at -4 V applied gate voltage), while these imperfect recoveries being accompanied by a 0.75 V shift of the threshold voltage towards more negative values (i.e. the final recovery curve at 96 hours after test versus the original curve before bias stress). The results displayed in **Figure 10** prove therefore the limitation of Indanthrene Blue when high robustness to electrical stress applications is sought.

Concluding from the knowledge gained through the completion of this type of electrical test, we found difficult to place our investigated molecules in the context of the performance of the classic van der Waals bonded semiconductors, since a need of standardization of these test is imperiously necessary. With this respect, the literature offers very broad view of bias stress conditions, with the time of the test ranging from minutes, to hours, days and even weeks [83, 84, 85,86].

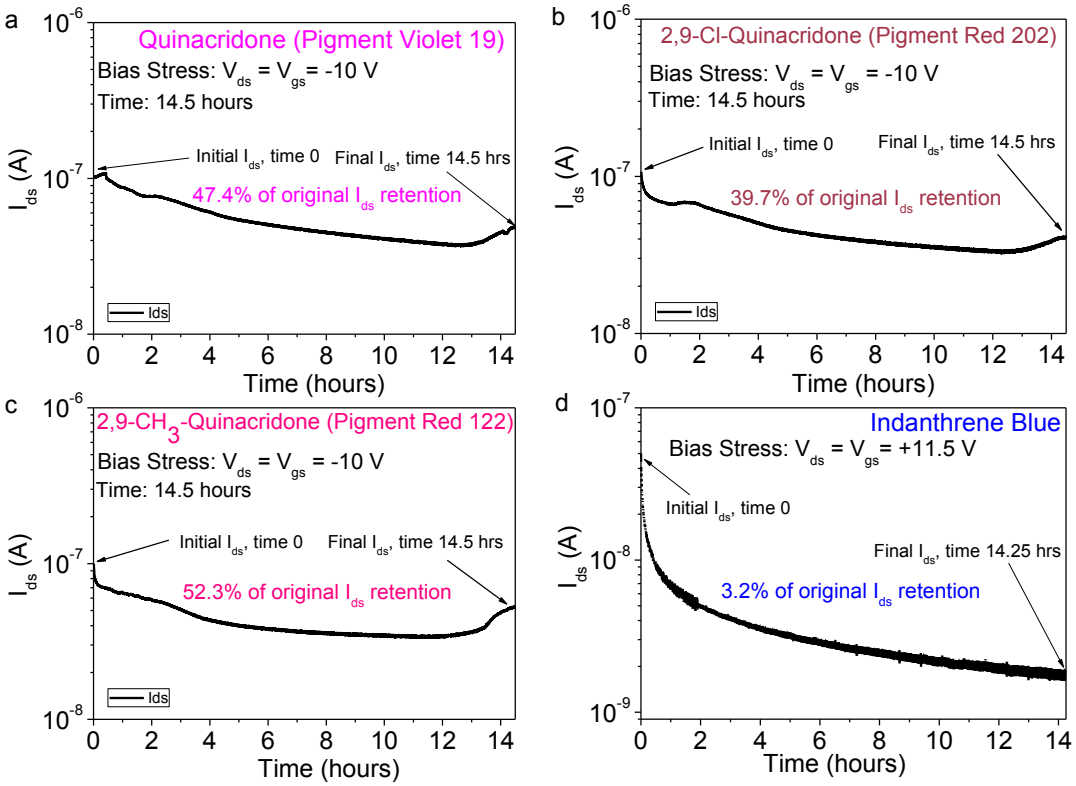

Figure 9: *Electrical stability consisted on application of a constant drain and gate voltage of -10 V for 14.5 hours for:* ***a)*** *Quinacridone;* ***b)*** *dichloro-Quinacridone;* ***c)*** *dimethyl-Quinacridone; and* ***d)*** *Electrical stability consisted on application of a constant drain and gate voltage of +11.5 V for 14.25 hours for Indanthrene Blue (batch TCI Europe). All the samples were fabricated on Al gate, AlOx-pentacontane dielectric, and Au source and drain electrodes.*

Another set of experimental data meant to assess the stability of the 3 Quinacridone pigments and Indanthrene Blue dye, involved thermal stress. In this experiment, OFETs fabricated in identical configuration and layer thickness, each bearing one individual semiconductor out of the four enumerated were measured in glove box immediately after their fabrication in order to record the base line; then were thermally heated on top of a hot plate (also inside glove box) for 30 minutes; cooled down to the room temperature by slow ramping down the temperature on the top of a hot plate; and finally re-measured at room temperature. The annealing temperatures were progressively increased with an increment of 25°C, and the respective transfer curves obtained after subsequent cooling down of each individual device are presented in **Figure 11.** The highest temperature displayed on the graph implies that the respective OFET sample showed no transistor transfer characteristics after the completion of the successive heating with an increment of 25°C for 30 minutes: i.e. 300°C for quinacridone, 250°C for Pigment Red 122, 225°C for Pigment Red 202 and 250°C for Indanthrene Blue respectively. Each graph in **Figure 11** show one transistor only, that was subjected to all the temperatures displayed in the legend for 30 minutes time at each temperature. Interestingly, each semiconductor of the four investigated resisted

to a series of successive heating and cooling cycles up to temperatures of at least 200°C, with Quinacridone OFET being the champion material that showed a distinct transfer characteristic even after the heating cycle of 30 minutes at 275 °C, after which the respective device irreversibly degraded when heat treated at 300°C for 30 minutes. We repeated the experiment for another Quinacridone OFET belonging to the same batch and observed that even 287.5 C was enough to irreversibly damage the sample. Interestingly though, the heat treated OFET samples changed progressively the color during testing, and finally the four semiconductors became more pale colored compared to the initially bright colored sampled (*e.g.* reddish-pink for Quinacridones and intense blue for Indanthrene Blue).

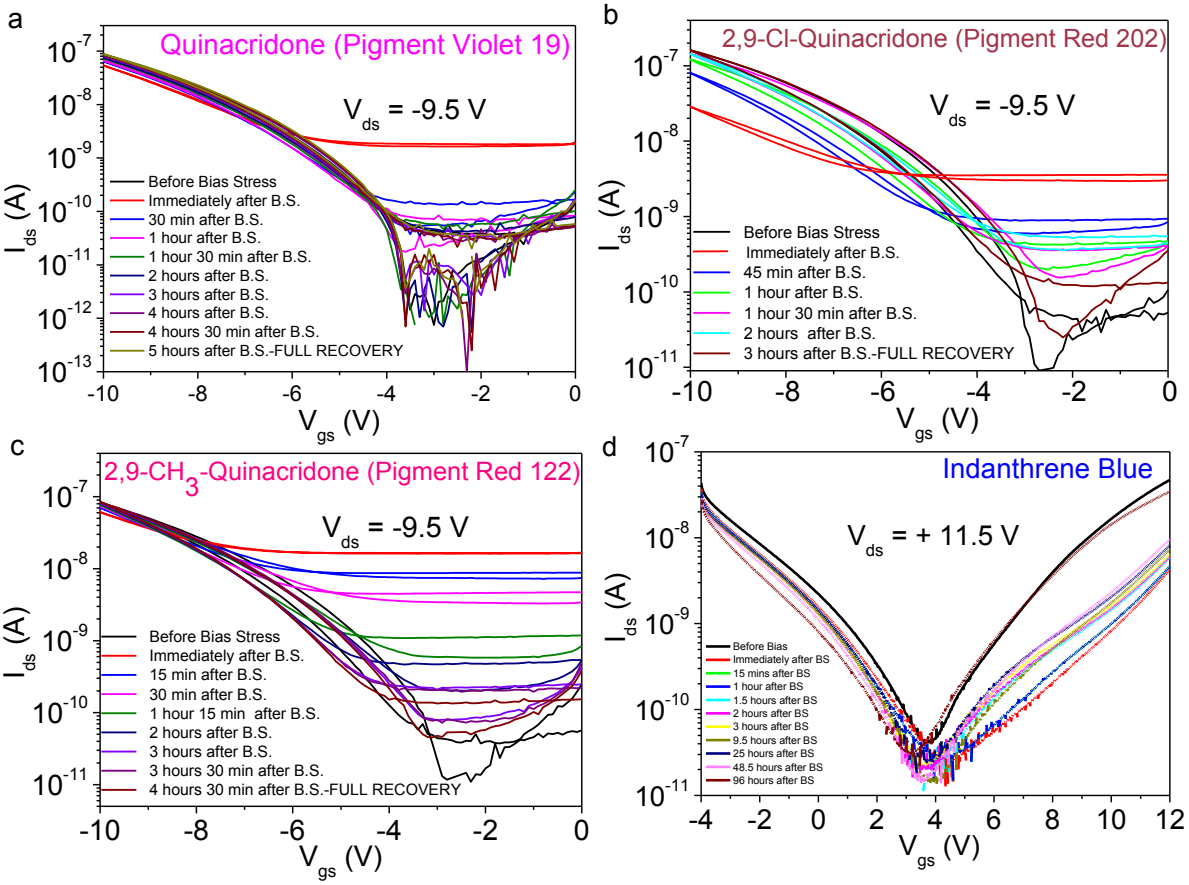

Figure 10: *The behavior of the transfer characteristics before and after bias of 14.5 hours:* ***a)*** *Quinacridone OFET;* ***b)*** *dichloro-Quinacridone OFET;* ***c)*** *dimethyl-Quinacridone OFET;* ***d)*** *The behavior of the transfer characteristics before and after bias of 14.25 hours of Indanthrene Blue OFET, batch of TCI Europe. All samples were fabricated on Al gate, AlOx-pentacontane dielectric, and Au source and drain electrodes. In panel d) only unidirectional curves are shown, in order to avoid cluttering the graph.*

We studied the event and realized that the effect is caused by the migration of the crosslinked polyethylene to the surface of the semiconductor [87], which appears to be the killing argument for the loss of semiconducting behavior of each transistor. Different than the three Quinacridones OFETs, when subjected to identical thermal test, the Indanthrene Blue OFET did not show a marked improvement of mobility with temperature of annealing. But contrary, the sample progressively degraded, as it is visible from the graph shown in **Figure 11d**), both in terms of mobility and threshold voltage stability. The ultimate temperature where both channels of the Indanthrene OFET showed semiconducting properties was 200°C, while for the subsequent temperatures the electron channel ceased to function; the hole channel was last reliably measured at 225°C, and finally became inactive after the 30 minutes annealing at 250°C (line not shown to avoid cluttering). Nevertheless, the final working curves for the OFET rendered mobilities in the range of 10^{-5} cm²/Vs, a fact that places Indanthrene Blue behind the three analyzed Quinacridones on the pecking order of temperature stability. A follow-up experimental data with the three Quinacridones and Indanthrene Blue deposited on more robust dielectrics with respect to temperature stability than the cross-linked polyethylene may offer an improved picture of the thermal stability of such molecules. Nevertheless, the values recorded here are absolutely remarkable, faring well with the performance of materials investigated elsewhere in similar tests for two van der Waals semiconductors (C10-DNTT and DPh-

DNTT) [88, 89]. Interestingly also, in our work the degradation of the devices seem to be due to the poor performance of the dielectric interface (for Quinacridones at least), while in fact the high temperature annealing is producing a beneficial effect with respect to mobility value increase for Quinacridone pigments (see the highest value of square root of drain current for the Quinacridone sample heat-treated at 225°C in **Figure S13** or the similar data of Pigment Red 122 heat treated at 150°C **Figure S13 c)**. These observations are in line with our preliminary data displayed in **Figure S10** with respect to thermal stability and annealing of Quinacridone. Importantly, the drift in threshold voltage recorded at least for Quinacridone and Pigment Red 122 during the thermal annealing test displayed in **Figure S13** (*i.e.* in the range of 1.3 V to 1.5 V, or in other words within 13% to 15% of the OFET operating voltage) compares well with the respective drift of the DNTT derivatives analyzed in Ref. [89].

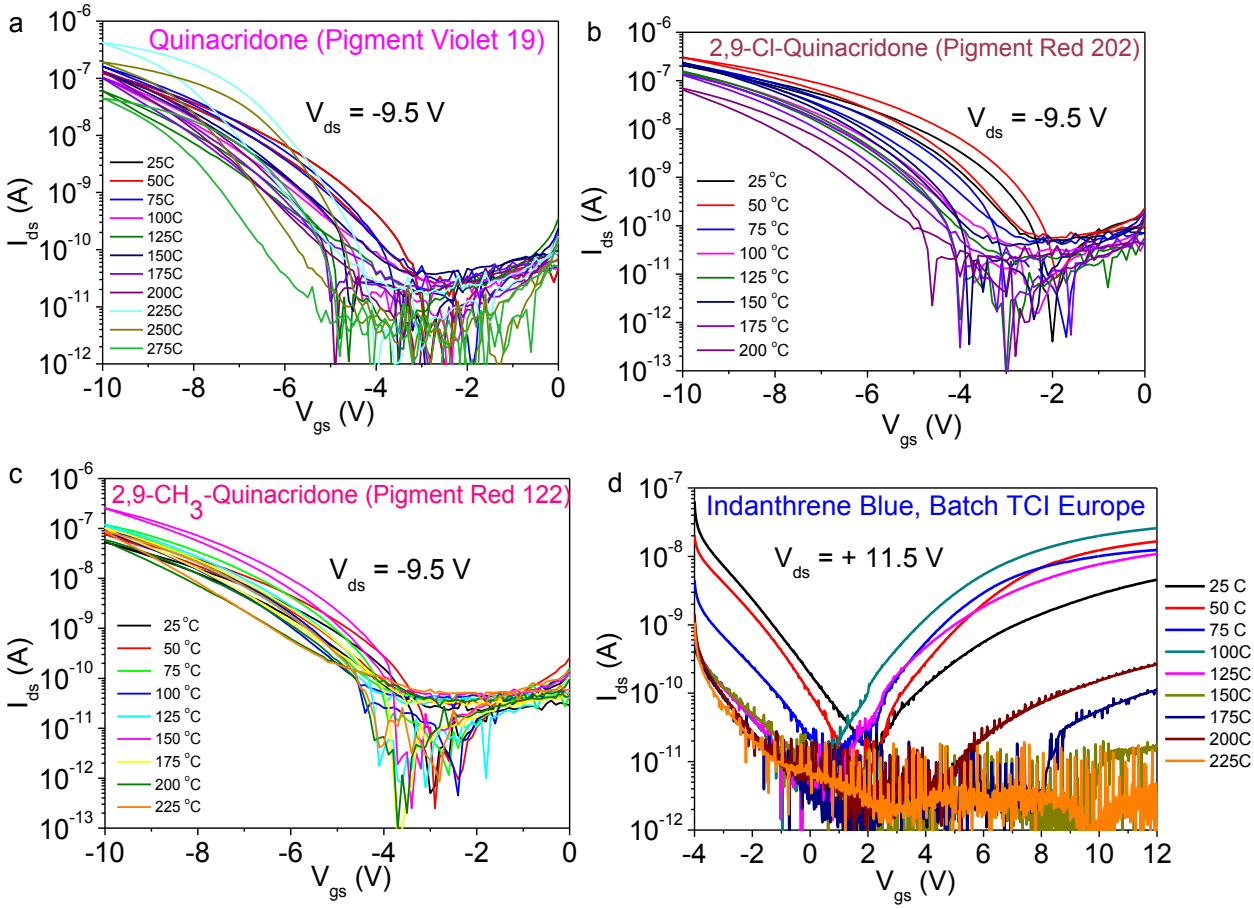

Figure 11: *Thermal stability of OFETs with:* ***a)*** *Quinacridone;* ***b)*** *dichloro-Quinacridone;* ***c)*** *dimethyl-Quinacridone; and* ***d)*** *Indanthrene Blue. All the samples were fabricated on Al gate, AlOx-crosslinked polyethylene dielectric, and Au source and drain contact electrodes. The thermal-stress experiment consisted on subjecting the fully fabricated OFETs to a series of temperatures (indicated on the transfer characteristics on the panels in the left columns) with an increment of 25 °C for a period of 30 minutes, followed by cooling down to room temperature and measurement of the transfer characteristics at room temperature. Each of the panels show one OFET sample only: i.e. the respective samples in each panel withstood all the previous temperatures displayed in the legends for a period of 30 minutes. Indanthrene Blue stemmed from a TCI Europe Batch synthesized in the year 2016; OFET produced in the year 2018.*

We close the experimental of this section dedicated to electrical stability of H-bonded molecules under various external factors, by placing in context the thermal stability of the investigated molecules, the three quinacridone pigments and the indanthrene blue dye. **Figure 12** shows that indeed, the materials having higher resistance to decomposition (Quinacridone and Pigment Red 122) also represent the best candidates for the development of OFET devices where resistance to temperature is a prerequisite, as described in **Figure S10 d)**.

The collection of research efforts highlighted in this Chapter of the Perspective Article with respect to electrical stability of materials under various influential factors demonstrates that high performance of the organic semiconductors in organic electronic devices is possible if one: (i) selects the optimum material for the desired application; (ii) optimizes the fabrication process to render ideal film deposition (thickness, orientation, etc.); (iii) and has available the right in-

strumentation, fabrication recipe and personnel skill. This chapter presented through various examples the key issues related to the handling of hydrogen bonded semiconductors and their development in functional devices. Many pieces of the puzzle are still unsettled to their intimate place, as it is the fundamental knowledge regarding the ultimate potential of these materials. Nevertheless, it seems fair to assume that when the fundamental principles of functionality of H-bonded semiconductor will be fully understood, then this class of molecules will allow the establishment of stronger molecular bonds and long range ordered structures, with performance surpassing the one provided by van der Waals semiconductors, and possibly approaching the one of their inorganic-based, covalently bonded counterparts. However, to reach this goal it is important that only (obsessively) high purity materials be employed in all the subsequent studies.

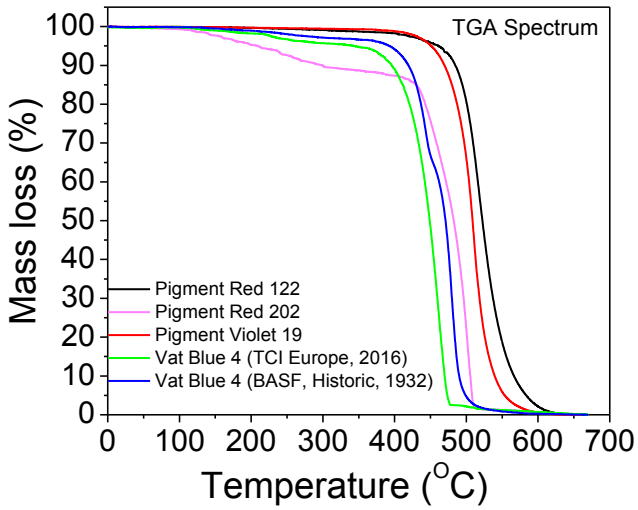

Figure 12: *Thermogravimetric analysis of the investigated powders for thermal stability in OFET devices. The only material not explored in OFET for such test was the historic dye, Indanthrene Blue. The graph shows a good correlation between the resistance to decomposition and the resistance to thermal annealing, described in the* ***Figures 11*** *and* ***S13****.*

A summary of the OFET devices performance subjected to aging, bias stress and thermal annealing is listed in **Table 2**.

Table2: *Summary of OFET data for devices subjected to aging, bias stress and thermal annealing.*

	Negative Quadrant	Positive Quadrant						
Indigo	110	105	-	-	-		-	
6,6'-Br-Indigo (Tyrian Purple)	275	250	-	-	-		-	
6,6'-Cl-Indigo	22	14	-	-	-		-	
Epindolidione	-	-	50% (140 days)	-	-		-	
Quinacridone	120	220	70% (160 days)	47.4%	100%-5 hours [a]		275°C	
Pigment Red 202	-	-	-	39.7%	100%-3 hours [a]		200°C	
Pigment Red 122	-	-	-	52.3%	100%-4.5 hours [a]		225°C	
Indanthrene Blue (TCI Europe, 2016)	-	-	-	3.2% [b]	Hole Channel	Electron Channel	Hole Channel	Electron-Channel
					75%-96 hours	65%-96 hours	225°C	200°C

[a](hole channel only); [b](14.25 hours Bias Stress);

Chapter 3. OFETs Stability in aqueous environment: effect of pH change and surface functionalization

When electronics meets biology, the crucial parameter is not the device operational stability in air, but in aqueous environment. Motivated by possible applications of air stable Epindolidione OFETs in bioelectronics, these devices needed to be evaluated in aqueous environment**.** For this purpose, in the bottom gate/top contact devices with the SD gold top contacts directly evaporated on EPI surface (Figure 2), the entire transistor active area was confined by using a poly(dimethylsiloxane) rubber block. No passivation of gold top contacts was necessary. The rubber block acted as a well for a water solution (40 μL volumes were used) that could be put directly in contact with the EPI surface and the EPI/Au interface. The use of a high capacitance gate dielectric, AlO_x with a thickness of ≈8 nm modified by a monolayer of n-octadecyl phosphonic acid, allowed to keep operating voltages in the range of 1-2 V. The OFET performances were evaluated in water solutions at various pH in the range 3-10 by measuring the transfer characteristics over 60 cycles, using the same devices sequentially in each series of different aqueous media. [58] For these devices the IV characteristics are shown in the **Figure 13**. After a total of 360 cycles in the six aqueous environments, an almost unperturbed transistor performance was found compared to the one recorded at the beginning of the experiment. It was also observed that, due to ionic currents between source and drain electrodes or dielectric screening effects arisen in the wet environments, 10 times higher OFF currents were recorded with respect to the dry state, while the ON currents and the threshold voltages remained constant during the 60 cycles in each environment.

The peculiar solid-state aggregation pattern driven by cooperative H-bonds and π-π stacking of HBPs is one of the factors accounting for the above demonstrated outstanding stability in water solution. In particular, evaporated crystalline thin films of Quinacridone and Epindolidione were investigated from the morphological and structural point of view to elucidate their organization. AFM topographies are a very immediate tool to demonstrate their aggregation into crystallites: the Figure 14 reports the 2.5x2.5 μm^2 surface morphologies acquired in tapping mode on the two evaporated semiconductors. The clear presence of grains in both morphologies is a direct proof of the crystalline organization of the two materials. Grain dimension was larger (300-400 nm) in Epindolidione films than in Quinacridone (200-300 nm) ones. Moreover, Quinacridone aggregates were rod-shaped and thinner (10-20 nm) than Epindolidione crystallites (60-80 nm). Interestingly, the spontaneous tendency of EPI and QNC to form self-assembled nano- and micro-structures was confirmed in wet preparation experiments also with further microscopical and XRD investigation. [90,91]

All these results demonstrated that the Epindolidione transistors could be considered as highly stable and effective devices for application in water environment, a fundamental requisite for any implication in bioelectronics. With this respect, the integration of biological entities into or on the surface of Epindolidione or Quinacridone active layers would open opportunities in sensing application, among others. This groundbreaking possibility currently attracts much interest from the scientific community [92, 93, 94,95, 96, 97, 98,99] due to the predictable technological impact. Hydrogen bonded pigments (HBPs) are indeed among the very few organic materials meeting the requirements of stability, efficiency and fast response[107,108] that are necessary to enable fundamental studies on biointerfaces.

The above described bottom-gate/top-contact geometry with a rubber block for solutions confinement was very useful to enable a series of experiments in which the poly-crystalline EPI surface was in direct contact with solutions containing specific chemicals: this step was propaedeutic to further functionalization of the device with biomolecules (proteins), that are typically handled in buffer solutions. The devices were operated in the linear regime with low V_{SD} values (0.1–0.5 V) and V_G < 3–3.5 V. This allowed to avoid any electrochemical reactions and parasitic currents. [109] Epindolidione field effect transistors operational stability was preventively evaluated in phosphate buffer saline (PBS) solution, after washing with water and drying, during incubation with the protein Streptavidin (SA) in PBS solution and after further washing and drying: the IV characteristics for the device subjected to these successive treatments are reported in the Figure 15d. Importantly, while the interaction with both solutions does modify their electrical properties, the devices continue to operate with similar mobility. In particular, the protein SA exhibits unspecific interaction with the active layer surface.

In order to further develop the idea of HBPs involvement in biointerfaces, we also performed a real bioconjugation reaction on the EPI surface with functional proteins. In particular, the organic pigments Quinacridone and Epindolidione in the solid state offer the possibility of a straightforward surface functionalization protocol with proteins based on the reactivity of their secondary amine (*i.e.* N-H) groups. We devised a two-step bioconjugation protocol and demonstrated the functionalization of evaporated crystalline thin films of Epindolidione with a layer of two proteins: the reaction center (RC) from *Rhodobacter Sphaeroides*, the key bacterial photoenzyme fueling the photosynthetic processes, and streptavidin, a protein that forms an archetypical noncovalent lock-and-key binding pair with the biomolecule biotin used in numerous biochemical procedures [110]. In particular, for the bioconjugation of the bacterial Reaction Center protein, we adapted methods previously developed for the bioconjugation with organic fluorophores [111, 112, 113]. The bioconjugation proceeds via the formation of an amide bond between the surface -N-H groups and an activated carboxyl derivative (a N-hydroxysuccinimidyl ester). For this purpose, aliphatic bifunctional linkers are required, providing two end-functionalities, the first for binding the pigment surface and the second for immobilizing the protein. We achieved this goal by using two chemical linkers, differing for the end group: the disuccinimidyl suberate (SUB) and the N-succinimidyl-D-biotinate linker (B7). The **Figure 15 f** depicts the mechanism of immobilization in the case of B7 on EPI.

In both cases the first step consists in the treatment of the semiconductor thin film surface with a water solution of the linker. After incubation with the linker and washing out the excess with distilled water, the surface is incubated with a solution of the protein. The washing of the surface will not remove the covalently linked protein. AFM investigation showed the preserved surface morphology and aggregation pattern of both QNC and EPI, with limited variation due to surface particles swelling as observed for other hydrogen bonded organic nanoparticles. [114]

The response of EPI field effect transistor to SUB or B7 covalent functionalization is shown in the Figure 15b-c, respectively. After functionalization with B7, even if the off current increases to ~100 pA, an outstanding stability of the performance was observed over hundreds of measurement cycles, and mobility measured in air was unaffected. Mobility decreased in the case of SUB from 0.1 $cm^2 V^{-1} s^{-1}$ to 0.06 $cm^2 V^{-1} s^{-1}$ after reaction; however, devices were stable in this state over measurement for at least 5 days. Devices reactivity to protein binding was in the case of the Reaction Center unsatisfactory: the immediate degradation of the FET, with no measurable modulation occurred after the start of incubation. This was attributed to the necessity of stabilizing this transmembrane protein in solution with the presence of the highly polar LDAO surfactant: test experiments performed exposing devices to a solution of LDAO in water had an identical degradation effect. Devices interaction with the protein SA gave more promising results: exposure of B7 modified OFETs to SA solutions originated a marked drop in the threshold voltage, by about 1 V, and an increase in current. The response of the devices was enhanced relative to the one given by the unfunctionalized FETs incubated with streptavidin discussed above. This characteristic was retained after washing the devices with PBS solution and drying.

Every experiment carried out on these devices, involving the treatment of the surface with a biomolecule, water or a buffer solution, leaded to operational devices with a shift of their parameters, depending on the kind of surface modification. Importantly, it was clear that the OFETs based on Epindolidione retain their operational stability upon surface functionalization and can be an ideal platform for biointerfaces.

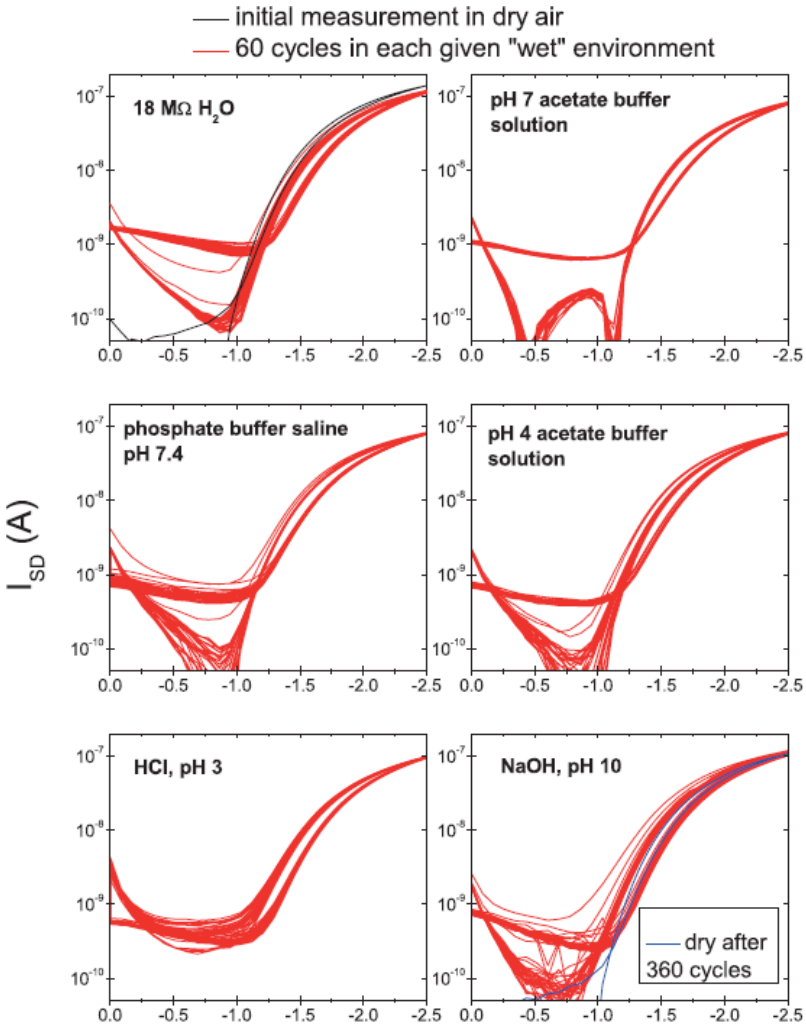

Figure 13: *Low-voltage operating transistors with Epindolidione semiconductors on Al gate, AlOx-Tetratetracontane dielectric, and Au source and drain electrodes, measured in air (black curve) and then measured in 360 successive cycles (red lines) in aqueous environments of different acidities, with 60 cycles carried out at each pH. A drain voltage of – 0.5 V was employed for raising each transfer characteristics. Samples were rinsed (equilibrated) in deionized water when moving from one electrolyte to the other. No encapsulation was employed for the OFETs during the measurements. Reproduced with permission from Ref. [58]*

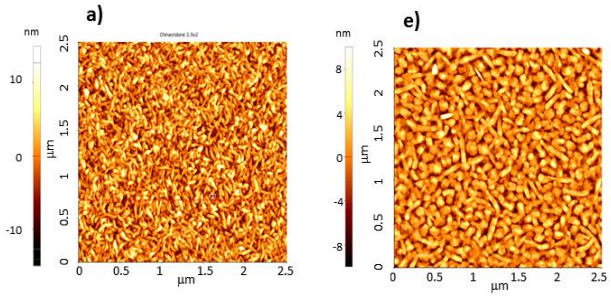

Figure 14: *2.5 x 2.5 µm² non-contact mode atomic force microscopy topographies of: evaporated Quinacridone (a); evaporated Epindolidione (b). Reproduced with permission from Ref. [117].*

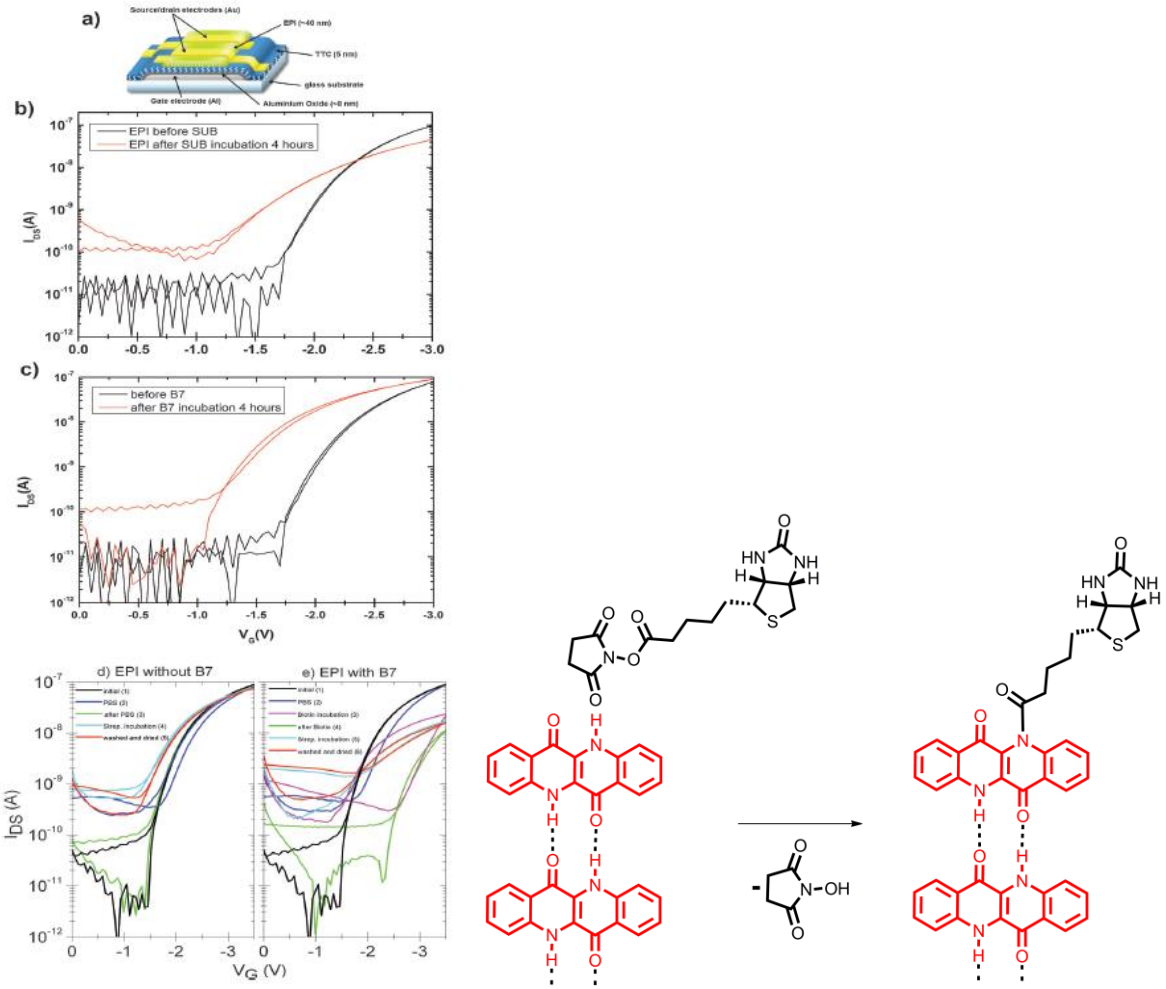

Figure 14: ***a)*** *bottom gate/top contact EPI OFET device geometry. A layer of TTC deposited on top of AlO_x generates the low capacitance dielectric;* ***b)*** *Epindolidione OFETs measured before and after SUB functionalization;* ***c)*** *Epindolidione OFETs measured before and after B7 functionalization;* ***d)*** *IV characteristics of pristine EPI devices in dry air (1), in PBS solution (2), after washing with water and drying (3), during incubation with SA in PBS solution (4), and after further washing and drying (5);* ***e)*** *same investigation as* ***d)*** *performed on devices after incubation with B7. A VSD of 500 mV was used in all measurements. Reproduced with permission from Ref.[117].*

Chapter 4. Photo(Electro) Catalysis with H-bonded pigments

Semiconductor-mediated photocatalysis and photoelectrocatalysis is a major subject of research and development in the field of sustainable energy. Reactions such as water splitting to produce H_2, reduction of CO_2 into hydrocar-

bon fuels, or generation of hydrogen peroxide represent energy conversion strategies where semiconductors play the key role. The overwhelming majority of this work relies on inorganic semiconductors. Organic semiconductors are considered unstable and fragile, especially in environments where water, oxygen, and light can conspire to induce degradation. In the field of organic solar cells or organic light-emitting diodes, for instance, considerable attention is devoted to protecting components from water or oxygen induced degradation. For these reasons, organic semiconductors are seldom relied upon for photo(electro)catalysis. H-bonded pigments, however, by virtue of their stability and favorable light-absorbing properties, have proven suitable for catalytic reactions in aqueous environments.

Epindolidione and quinacridone deposited on thin film gold electrodes were studied as photoelectrodes in oxygenated aqueous electrolytes in a pH range of 1-12 by Jakešová *et al.* (**Figure 18b**)) [129]. For both materials, a pronounced photocathodic effect was found wherein dissolved oxygen was selectively reduced to hydrogen peroxide, H_2O_2. In the case of photoelectrocatalysis in a photocathode, photogenerated electrons reduce oxygen, while the holes are transported to the underlying electrode. This process was found to proceed with high faradaic efficiency between 80-95% with respect to hydrogen peroxide. The two pH regimes for reduction of oxygen to peroxide were supported by the H-bonded pigments: The low-pH process with $2H^+$ and the high-pH process utilizing H_2O as a proton source and producing hydroxyl ions as a byproduct (**Figure 18c**). Throughout these photocathodic experiments, the H-bonded pigments demonstrates outstanding stability. Three-electrode photoelectrocatalytic experiments were run for four days under continuous simulated solar irradiation, without degradation of the semiconductor layers or catalytic activity. In two-electrode systems, epindolidione showed the best performance with continuous photogeneration of hydrogen peroxide over 48h (**Figure 18d**). The highly-selective and efficient photocathodic reaction afforded by these H-bonded pigments was in fact the first example of a semiconductor catalyst intrinsically capable of photoelectrochemical reduction of oxygen to hydrogen peroxide. In the seminal example of catalytic photocathodes, absorption and photogeneration limited the overall catalytic current. This was overcome by depositing the H-bonded pigment onto an organic donor/acceptor heterojunction capable of generating much more photocharge due to wide absorption. Such composite photocathodes demonstrated up to an order of magnitude higher cathodic currents for hydrogen peroxide generation and represent the state-of-the-art in terms of photochemical hydrogen peroxide generation [130]. These devices once again showcase the outstanding catalytic stability offered by H-bonded pigments within an exceptionally wide range of pH values. It should be stated that many inorganic materials show favorable photocatalytic properties, however are stable within a narrow pH window.

What is remarkable about the H-bonded pigments is both stability in many conditions and a very good selectivity for oxygen reduction to hydrogen peroxide (**Figure 19a)**). The latter is the result of the arrangement of carbonyl groups which favor two-electron redox chemistry, as each carbonyl group on epindolidione or quinacridone accommodate one electron upon reduction, the whole molecule can carry a net charge of -2. The two-electron selectivity afforded by the carbonyl group arrangement in H-bonded pigments present in peroxide synthesis is also seen in the reaction of electrochemical carbon dioxide capture from solution (**Figure 19b)**). This is in in the strict sense a catalytic reaction, since the reactant and product are both CO_2. However, the electrochemistry with respect to the H-bonded pigment is reversible: Upon electrochemical reduction in CO_2-containing electrolyte, reduced quinacridone reacts with CO_2 to form a dicarbonate salt [131]. The salt is stable and thus serves as a method of electrochemical capture of CO_2. The CO_2 can be released back by heating the film, or alternatively, electrochemically oxidizing the film. This results in the liberation of CO2 and restoration of the original H-bonded quinacridone. Since the reduction potential of quinacridone is too cathodic to allow this process to occur in water, only operation in acetonitrile electrodes is possible. The electrochemical capture/release concept was later extended to naphthalene bisimide carbonyl-containing compounds which could be reversibly reduced in aqueous electrolytes as well [132]. The CO_2 capture-release cycle in all cases serves to demonstrate the favorability of 2-electron/2-proton redox chemistry that characterizes many H-bonded pigments.

All the aforementioned cases of catalytic behavior in H-bonded pigments feature the material deposited on top of an electrode. The case of photocatalysis, where both photogenerated electrons and holes in a single material carry out respective redox reactions, is also observable in the case of the H-bonded pigment epindolidione (**Figure 19c**) [133].Thin films of Epindolidione can be irradiated in various oxygenated aqueous conditions in the presence of sacrificial electron donors (easily-oxidizable molecules) such as oxalate, formate, or phenol. In these cases, oxygen is photoreduced to hydrogen peroxide, which accumulates in solution. Simultaneously, photogenerated holes oxidize the various electron-rich molecules in solution. The latter mechanism can be proven by measuring photoanodic current. The problem in the case of pure photocatalysis, in contract to photoelectrocatalysis, is that photogenerated holes can lead to self-oxidation of epindolidione, which is irreversible. Therefore, in the case of photocatalysis, oxidation of substrates in solution competes with autooxidation of the material itself. In this respect, epindolidione must be improved in terms of stability with respect to oxidation. This problem does not exist in the case of photoelectocatalysis, since photogenerated holes are rapidly driven out to the underlying electrode.

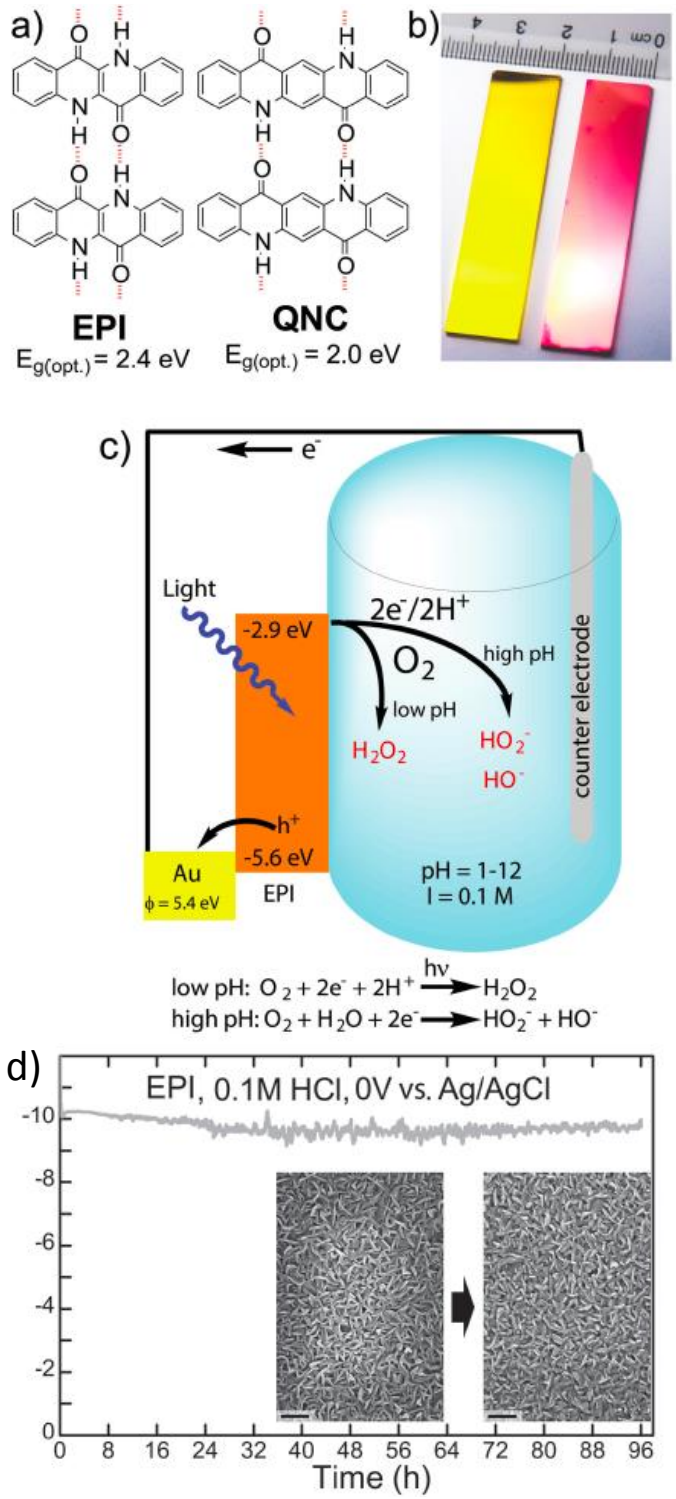

Figure 19: ***a)*** *The films of epindolidione and quinacridone have visible-region band gaps suitable for harvesting solar energy to fabricate photocathodes;* ***b)*** *Photocathodes are made by vacuum evaporation of the pigments onto thin films of evaporated Cr/Au;* ***c)*** *Photocathodes in aqueous electrolytes show overwhelming preference for reduction of oxygen to hydrogen peroxide. Photogenerated holes are extracted into the circuit;* ***d)*** *Epindolidione photocathodes show excellent robustness in terms of photocurrent, faradaic efficiency, and morphological stability over several days of continuous operation. Reproduced with permission from Ref [129].*

The picture that emerges in the case of H-bonded pigments is that they are promising materials for catalysis applications in aqueous conditions, and that hydrogen peroxide is the dominant product in all cases. The two-electron fa-

vorability of the H-bonded pigments suggests also the possibility of proton reduction to H_2. However, hydrogen evolution has been found only in trace amounts. Nevertheless, the rapidly growing interest in using hydrogen peroxide as a liquid chemical energy carrier suggests that H-bonded pigments may be ideally poised to making meaningful contributions to this field. Conceptually, H-bonded pigments as hydrophilic molecules with a rich chemistry are one of the only examples of organic semiconductors with intrinsic catalytic behavior. Therefore, it is an inviting topic for synthetic chemists to address to produce more efficient and stable organic catalysts.

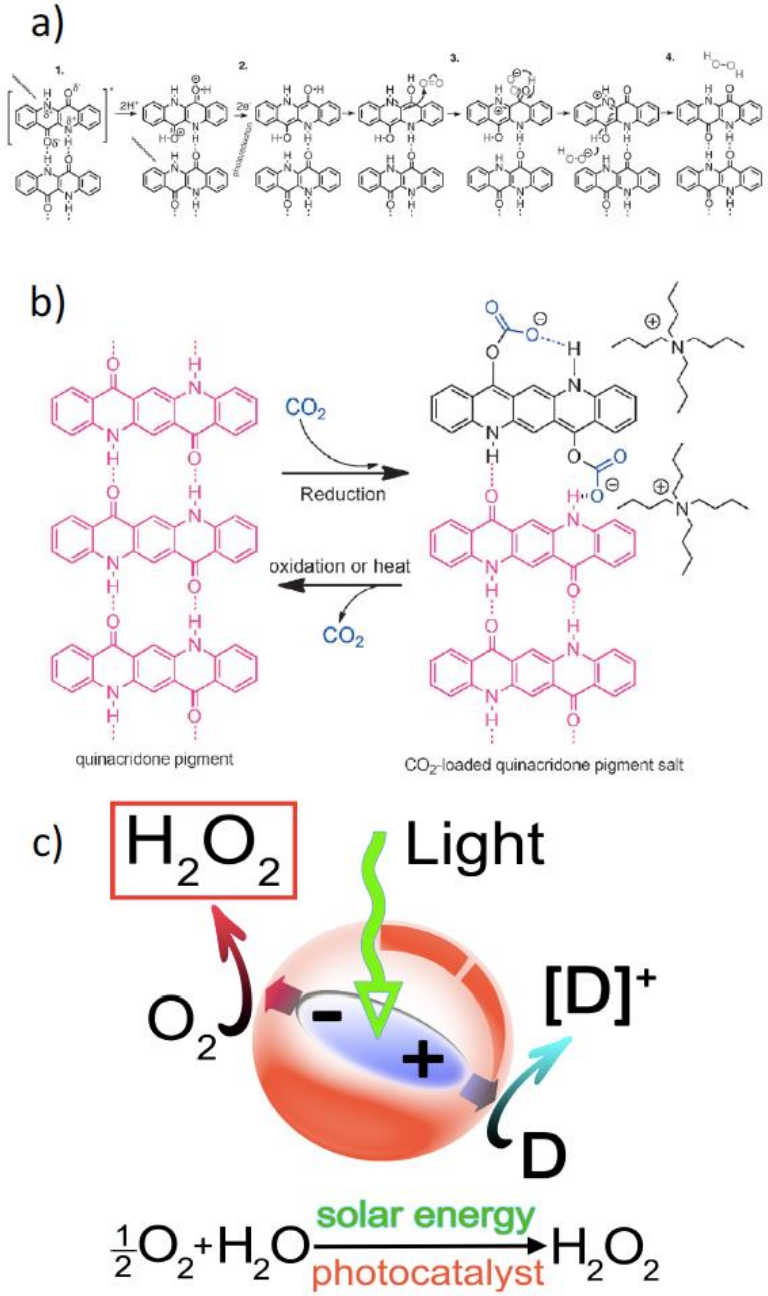

Figure 20: ***a)*** *The proposed mechanism for selective 2-electron reduction of oxygen to hydrogen peroxide with epindolidione;* ***b)*** *Electrochemical capture and release of carbon dioxide using quinacridone. Though not strictly a catalytic reaction, this process makes use of the reversible redox chemistry of the carbonyl functional groups;* ***c)*** *The case of pure photocatatlysis for the photochemical evolution of hydrogen peroxide. Various electron donors in solution can be consumed in this reaction. A major focus of research is to increase the stability of the H-bonded pigment with respect to autooxidation under these conditions. Reproduced with permission from Ref [133].*

Chapter 5. H-bonded Semiconductors and their Suitability for Biodegradation

Because of the high stability of H-bonded organic pigments to various external factors exemplified in this article, it does not come to a surprise that they are also highly resistant to microbial or enzyme attack. In addition, their extremely low solubility in water dramatically reduces their bioavailability, making it difficult for these molecules to become part of cellular metabolism. However, due to the wide functional and metabolic diversity of microorganisms in nature, numerous species of bacteria, fungi and even plants are capable of causing, to a different extent, the degradation of this type of compounds. Indigo and indigoids such as indigo carmine (indigo-5,5′-disulfonic acid), tyrian purple (6,6'-dibromoindigo) or anthraquinone-based dyes such as Remazol Brilliant Blue R, are among the few H-bonded pigments whose biodegradation have been more extensively studied due to their wide application in the textile industry. However, the biodegradation of other organic semiconductors such as epindolidiones and quinacridones have not been described so far. This heading of this Perspective Article will highlight some important achievements of the biodegradation scientific community, and will place the respective results in the viewpoint of necessary milestone to reach in order to place the Hydrogen bonded semiconductor class of molecules in the rank of materials with sustainable development.

5.1 Degrading enzymes and microorganisms

5.1.1 Biodegradation of indigo and indigoids

Despite their perception as "materials of natural origin", or "bio-based" materials, Indigo and indigo carmine dyes are reported to be toxic to microbes, plants and animals, so the discharge into wastewaters will cause damage to the environment [134]. Recently, the capacity of indigo to act as an organic semiconductor has been described, with important biotechnological perspectives [31, 135, 136, 137] therefore a demand for an efficient and eco-friendly methods to eliminate this pollutant [138] is of immediate interest. The bioremediation has been regarded as a feasible and cost-effective method for the removal of indole polluted systems. Among the microorganisms capable of degrading this compound are fungi and bacteria, although the ability of plants or plant residues (phytoremediation) to eliminate these semiconductors from disturbed ecosystems has also been reported.

Basidiomycetes and especially white-rot fungi (WRF) either in living or inactivated form, such as *Phanerochaetes, Pleurotus, Trametes, Coriolus, Ganoderma, Pycnoporus, Irpex*, *Pycnoporus*, *etc.*[139,140,141,142] have received much attention because of their ability to degrade xenobiotic compounds. Owing to extracellular non-specific free-radical-based ligninolytic enzymes of WRF, laccases, lignin-peroxidases and manganese-peroxidases can degrade indigo and its derivatives [140,143,144]. Degradation efficiency can be improved by the addition of a nitrogen source and vitamins (Levin et al., 2010). Synergistic action of laccase isoforms in *Trametes hirsuta* has also been described [145,146]. In addition, the use of redox mediators significantly increased biodegradation [147,142,148]. Even biotransformation of indigo carmine can be carried out by using lyophilized mycelia where extracellular enzymes were absent [149]. Fungal co-culture system comprised of *Coprinopsis cinerea* (Basidiomycetes) and *Gongronella* (Mucoromycetes) produced 900 times higher laccase activity than that in pure culture and identifying inducible laccases in co-culture [150].

Ascomycetes also can be used to degradation of this semiconductor. *Scytalidium thermophilum* laccase can drive indigo transformation. However, the toxicity of the media is persistent [151]. *Myrothecium verrucaria* a non-ligninolytic fungus degrades indigo with the intervention of bilirubin oxidase [152]. *Curvularia lunata* is able to degrade indigo with production of less toxic intermediates than *Phaneroachaetes chrysosporium* [153]. Some yeasts, such as *Diutina rugosa*, a recently described genus, have been successfully used in the indigo carmine biotransformation at very low pH values. The enzyme analysis revealed significant inductions and major roles played by NADH-DCIP reductase and lignin-peroxidase in the asymmetric cleavage, initial reduction and deamination of indigo [154]. The use of fungi-bacteria co-cultures (*Aspergillus alliaceus, Bacillus cereus* and *Bacillus pumilus)* seems to be an efficient alternative for the degradation of indigo carmine towards the complete mineralization due to the synergistic action of the above species involved [155].

Apart from fungi, laccases have also been detected in a wide range of bacterial species including *Azospirillum lipoferum*, *Cupriavidus* sp., *Marinomonas mediterranea*, *Escherichia coli*, *Bacillus* sp., *Pseudomonas* sp. and several *Streptomycetes* (156, 157, 158]. *Achromobacter xylosoxidans* isolated from denim-manufacturing mill sludge where able to use isatin and anthranilic acid (both intermediate metabolites of indigo carmine degradation) as carbon source [159]. Unlike fungal laccases, bacterial laccases are resistant to inactivation caused by high temperatures and alkaline conditions, tolerate the presence of NaCl and organic solvents [156, 160] and are effective in absence of redox mediator [161].

5.1.2 Biodegradation of anthraquinone dyes

Although anthraquinone-biodegrading systems have not been described, some anthraquinone derived dyes with potential semiconductor capacity have been biotransformed such as, for example, Remazol Brilliant Blue R. Laccases show ability to decolorize this pollutant. They can be broken down into smaller molecules with potential lower toxicity levels [142]. For example, laccases from *Scytalidium thermophilum, Polyporum* sp., *Armillaria* sp., can totally and rapidly decolor under optimized conditions [151, 162, 163]. Manganese peroxidases from several fungi can also biotransform this

compound [141]. Some plants as *Rumex hydrolapatum*, *Rumex acetosa*, *Rheum rhabarbarum* and *Apium graveolens* were screened for removal of sulfonated anthraquinones in hydroponic solutions [164,165, 166]. In *Rheum rhabarbarum*, cytochromes P450 and peroxidases are important roles in the detoxification of sulphonated anthraquinones [165]. Although these studies are a first step in the elimination of anthraquinone derivatives, so far complete mineralization has not been achieved.

5.2 Phytoremediation

Phytoremediation involves the use of plants in the recovery of disturbed systems. It is an ecofriendly, passive, solar energy driven and cost-effective strategy for the decolonization and detoxification of recalcitrant synthetic dyes [166]. Some plants can extract, sequester, detoxify and/or volatilize xenobiotic organic and even inorganic pollutants [167; 168] using their own enzymatic machineries or in association with their microbiome, fundamentally rhizosphere and endosphere . Oxidoreductases from plants such as lignin peroxidase, laccase, tyrosinase, azoreductase, etc., can break the complex structures of dyes [166]. Hellophytes (*Phragmites australis, Alternanthera philoxeroides, Typha domingensis, Junus* sp.), ornamental plants (*Ipomoea hederifolia, Aster amellus, Portulaca grandiflora, Zinnia angustifolia, Petunia grandiflora, Glandularia pulchella*) and many ferns and herbs, have been extensively used for dye removal [166, 169,170]. Recently, aquatic plants such as *Pistia stratiotes* or *Lemna minor* have been used successfully in the elimination of carcinogenic azo red dye, although plants cannot be reused and at high concentrations suffer irreversible damage [171, 172]. Some of these plants have been used in phytoreactors and constructed wetlands, obtaining interesting results in biotransformation, although not always the derived products were non/less toxic than untreated compounds [166,173]. Plant tissue cultures can be an alternative for the degradation of these compounds. They offer advantages like they lack chlorophyll and other plant pigments, reproducibility, homogeneity of the plant material, reduced problems of uptake and transport, easy manipulation and more quick results.

Currently, the concept of plant-metaorganism is widely accepted and the term phytoremediation includes the microbiota associated with the plant. Thus, *Alternanthera philoxeroides* can remove Reactive Green dye (i.e. Fast Green FCF) with its own laccases system. Interestingly, the inoculation with plant growth promoting (PGB) *Klebsiella* (rhizophytic bacteria) significantly increased the degradation of the pollutant by a bacterial azoreductase [169, 174]. Ornamental plants at constructed wetland accumulated and degraded dyes without any severe toxicity on studied plants and synergism between plants and microbes was involved in effective dye removal [170]. It has been evaluated on-site performance of endophyte-assisted pilot-scale horizontal flow constructed wetlands to remove dye contaminated water. Treated wastewater was found to be non-toxic and the inoculated bacteria showed persistence in the wastewater as well as rhizo- and endosphere of *Leptochloa fusca* [175]. These endophytes are usually PGB, so they not only purify the water, but also favor the development of the plants in the system, thus improving their effectiveness [176].

As far as we are aware of, only one phytoremediation system capable of degrading indole has been described. *Phomopsis liquidambari*, an endophytic fungus isolated from *Bischofia polycarpam* oxidizes indigo with an additional contribution of organic matter. Indole metabolic pathway was similar with endophytic metabolisms of indole acetic acid in plant compounds [177]. These results indicate a possible application of the endophytic fungus and bacteria in bioremediation of indole and possibly other N-heterocyclic aromatic. Mora *et al.* [178] used lignocellulosic residue to promote the synthesis of MnO_2 nanoparticles. These fibers-nanoparticles were used to degrade the indigo carmine dye. This may be another eco-alternative to deal with the degradation of organic semiconductors.

5.3 Metabolic pathways and biotransformation reactions.

Despite the large environmental impact of pigments in waste waters and the increasing number of degrading microorganisms capable to transform stable H-bonded pigments into less toxic compounds, little is known about the metabolic pathways and biological mechanisms driven the process. The laccase enzymes have been shown to decolorize anthraquinone, indigo and derivatives [179;180;181;138] more efficiently than other classes of dyes [180]. The first step in indigo and indigo derivatives degradation by laccase is an electrochemical oxidation to dehydroindigo [182] which is easily attacked by nucleophiles molecules such as water. Four electrons are necessary to oxidize indigo dyes by laccases from *Trametes hirsuta* and *Sclerotium rolfsii* [183] to form isatin (indol-2,3-dion). There is a further degradation of isatin to isatic acid which is not an stable compound and is decarboxylated spontaneously to anthranilic acid (2-aminobenzoic acid). This compound is included in the List I of DEA (United States Drug Enforcement Administration) considered as a methaqualone with sedative and hypnotic properties. Previously, it was shown that indole was metabolized by a *Bacillus* sp. to further metabolites such as salicylic acid from anthranilic acid and a catechol as the end product (considered non-toxic) [184]. Other strains such as *Cupriavidus* sp. strain KK10 produce more than 20 intermediate products during indole degradation such as isatin, N-formylanthranilic acid, anthranilic acid, salicylic acid, gentisic acid, 1,2,4-trihydroxybenzene, 2-oxindole or indole-2,3-dihydrodiol [185].The degradation of anthraquinone dyes by laccase of *Polyporus sp*. S133 [186] or *Trametes pubescens* [187] can be broken down forming smaller molecules through hydroxylation, deamination, and oxidation reactions. According to the metabolites obtained during the laccase degradation of *T. pubescens*, those were less toxic than their corresponding parent compounds. Therefore, the efficiency of dye biodegradation depends on the type of

laccase-producing organism and the laccase kinetics. The enzymatic velocity is affected by adsorption, transport, pH, accessibility and redox potential of the enzyme and the substrate [183]. Recently, the genes involved on indole degradation *iff* and *ant* cluster from different bacteria such as, *Burkholderia* sp. IDO3, *Acinetobacter* sp. O153, *Acinetobacter* sp. JW have been identified [188; 138; 189]. The indole oxidation is mediated by IifC and IifD flavin-dependent two-component oxygenase system. Many oxygenases have proven to oxidize indole to indigo [134]. However, the lifB enzyme avoids the formation of indigo carmine. The final product, anthranilic acid, is formed by IifA, an enzyme which is both structurally and functionally comparable to cofactor-independent oxygenases (138). Moreover, the *iif* cluster was identified in the genomes of a wide range of bacteria, suggesting the potential of widespread lif-mediated indole degradation [190;138;189]. Ma et al. [134] using bioinformatics analyses, identified a new indigo carmine degrader enzyme forming a phylogenetically separated branch from other related aromatic oxygenases.

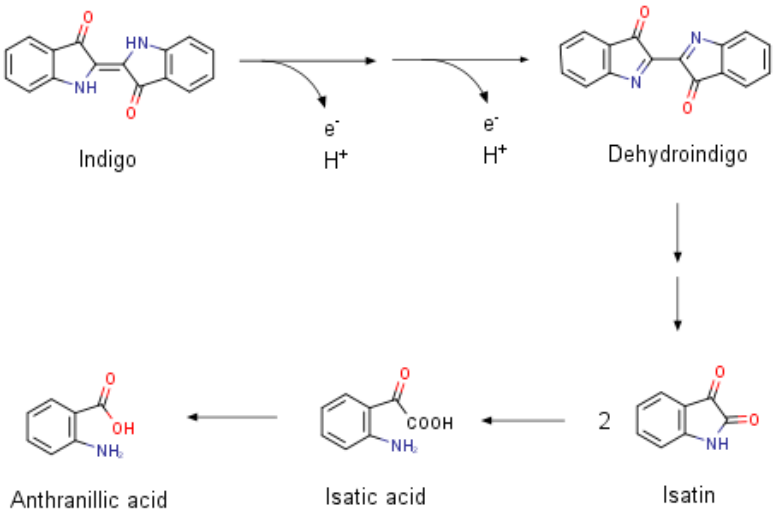

Scheme 9: *Proposed biodegradation pathway of indigo. Adapted from reference [183]. Reproduced with permission.*

5.4 Bioremediation

Aimed to develop biological processes for efficient H-bonded pigments degradation and detoxification, many microbial and enzymatic bioreactor systems have been devised. However, most of these studies assessed the effectiveness based on the decolorization of the aqueous medium. This means that only biotransformation of the pigment is usually measured, without information about the fate and intermediates or final products of the biodegradation process, which can be useful from the technical and applied point of view but gives no information about the degree of mineralization of the organic pollutant, i.e., conversion to CO_2. Among novel bioreactor developments, combined processes can be attractive and efficient alternatives to traditional activated sludge based biological treatments. For example, a CSTR bioreactor containing activated sludge was capable to reduce the color of indigo polluted waste waters by 75% while a fixed film bioreactor reached 80% decolorization. However, a combination of both bioreactors in series reached a 97.3% color removal working at a hydraulic retention time of 4 day under aerobic conditions [191]. Another composite system was designed for bioelectrochemical degradation of indigo carmine. The process consisted in a new anode formed by microporous activated carbon fiber felt with immobilized laccase from the withe rot fungus *Pycnoporus sanguineus* that achieved 83.6% color reduction in 1 h [192].

Immobilized microbial cells have been also developed for the almost complete decolorization (98%) of 250 ppm of indigo carmine after 12 days in a solid-state bioreactor with *Phanerochaete chrysosporiurn* grown on wood shavings. The fungus showed manganese-peroxidase and lignin-peroxidase activity [193]. Bioagmentation assays have been performed by the addition of two different *Bacillus* species into activated sludge: The results demonstrated a stable balance between the foreign microorganisms and those in the sludge, achieving a color and a chemical oxygen demand of 98% and 99% respectively [155]. The complete mineralization of indigo has not been reported so far [194] though *Acinetobacter* sp. partially transforms indol into CO_2 and organic nitrogen into ammonia and nitrate. However, a parallel toxicological characterization proved that some metabolites were more toxic than indole itself [195].

The use of microbial consortia can substantially improve the degradation of this compound since they can produce non-toxic products [196]. The synergistic action of three *Bacillus* in a consortium is capable of considerably reducing the toxicity of the medium [197]. Although studies have been carried out on the structure and dynamics of microbial populations in consortia involved in the biological synthesis of indigo carmine (e.g. Ref. [198]), nothing is known about the

behavior of degradative consortiums, even though many of them are used in bioreactors to purify water contaminated with dyes, *e.g.* Ref. [191]

Treatment of textile wastewater containing anthraquinone dyes is a huge challenge due to its complex aromatic structure and toxicity. For example a study dealing with the degradation and detoxification of Reactive Blue 4 using bacterial granules showed that this system decolorized at wide range of pH and temperature. The dye is phytotoxic, cytotoxic and genotoxic whereas its biotransformed product were non-toxic [199].

Instead of microorganisms, laccases can be immobilized onto several matrix [200]. Thus, *Bacillus* spore-associated laccase can serve as a robust and efficient green catalyst for indigo carmine degradation [200]. Laccase from *Ganoderma* sp. KU-Alk4 was immobilized in copper-alginate beads and used in a 5 L airlift bioreactor, showing a complete (100%) degradation of indigo carmine (25 mg/L) in 1 day. In this case, the product of the reaction was identified as isatin sulfonic acid. Enzyme catalysts was stable and active through 20 days of continuous work. This biocatalyst also showed a high efficiency in Remazol Brilliant Blue R removal (100%) in 2 h [201]. A novel laccase-like multicopper oxidases from the fungus *Myrothecium roridum* yielded a 95% elimination of the indigo carmine (50 mg/L) within 3 hours or 98% (200 mg/L) in 8 h [202].

Extreme and harsh conditions applied to a laccase-producing fungus can alter the properties of the enzyme, leading to higher catalytic activity. An enzymatic extract showing laccase activity from 0.2 kGy electron beam irradiated endophytic fungus *Phomopsis* sp. was able to decolorize 95% of Remazol Brilliant Blue R (50 mg/L) within 48 h without the aid of redox mediators. The above anthraquinone-based dye was converted into lower-mass, non-toxic compounds, after a series of chemical reactions involving oxidation, hydroxylation, deamination and ring cleavage [203].

CONCLUSIONS

The class of inorganic semiconductors exhibit reliability and performance due to their covalently bonded inner structure of the component materials that allow: (i) lego-type assembly of atom layer by atom layer; (ii) single crystalline units' assembly; and finally (iii) control of electronic and photonic properties by individual elements, their position, their mixture/doping level and their chemical structure. In this Perspective article we showed thorough complementary examples that Hydrogen-bonded molecules are also promising candidates for the establishment of a novel class of organic semiconductors that has the potential to open research avenues leading to the above mentioned characteristics of inorganic semiconductors. Moreover, these hydrogen bonded molecules will have the ability to resist degradation and offer stability in device operation. When we will be able to control carefully both the purity of the precursor hydrogen bonded semiconductor, and the deposition technique in such a way to generate films of improved molecular alignment, then this novel class of semiconductor materials may become viable candidates for the establishment of high performance, cost effective electronics, in line with the original promise of organic electronics research field. In this article we analysed the behavior of the selected Hydrogen-bonded semiconductor materials by employing OFET architecture as a critical evaluation tool. We showed that purity of materials is of paramount importance for the advancement of the field and further suggest that both the purity and (eventually) the cost of synthesis of organic semiconductors be the two critical factors necessary to be reported in any of the future publications of the field.

These Hydrogen bonded materials are also abundant and low cost. To give a simple example along these lines, we compare directly in the following the price of Quinacridone and DNTT. Quinacridone is produced in multi tons/day amount by chemical industry (mainly in mainland China) and sold on online forums (*e.g.* the Alibaba portal) for modest prices that can reach ridiculously low levels of 15 cents/ kilogram for orders exceeding one metric ton. Noteworthy the production potential of several such chemical companies exceeds tens of metric tons/week, while the synthesis yield surpassed the value of 99% even with the methodology available in 1967 [47]. In the same time, DNTT and many of its high performance derivatives that are highly acclaimed by the organic electronics community are produced in multi-grams amounts only through tenuous synthetic processes at laboratory relevant levels, with yields ranging at best between 70% and 85% that involve tenuous removal steps of isomeric products by column chromatography [204]; DNTT is the only member of DNTT family commercially available at Sigma-Aldrich at prices circumventing around 2000 Euros/gram (1060 Euro/500 mg at the time of writing this text), basically more than 10 (ten) million times higher than the price of Quinacridone. Interestingly both materials require several steps of vacuum purification in order to deliver meaningful results as semiconductor materials, as we observed in our laboratory with the "as purchased DNTT" from Sigma-Aldrich and the "as purchased Quinacridone" from TCI Europe suppliers respectively. One train sublimation purification step was necessary to bring DNTT-based OFET performance to levels higher by one order of magnitude, *i.e.* mobility of ~1 to 3 cm^2/Vs (see footnote [1], perfectly in line with our previous observations of importance of purification for recording meaningful re-

[1] A. Petritz[a], E. Karner-Petritz[a], B. Stadlober[a] ([a]Joanneum Research mbH)-unpublished results; Research performed, 2018

sults, exemplified in this publication by Indigo (see **Figure 3a),** or with our recent observations involving pentacene and C_{60} [67, 205]). Nevertheless, the train sublimation step for DNTT came at a cost; we conservatively collected only 80% of the sublimed material, although collecting higher amount could have represented a viable option too; however we did not explore it further. Repeating the same procedure for Quinacridone, the conservative loss of 20% of the sublimed material proved affordable, given the modest retail price of Quinacridone. With this respect, hydrogen-bonded materials bearing natural cores (*e.g.* Indigo, Acridone, Anthraquinone, Naphthoquinone) may offer the interested researchers plethora of low cost choices and variability in molecular design, applicability and functionality as well as stability. Many of these syntheses are already known, and many of these derivatives are already mass produced by chemical industry. Noteworthy, the reference Labana and Labana [47] lists in excess of 100 linear trans-quinacridones already documented in 1967 (noteworthy both authors were affiliated to Xerox Company, a company seemingly interested in launching these molecules in the ink printing formulations). Many of the tabulated linear trans-quinacridones in Ref. [47] have assigned synthesis yields in excess of 90% or even approaching 100% as is the case of parent Quinacridone. If Tyrian purple (6,6'-Br-Indigo) proved to outclass Indigo in performance (see Chapter 2 here), then couldn't be at least one Quinacridone derivative able to reach a similar feat? As it is visible in this Perspective article, we picked up two such trans-Quinacridones, but many more await their investigation, and the results may be truly surprising and intriguing. This is in fact to be expected, given the large variety of trans-quinacridone molecules, visible simply by inspecting the very color of such compounds listed in Ref. [47], which ranges from orange to brown, red, grayish-blue and even violet tints. Considering these 100+ molecules as a singular class of linear trans-quinacridones, the derivatization potential at the core Quinacridone molecule seems immense; and similar lines of thought can be drawn for Anthraquinones, Indigos and even Naphthoquinones. It is worth mentioning also that despite our focus of this Perspective article on OFET structures only, Quinacridone and the two Quiancridone pigments exemplified here showed potential for the development of homojunction photovoltaics. In the latter case, the design of a "single material absorber in a single layer", deposited either via vacuum evaporation or solution processing represent a viable alternative to follow for the development of organic devices mimicking the architecture of highly performant silicon PVs. Despite their narrow absorption, the three analyzed Quinacridones rendered power conversion efficiencies in the range of 0.1% to 0.2% [32, 206] in homojunction architecture, but possibly other molecules (including Anthraquinones) displaying much broader absorption may render well improved results.

If in the organic photovoltaics field (OPVs), the development of mixed organic-inorganic structures based on the ABX_3 perovskite crystal structure [207, 208] is producing already exciting results, in the organic field effect transistors field (OFETs), urgent refreshment in new materials and ideas are necessary [14]. Could Hydrogen-bonded semiconductor assemblies represent the next revolution, and take the organic electronics field to more distant borders? This event seems highly reasonable, especially since many such molecules have extraordinary appeal due to their combined features of: natural heritage; high availability and/or low synthesis cost; stability in operation and aging (broadly highlighted here in Chapter 2 from very different angles); biocompatibility and amenability for biomolecule binding (highlighted here in the Chapters 3 and 4) and finally due to their bio-degradation routes, which proved already their effectiveness (highlighted in Chapter 5 of this article). These prerequisites are central to the development of our modern society that centers its strategic growth on sustainable evolution (Sustainable Development Goals of United Nations). As carefully analyzed by T.G. Gutowski and co-workers in their seminal work [1], in many inorganic electronics fabrication processes, the energy expanded is in excess of 1000 times, and surpassing even 1 million times the energy required to evaporate (sublime) metals like Copper or Iron. Noteworthy, the respective fabrication processes consume the above mentioned colossal energy while delivering only multi gram/hour of finite products. Hydrogen-bonded semiconductors may therefore bridge the gap of performance that exist between organic and inorganic electronics by reaching to the original promise of the organic electronics while offering a lot of excitement to the synthetic chemistry, theoretical and experimental physics, materials engineering and device manufacturing fields, for decades to come.

Funding Sources

This work was financially supported by the Wittgenstein Prize to Prof. Sariciftci by the Austrian Funds for Advancement of Science (FWF)", Project No Z222-N19; Mihai Irimia-Vladu acknowledges the research support to the Austrian Research Promotion Agency (FFG), Project COMPOSTRONICS, Project No. 5730587 and Project 3DFormOFETs, Project No. 842496; Gianluca Farinola thanks to the European Commission through the EU Project HyPhOE, Project No. 800926; Yasin Kanbur thanks to Turkish TUBITAK-BIDEB platform for the international post-doctoral research fellows; Angela Vlad is thankful to the Executive Agency for Higher Education, Research, Development and Innovation Funding (UEFISCDI) Romania, in the frame of project number PN-III-P1-1.1-MC-2018-1670; Eric D.Glowcki is grateful to the Knut and Alice Wallenberg foundation for support within the framework of the Wallenberg Centre for Molecular Medicine and the Wallenberg Wood Science Centre 2.0; Cristian-Vlad Irimia thanks the FFG Austria, with financial support within the program "Practical Training for Talented Pupils", Project DeftFAB, Project No. 867266 OTHERS?....

Notes

This article is dedicated to Professor Dr. Jean-Luc Brédas, an honorable friend and colleague, whose work illuminated many of us in the field of Organic Electronics.

ACKNOWLEDGMENT

We gratefully acknowledge our colleague and friend, Emeritus Professor Dr. Gundula Voss, who co-authored many of our original papers and brought the chemical modification of Indigo into our Institute in Linz, Austria. Her energy and knowledge have been unsurpassed. We also thank Prof. Horst Hartmann of Technical University Dresden, Germany for help in procuring one gram of historic Indanthrene Blue from the Historic Dyestuff Collection in Dresden.

ABBREVIATIONS

OFET: Organic Field Effect Transistor
WEEE: Waste from electrical and electronic equipment
OLED: organic light emitting diode
OPV: organic photovoltaic device (organic solar cell)
HPP: High-Performance Pigment
DPP: diketo pyrrolo pyrrole
LUMO: lower unoccupied molecular orbital
HOMO: higher occupied molecular orbital
EU: European Union
USA: United States of America
DNTT: dinaphtho[2,3-b:2',3'-f]thieno[3,2-b]thiophene
H: hydrogen
CO_2: carbon dioxide
H_2O: water
TTC: tetratetracontane
TMSC: trimethyl silyl cellulose

REFERENCES

[1] Gutowski, T. G.; Branham, M. S.; Dahmus, J. B.; Jones, A. J.; Thiriez, A.; Sekulic, D. P. Thermodynamic Analysis of Resources Used in Manufacturing Processes. *Environ. Sci. Technol.* **2009**, *43(5)*, 1584-1590.

[2] Williams, E.; Energy Intensity of Computer Manufacturing: Hybrid Assessment Combining Process and Economic Input–Output Methods. *Environ. Sci. Technol.* **2004**, *38(22)*, 6166-6174.

[3] Bhakvi, D. P.; Gutowski, T. G.; Sekulic´, D. P. (Edts.) Thermodynamic and the Destruction of Resources, Cambridge Univ. Press, 1st Edition. **2011,** 163–189.

[4] Baldé, C. P.; Forti V.; Gray, V.; Kuehr, R.; Stegmann, P. The Global E-waste Monitor – **2017**, United Nations University (UNU), International Telecommunication Union (ITU) & International Solid Waste Association (ISWA), Bonn/Geneva/Vienna.

[5] Kim, D.-H.; Lu, N.; Ma, R.; Kim, Y.-S.; Kim, R.-H.; Wang, S.; Wu J.; Won, S. M.; Tao, H.; Islam, A.; Yu, K. J.; Kim, T.; Chowdhury, R.; Ying, M.; Xu, L.; Li, M.; Chung, H.-J.; Keum, H.; McCormick, M.; Liu, P.; Zhang, Y.-W.; Omenetto, F. G.; Huang, Y.; Coleman, T.; Rogers, J. A. Epidermal Electronics. *Science* **2011**, *333*, 838–843.

[6] Kang, S. K.; Murphy, R. K. J.; Hwang, S. W.; Lee, S. M.; Harburg, D. V.; Krueger, N. A.; Shin, J.; Gamble, P.; Cheng, H.; Yu, S.; Liu, Z.; McCall, J. G.; Stephen, M.; Ying, H.; Kim, J.; Park, G.; Webb, R. C.; Lee, C. H.; Chung, S.; Wie, D. S.; Gujar, A. D.; Vemulapalli, B.; Kim, A. H.; Lee, K. M.; Cheng, J.; Huang, Y.; Lee, S. H.; Braun, P. V.; Ray, W. Z.; Rogers, J. A. Bioresorbable silicon electronic sensors for the brain. *Nature* **2016**, *530*, 71–76.

[7] Feig, V. R.; Tran, H.; Bao, Z. Biodegradable Polymeric Materials in Degradable Electronic Devices. *ACS Cent. Sci*. **2018**, *4*, 337–348.

[8] Lipomi, D. J.; Vosgueritchian, M.; Tee, B. C.; Hellstrom, S. L.; Lee, J. A.; Fox, C. H.; Bao, Z. Skin-like pressure and strain sensors based on transparent elastic films of carbon nanotubes. *Nat. Nanotechnol.* **2011**, *6*, 788–792.

[9] Bauer, S.; Bauer-Gogonea, S.; Graz, I.; Kaltenbrunner, M.; Keplinger, C.; Schwödiauer, R. 25th Anniversary Article: A soft future: from robots and sensor skin to energy harvesters. *Adv. Mater.* 2014, *26*, 149–162.

[10] Kaltenbrunner, M.; Sekitani, T.; Reeder, J.; Yokota, T.; Kuribara, K.; Tokuhara, T.; Drack, M.; Schwödiauer, R.; Graz, I.; Bauer-Gogonea, S.; Bauer, S.; Someya, T. An ultra-lightweight design for imperceptible plastic electronics. *Nature* **2013**, *499*, 458–463.

[11] Noy A. Bionanoelectronics. *Adv. Mater.* **2011**, *23*, 807–820.

[12] Mei, Y.; Diao, A.L.; Appleton, L.; Fang, T. Bao, Z. Integrated Materials Design of Organic Semiconductors for Field-Effect Transistors. *J. Amer. Chem. Soc.* **2013**, *135*, 6724–6746.

[13] Facchetti, A. Semiconductors for Organic Electronics. *Materials Today* **2007,** *10(3)*, 28-37.

[14] Klauk, H.; Will We See Gigahertz Organic Transistors?. *Adv. Electron. Mater.* **2018**, *4(10)*, 1700474.

[15] Operamolla, A. Farinola, G. M. Molecular and Supramolecular Architectures of Organic Semiconductors for Field-Effect Transistor Devices and Sensors: A Synthetic Chemical Perspective. *Eur. J. Org. Chem.* **2011**, 423-450.

[16] Marzano, G. Ciasca, C. V. Babudri, F. Bianchi, G. Pellegrino, A. Po, R. Farinola, G. M. Organometallic Approaches to Conjugated Polymers for Plastic Solar Cells: From Laboratory Synthesis to Industrial Production. *Eur. J. Org. Chem.* **2014**, 6583-6614.

[17] Ragni, R. Operamolla, A. Farinola, G. M. Synthesis of electroluminescent conjugated polymers in "Organic light-emitting diodes (OLEDs): materials, devices and applications. Alastair Buckley (Ed.), Woodhead Pub. Lim., Sawston, Cambridge, UK, **2013**.

[18] Facchetti, A. π-Conjugated Polymers for Organic Electronics and Photovoltaic Cell Applications, *Chem. Mater.* **2011**, *23*, 733-758.

[19] Wang, C.; Dong , H.; Lang, J.; Hu, W. Organic semiconductor crystals. *Chem. Soc. Rev.* **2018**, *47*, 422-500.

[20] Coropceanu, V.; Cornil, J.; da Silva Filho, D. A.; Olivier, Y.; Silbey, R.; Brédas, J.-L. Charge Transport in Organic Semiconductors. *Chem. Rev.* **2007**, *107(4)*, 926-952

[21] Coropceanu, V.; Li, H.; Winget, P.; Zhu, L.; Brédas J.-L. Electronic-Structure Theory of Organic Semiconductors: Charge-Transport Parameters and Metal/Organic Interfaces. *Ann. Rev. Mater. Res.* **2013**, *43*, 63-87.

[22] Brondijk, J. J.; Roelofs, W.S.C.; Mathijssen, S.G.J.; Shehu, A.; Cramer, T.; Biscarini, F.; Blom, P.W.M.; Leeuw, de D.M. Two-dimensional charge transport in disordered organic semiconductors. *Phys. Rev. Lett.* **2012**, *109*, 056601.

[23] Kheradmand-Boroujeni, B.; Klinger, M. P.; Fischer, A.; Kleemann, H.; Leo, K.; Ellinger, F. A Pulse-Biasing Small-Signal Measurement Technique Enabling 40 MHz Operation of Vertical Organic Transistors. *Sci. Rep.* **2018**, *8,* 1–9.

[24] Steckl, A. J. DNA: A New Material for Photonics?. *Nature Phot.* **2007**, *1*, 3-5.

[25] Irimia-Vladu, M.; Troshin, P. A.; Reisinger, M.; Shmygleva, L.; Kanbur, Y.; Schwabegger, G.; Bodea, M.; Schwödiauer, R.; Mumyatov, A.; W Fergus, J.; Razumov, V. F.; Sitter, H.; Sariciftci, N. S.; Bauer S. Biocompatible and biodegradable materials for organic field-effect transistors. *Adv. Funct. Mater.* **2010**, *20(23)*, 4069-4076.

[26] Tobjörk, D.; Österbacka, R. Paper Electronics, *Adv. Mater.* **2011**, *23*, 1935-1961.

[27] Tao, H.; Kaplan, D. L.; Omenetto, F. G. Silk Materials – A Road to Sustainable High Technology, *Adv. Mater.* **2012**, *24*, 2824-2837.

[28] Pron, A.; Gawrys, P.; Zagorska, M.; Djurado, D.; Demadrille, R. Electroactive materials for organic electronics: preparation strategies, structural aspects and characterization techniques. *Chem. Soc. Rev.* **2010**, *39*, 2577-2632.

[29] Coropceanu, V.; Cornil, J.; da Silva Filho, D. A.; Olivier, Y.; Silbey, R.; Brédas, J.-L. Charge Transport in Organic Semiconductors. *Chem. Rev.* **2007**, *107*, 926-952.

[30] Głowacki, E. D.; Coskun, H.; Blood-Forsythe, M. A.; Monkowius, U.; Leonat, L.; Grzybowski, M.; Gryko, D.; White, M. S.; Aspuru-Guzik, A.; Sariciftci N. S. Hydrogen-bonded diketopyrrolopyrrole (DPP) pigments as organic semiconductors. *Org. Electron.* **2014**, *15(12)*, 3521-3528.

[31] Irimia-Vladu, M.; Głowacki, E. D.; Troshin, P. A.; Schwabegger, G.; Leonat, L.; Susarova, D. K.; Krystal, O.; Ullah, M.; Kanbur, Y.; Bodea, M. A.; Razumov, V. F.; Sitter, H.; Bauer, S.; Sariciftci, N. S. Indigo-a natural pigment for high performance ambipolar organic field effect transistors and circuits. *Adv. Mater.* **2012**, *24(3)*, 375–380.

[32] Głowacki, E. D.; Leonat, L.; Irimia-Vladu, M.; Schwödiauer, R.; Ullah, M.; Sitter, H.; Bauer, S.; Sariciftci, N. S. Intermolecular hydrogen-bonded organic semiconductors-quinacridone versus pentacene. *Appl. Phys. Lett.* **2011**, *101*, 023305.

[33] Irimia-Vladu, M.; Glowacki, E. D.; Bauer, S.; Sariciftci, N. S. (Edts.) Green Materials for Electronics. Wiley-VCH Verlag GmbH & Co. KGaA, **2017**.

[34] Kanbur, Y.; Irimia-Vladu, M.; Głowacki, E. D.; Voss, G.; Baumgartner, M.; Schwabegger, G.; Leonat, L.; Ullah, M.; Sarica, H.; Erten-Ela, S.; Schwödiauer, R.; Sitter, H.; Küçükyavuz, Z.; Bauer, S.; Sariciftci, N. S. Vacuum-processed Polyethylene as a Dielectric for Low Operating voltage Organic Field-effect Transistors. *Org. Electron.* **2012**, *13(5)*, 919-924.

[35] Głowacki, E. D.; Irimia-Vladu, M.; Kaltenbrunner, M.; Gasiorowski, J.; White, M. S.; Monkowius, U.; Romanazzi, G.; Suranna, G. P.; Mastrorilli, P.; Sekitani, T.; Bauer, S.; Someya, T.; Torsi, L.; Sariciftci N. S. Hydrogen-Bonded Semiconducting Pigments for Air-Stable Field-Effect Transistors. *Adv. Mater.* **2013**, *25(11),* 1563-1567.

[36] Wagner, T.; Györök, M.; Huber, D.; Zeppenfeld, P.; Głowacki, E.D.; Quinacridone on Ag (111): Hydrogen Bonding versus Chirality. *J. Phys. Chem. C* **2014**, *118(20)*, 10911-10920

[37] Villagomez, C. J.; Guillermet, O.; Goudeau, S.; Ample, F.; Xu, H.; Coudret, C.; Bouju, X.; Zambelli, T.; Gauthierg, S. Self-assembly of enantiopure domains: The case of indigo on Cu-111. *J. Chem. Phys.* **2010**, *132*, 074705.

[38] Linke, G. Molecular Stacks as a Common Characteristic in the Crystal Lattice of Organic Pigment Dyes: A Contribution to the "Soluble–insoluble" Dichotomy of Dyes and Pigments from the Technological Point of View. *Dyes Pigm.* **2003**, *59*, 1-24.

[39] Paulus, E. F.; Leusen, F. J. J.; Schmidt, M. U. Crystal structures of quinacridones. *Cryst. Eng. Comm.* **2007**, *9*, 131–143.

[40] Wei, H.-L.; Shi, Y.-R.; Liu, Y.-F. A theoretical study of charge-transport parameters for a hydrogen-bonded organic semiconductor: the indigo and s-indaceno [1,2-b:5,6-b′] dithiophene-4,9-dione derivatives. *Semicond. Sci. Technol.* **2016**, *31* 065016.

[41] Winkler, C.; Mayer, F.; Zojer E. Analyzing the Electronic Coupling in Molecular Crystals—The Instructive Case of α-Quinacridone. *Adv. Theory Simul.* **2019**, 1800204, DOI: 10.1002/adts.201800204.

[42] Hao, Z.; Iqbal A. Some aspects of organic pigments. *Chem. Soc. Rev.* **1997**, *26*, 203-213.

[43] Smith H. M. (Edt.) High Performance Pigments. Second Edition, Wiley-VCH, Weinheim, Germany, **2009**.

[44] Voss, G.; Gerlach, H. Regioselektiver Brom/Lithium-Austausch bei 2,5-Dibrom-1-nitrobenzol. – Eine einfache Synthese von 4-Brom-2-nitrobenzaldehyd und 6,6′-Dibromindigo. *Chem. Ber.* **1989**, *122(6)*, 1199-1201.

[45] Klimovich I. V.; Leshanskaya, L. I.; Troyanov, S. I.; Anokhin, D. V.; Novikov, D. V.; Piryazev, A. A.; Ivanov, D. A.; Dremova, N. N.; Troshin P. A. Design of indigo derivatives as environmentfriendly organic semiconductors for sustainable organic electronics. *J. Mater. Chem. C* **2014**, *2*, 7621-7631.

[46] Struve, W. S. Process for the preparation of linear quinacridones. U.S. Patent 2821529, **1958**.

[47] Labana S. S; Labana, L. L. Quinacridones. Chem. Rev. **1967,** *67(1)*, 1-18.

[48] Ainley, A. D.; Robinson, R. The epindoline group. Part I. Trial of various methods for the synthesis of epindolidiones. *J. Chem. Soc.* **1934**, 1508-1520.

[49] de Diesbach, H.; Schurch, A.; Cavin, G. Contribution à l'étude des hydroxy-4-phénylamino-3-quinoléines. *Helv. Chim. Acta*, **1948**, 31(3), 716-724

[50] Haucke, G.; Graness. G. Thermische Isomerisierung von Indigo. *Angew. Chem.* **1995**, *107*, 116-117.

[51] Haucke, G.; Graness, G. Thermal Isomerization of Indigo. *Angew. Chem. Int. Ed. Engl.* **1995,** *34*, 67-68.

[52] Aldridge, G. R.; Jaffe, E.; Jaffe, E. E.; Matrick, H. Quinolonoquinolone Pigments And Substituted Derivatives Thereof. U.S Patent 3334102, **1967.**

[53] Jaffe, E. E. Matrick, H. Synthesis of epindolidione. *J. Org. Chem.* **1968**, *33*, 4004-4010.

[54] Van Slyke, S. A. ; Tang, C. W. Organic electroluminescent devices having improved power conversion efficiencies. U.S. Patent 4539507, **1985**.

[55] Kaul B. A.; Piastra, B.; Wolf, V.; Prokschy, F.; Schmidt, M.U. Epindolidione pigments. U.S. Patent 7307170, **2007.**

[56] Weiss, D.; Burberry, M. Photoconductivity studies of indium/epindolidione/indium tin oxide sandwich cells. *Thin Solid Films* **1988**, *158*, 175-187.

[57] Pron, A.; Rannou, P. Processible conjugated polymers: from organic semiconductors to organic metals and superconductors. *Prog. in Polym. Sci.* **2002**, *27*, 135-190.

[58] Głowacki, E. D.; Romanazzi, G.; Yumusak, C.; Coskun, H.; Monkowius, U.; Voss, G.; Burian, M.; Lechner R.T.; Demitri, N.; Redhammer, G. J.; Sünger, N.; Suranna, G. P.; Sariciftci, N. S. Epindolidiones—Versatile and Stable Hydrogen-Bonded Pigments for Organic Field-Effect Transistors and Light-Emitting Diodes. *Adv. Funct. Mater.* **2015**, *25*, 776-787.

[59] Jones, A.O.F.; Röthel, C.; Lassnig, R.; Bedoya-Martínez O.N.; Christian, P.; Salzmann, I.; Kunert, B.; Winkler, A.; Resel, R. Solution of an elusive pigment crystal structure from a thin film: a combined X-ray diffraction and computational study. *CrystEngComm.* **2017**, *19*, 1902-1911.

[60] Jaffe E. E. *J. Oil Colour Chem. Assoc.* **1992**, *75*, 24-31.

[61] Kemp, D. S.; Bowen, B. R.; Muendel, C.C. Synthesis and conformational analysis of epindolidione-derived peptide models for .beta.-sheet formation. *J. Org. Chem.* 1990, *55(15)*, 4650-4657.

[62] Yang, C. Y.; Shi, K.; Lei, T.; Wang, J.; Wang, X.-Y.; Zhuang, F. D.; Wang, J. Y.; Pei, J. Epindolidione-Based Conjugated Polymers: Synthesis, Electronic Structures, and Charge Transport Properties. *ACS Appl. Mater. Interf.* **2016**, *8(6)*, 3714-3718.

[63] Bolto, B.A.; McNeill, R.; Weiss, D.E. Electronic Conduction in Polymers. III. Electronic Properties of Polypyrrole" (PDF). *Australian J. Chem.* **1963,** *16(6)*, 1090-1103.

[64] Shirakawa, H.; Louis, E. J.; MacDiarmid, A. G.; Chiang, C. K.; Heeger, A. J. Synthesis of electrically conducting organic polymers: Halogen derivatives of polyacetylene, (CH) x. *J. Chem. Soc. Chem. Commun.* **1977**, *16*, 578-580.

[65] Scharber, M. C.; Mühlbacher, D.; Koppe, R.; Denk, P.; Waldauf, C.; Heeger, A. J.; Brabec C. J. Design rules for donors in bulk-heterojunction solar cells-Towards 10% energy-conversion efficiency. *Adv. Mater.* **2006**, *18(6)*, 789-794,

[66] Dennler, G.; Scharber, M. C.; Brabec, C. J. Polymer-fullerene bulk-heterojunction solar cells" *Adv. Mater.* **2009**, *21(13)*, 1323-1338.

[67] Petritz, A.; Krammer, M.; Sauter, E.; Gärtner, M.; Nascimbeni, G.; Schrode, B.; Fian, A.; Gold, H.; Cojocaru, A.; Karner-Petritz, E.; Resel, R.; Terfort, A.; Zojer, E.; Zharnikov, M.; Zojer, K.; Stadlober, B. Embedded Dipole Self-Assembled Monolayers for Contact Resistance Tuning in p-Type and n-Type Organic Thin Film Transistors and Flexible Electronic Circuits. *Adv. Funct. Mater.* **2018**, *28*, 1804462.

[68] Pitayatanakul, O.; Higashino, T.; Kadoya, T.; Tanaka, M.; Kojima, H.; Ashizawa, M.; Kawamoto, T.; Matsumoto, H.; Ishikawa, K.; Mori T. High performance ambipolar organic field-effect transistors based on indigo derivatives. *J. Mater. Chem. C.* **2014**, *2*, 9311-9317.

[69] Głowacki, E. D.; Leonat, L.; Voss, G.; Bodea, M. A.; Bozkurt, Z.; Montaigne Ramil, A.; Irimia-Vladu, M.; Bauer, S.; Sariciftci N. S. Ambipolar organic field effect transistors and inverters with the natural material Tyrian Purple, *AIP Advances* **2011**, *1(4)*, 042132.

[70] Anthopoulos, T. D.; Setayesh, S.; Smits, E; Cölle, M, Cantatore, E.; de Boer, B.; Blom, P. W. M.; de Leeuw D. M. Air-Stable Complementary-like Circuits Based on Organic Ambipolar Transistors. *Adv. Mater.* **2006**, *18(14)*, 1900-1904.

[71] Petritz, A.; Wolfberger, A.; Fian, A.; Griesser, T.; Irimia-Vladu, M.; Stadlober B. Cellulose-Derivative-Based Gate Dielectric for High-Performance Organic Complementary Inverters. *Adv. Mater.* **2015**, *27(46)*, 7645-7656.

[72] Chen, Z.; Lee, M. J.; Ashraf, R. S.; Gu, Y.; Albert-Seifried, S.; Nielsen, M. M.; Schroeder, B.; Anthopoulos, T. D.; Heeney, M.; McCulloch, I.; Sirringhaus, H. High-Performance Ambipolar Diketopyrrolopyrrole-Thieno[3,2-b]thiophene Copolymer Field-Effect Transistors with Balanced Hole and Electron Mobilities. *Adv. Mater.* **2012**, *24*, 647–652.

[73] T. D. Anthopoulos, D. M. de Leeuw, E. Cantatore, S. Setayesh, E. J. Meijer, C. Tanase, J. C. Hummelen, P. W. M. Blom, Organic complementary-like inverters employing methanofullerene-based ambipolar field-effect transistors. *Appl. Phy. Lett*. **2004**, *85*, 4205.

[74] Zaumseil, J.; Donley, C. L.; Kim, J.-S.; Friend, R.H.; Sirringhaus, H. Efficient Top-Gate, Ambipolar, Light-Emitting Field-Effect Transistors Based on a Green-Light-Emitting Polyfluorene. *Adv. Mater.* **2006**, *18*, 2708–2712.

[75] Youn, J.; Kewalramani, S.; Emery, J. D.; Shi, Y.; Zhang, S.; Chang, H. C.; Liang, Y.; Yeh, C. M.; Feng, C. Y.; Huang, H.; Stern, C.; Chen, L.-H.; Ho, J. C.; Chen, M. C.; Bedzyk, M. J.; Facchetti, A.; Marks, T. J. Fused Thiophene Semiconductors: Crystal Structure–Film Microstructure Transistor Performance Correlations, *Adv. Funct. Mater.* **2013**, *23*, 3850–3865.

[76] Liu, C.; Liu, Z.; Lemke, H. T.; Tsao, H.N.; Naber, R. C. G.; Li, Y.; Banger, K.; Müllen, K.; Nielsen, M. M.; Sirringhaus, H. High-Performance Solution-Deposited Ambipolar Organic Transistors Based on Terrylene Diimides. *Chem. Mater.* **2010**, *22*, 2120–2124.

[77] Petritz, A.; Fian, A.; Głowacki, E. D.; Sariciftci, N. S.; Stadlober, B.; Irimia-Vladu M. Ambipolar inverters with natural origin organic materials as gate dielectric and semiconducting layer. *Phys. Status Solidi (RRL)* **2015**, *9(6)*, 358-361.

[78] Irimia-Vladu, M.; Fergus, J.W. Impedance Spectroscopy of Thin Films of Emeraldine Base Polyaniline and its Implications for Chemical Sensing. *Synth. Met.* **2006**, *156*, 1396-1400.

[79] Irimia-Vladu, M.; Marjanovic, N.; Bodea, M.; Hernandez-Sosa, G.; Montaigne Ramil, A.; Schwödiauer, R.; Bauer, S.; Sariciftci, N.S.; Nüesch, F. Small-molecule Vacuum Processed Melamine-C_{60}, Organic Field-Effect Transistors. *Org. Electron.* **2009**, *10(3)*, 408-415.

[80] Irimia-Vladu, M.; Marjanovic, N.; Vlad, A.; Hernandez-Sosa, G.; Montaigne Ramil, A.; Schwödiauer, R.; Bauer, S.; Sariciftci, N.S. Vacuum Processed, Polyaniline-C_{60} Organic Field Effect Transistors", *Adv. Mater.* **2008**, *20(20)*, 3887-3892.

[81] Irimia-Vladu, M.; Troshin, P. A.; Reisinger, M.; Schwabegger, G.; Ullah, M.; Schwödiauer, R.; Mumyatov, A.; Bodea, M.; Fergus, J. W.; Razumov, V.F.; Sitter, H.; Bauer, S.; Sariciftci, N. S.; Environmentally Sustainable Organic Field Effect Transistors. *Org. Electron.* **2010**, *11(12)*, 1974-1990.

[82] Kaltenbrunner, M.; Stadler, P.; Schwödiauer, R.; Hassel, A. W.; Sariciftci, N. S.; Bauer, S. Anodized Aluminum Oxide Thin Films for RoomTemperature Processed, Flexible, Low-Voltage Organic Non-Volatile Memory Elements with Excellent Charge Retention. *Adv. Mater.* **2011**, *23*, 4892–4896.

[83] Bisoyi, S.; Zschieschang, U.; Kang, M. J.; Takimiya, K.; Klauk, H.; Tiwari S. P. Bias-stress stability of low-voltage p-channel and n-channel organic thin-film transistors on flexible plastic substrates. *Org. Electron.* **2014**, *15*, 3173–3182,

[84] Park, S.; Cho E. N.; Yun I. Threshold voltage shift prediction for gate bias stress on amorphous InGaZnO thin film transistors. *Microelectronics Reliability* **2012**, *52*, 2215–2219,

[85] Kim, J.; Jang, J.; Kim, K.; Kim, H.; Kim, S. H.; Park C. E. The Origin of Excellent Gate-Bias Stress Stability in Organic Field-Effect Transistors Employing Fluorinated-Polymer Gate Dielectrics. *Adv. Mater.* **2014**, *26(42),* 7241-7246.

[86] Zschieschang, U.; Weitz, R. T.; Kern, K.; Klauk H. Bias stress effect in low-voltage organic thin-film transistors. *Appl. Phys. A* **2009**, *95*, 139–145.

[87] Kanbur, Y.; Coskun, H.; Głowacki, E. D.; Irimia-Vladu, M.; Sariciftci, N. S.; Yumusak C. High temperature-stability of organic thin-film transistors based on quinacridone pigments. *Org. Electron.* **2019**, *66*, 53-57.

[88] Kuribara, K.; Wang, H.; Uchiyama, N.; Fukuda, K.; Yokota, T.; Zschieschang, U.; Jaye, C.; Fischer, D.; Klauk, H.; Yamamoto, T.; Takimiya, K;. Ikeda, M.; Kuwabara, H.; Sekitani, T.; Loo, Y.-L.; Someya, T. Organic transistors with high thermal stability for medical applications. *Nature Commun*. **2012,** *3*, 723.

[89] Yokota, T.; Kuribara, K.; Tokuhara, T.; Zschieschang, U.; Klauk, H.; Takimiya, K.; Sadamitsu, Y.; Hamada, M.; Sekitani, T.; Someya T. Flexible Low-Voltage Organic Transistors with High Thermal Stability at 250 ° C. *Adv. Mater.* **2013**, *25*, 3639–3644.

[90] M. Sytnyk, E. D. Głowacki, S. Yakunin, G. Voss, W. Schöfberger, D. Kriegner, J. Stangl, R. Trotta, C. Gollner, S. Tollabimazraehno, G. Romanazzi, Z. Bozkurt, M. Havlicek, N. S. Sariciftci, R. Schindl, W. Heiss, "Hydrogen-Bonded Organic Semiconductor Micro- And Nanocrystals: From Colloidal Syntheses to (Opto-)Electronic Devices" J. Am. Chem. Soc. 2014, 136, 16522–16532.

[91] M. Sytnyk, M. Jakešová, M. Litviňuková, O. Mashkov, D. Kriegner, J. Stangl, J. Nebesářová, F. W. Fecher, W. Schöfberger, N. S. Sariciftci, R. Schindl, W. Heiss, E. D. Głowacki, "Cellular interfaces with hydrogen-bonded organic semiconductor hierarchical nanocrystals" Nat. Commun., 2017, 8, 91.

[92] Muskovich, M.; Bettinger, C. J. Biomaterials-Based Electronics: Polymers and Interfaces for Biology and Medicine. *Adv. Healthc. Mater.* **2012**, *1*, 248–266.

[93] Simon, D. T.; Gabrielsson, E.; Tybrandt, K.; Berggren, M. Organic Bioelectronics: Bridging the Signaling Gap between Biology and Technology. *Chem Rev.* **2016**, *116(21)*, 13009-13041.

[94] Amdursky, N.; Głowacki, E. D.; Meredith, P. Macroscale Biomolecular Electronics and Ionics. *Adv. Mater.* **2018**, *1802221*, 1–28.

[95] Li, H.; Shi, W.; Song, J.; Jang, H.-J.; Dailey, J.; Yu, J.; Katz, H.E. Chemical and Biomolecule Sensing with Organic Field-Effect Transistors. *Chem. Rev.* **2019**, *119* 3-35.

[96] Milano, F.; Punzi, A.; Ragni, R.; Trotta, M.; Farinola, G. M. Photonics and Optoelectronics with Bacteria: Making Materials from Photosynthetic Microorganisms. Adv. Funct. Mater. in press, DOI: 10.1002/adfm.201805521.

[97] Operamolla, A. Ragni, R. Milano, F. Tangorra, R. R. Antonucci, A. Agostiano, A. Trotta, M. Farinola, G. M. "Garnishing" the photosynthetic bacterial reaction center for bioelectronics. *J. Mater. Chem. C* **2015**, *3*, 6471-6478.

[98] Magliulo, M. Manoli, K. Macchia, E. Palazzo, G. Torsi, L. Tailoring Functional Interlayers in Organic Field-Effect Transistor Biosensors. *Adv. Mater.* 2015, *27*, 7528-7551.

[99] Rivnay, J.; Inal, S.; Salleo, A.; Owens, R.M.; Berggren, M.; Malliaras, G.G. Organic electrochemical transistors. *Nature Rev. Mater.* **2018**, *3*, 17086.

[107] Jiang, Y. Tian, B. Inorganic semiconductor biointerfaces. *Nature Rev. Mater.* **2018**, *3*, 473–490.

[108] Hopkins, J.; Travaglini, L.; Lauto, A.; Cramer, T.; Fraboni, B.; Seidel, J.; Mawad, D. Photoactive Organic Substrates for Cell Stimulation: Progress and Perspectives. *Adv. Mater. Technol.* **2019**, in press, DOI: 10.1002/admt.201800744.

[109] Stephanopoulos, N.; Francis, M.B. Choosing an effective protein bioconjugation strategy. *Nat. Chem. Biol.* **2011**, *7*, 876–884.

[110] Głowacki, E. D.; Tangorra, R. R.; Coskun, H.; Farka, D.; Operamolla, A.; Kanbur, Y.; Milano, F.; Giotta, L.; Farinola, G.M.; Sariciftci, N. S. Bioconjugation of hydrogen-bonded organic semiconductors with functional proteins. *J. Mater. Chem. C* **2015**, *3*, 6554-6564.

[111] Milano, F.; Tangorra, R. R.; Omar O. H.; Ragni, R.; Operamolla, A.; Agostiano, A.; Farinola, G. M.; Trotta, M. Enhancing the light harvesting capability of a photosynthetic Reaction Center by a tailored molecular fluorophore. *Angew. Chem. Int. Ed.* **2012**, *51*, 11019.

[112] La Gatta, S.; Milano, F.; Farinola, G. M.; Agostiano, A.; Di Donato, M.; Lapini, A.; Foggi, P.; Trotta, M.; Ragni, R. A highly efficient heptamethine cyanine antenna for photosynthetic Reaction Center: From chemical design to ultrafast energy transfer investigation of the hybrid system. *BBA – Bioenergetics* **2019**, *1860*, 350–359.

[113] Omar, O. H.; La Gatta, S.; Tangorra, R. R.; Milano, F.; Ragni, R.; Operamolla, A.; Argazzi, R.; Chiorboli, C.; Agostiano, A.; Trotta, M.; Farinola G. M. Synthetic antenna functioning as light harvester in the whole visible region for enhanced hybrid photosynthetic reaction centers. *Bioconj. Chem.* **2016**, *27*, 1614–1623.

[114] Operamolla, A. Casalini, S. Console, D. Capodieci, L. Di Benedetto, F. Bianco G. V., Babudri, F. Tailoring water stability of cellulose nanopaper by surface functionalization. *Soft Matter* **2018**, *14*, 7390-7400.

[129] Jakešová, M.; Apaydin, D. H.; Sytnyk, M.; Oppelt, K.; Heiss, W.; Sariciftci, N. S.; Głowacki, E. D.; Hydrogen-Bonded Organic Semiconductors as Stable Photoelectrocatalysts for Efficient Hydrogen Peroxide Photosynthesis. *Adv. Funct. Mater.* **2016**, *26*, 5248–5254.

[130] Gryszel, M.; Markov, A.; Vagin, M.; Głowacki, E. D. Organic Heterojunction Photocathodes for Optimized Photoelectrochemical Hydrogen Peroxide Production. *J. Mater. Chem. A* **2018**, *6*, 24709–24716.

[131] Apaydin, D. H.; Głowacki, E. D.; Portenkirchner, E.; Sariciftci, N. S. Direct Electrochemical Capture and Release of Carbon Dioxide Using an Industrial Organic Pigment: Quinacridone. *Angew. Chem. Int. Ed. Engl.* **2014**, *53(26)*, 6819–6822.

[132] Apaydin, D. H.; Gora, M.; Portenkirchner, E.; Oppelt, K. T.; Neugebauer, H.; Jakesova, M.; Głowacki, E. D.; Kunze-Liebhäuser, J.; Zagorska, M.; Mieczkowski, J.; Sariciftci, N.S. "Electrochemical Capture and Release of CO_2 in Aqueous Electrolytes Using an Organic Semiconductor Electrode", *ACS Appl. Mater. Interf.* **2017**, *9*, 12919–12923.

[133] Gryszel, M.; Sytnyk, M.; Jakesova, M.; Romanazzi, G.; Gabrielsson, R.; Heiss, W.; Głowacki, E. D. General Observation of Photocatalytic Oxygen Reduction to Hydrogen Peroxide by Organic Semiconductor Thin Films and Colloidal Crystals. *ACS Appl. Mater. Interfaces* **2018**, *10*, 13253–13257.

[134] Ma, Q.; Zhang, X.; Qu, Y. Biodegradation and biotransformation of indole: advances and perspectives. *Front. Microbiol.* **2018**, *9*, 2625.

[135] Głowacki, E. D.; Voss, G.; Leonat, L.; Irimia-Vladu, M.; Bauer, S.; Sariciftci, N. S. Indigo carmine and Tyrian purple–from ancient natural dyes to modern organic semiconductors. *Israel J. Chem.* **2012**, *52(6)*, 540-551.

[136] Ganesh, V.; Manthrammel, M. A.; Shkir, M.; Yahia, I. S.; Zahran, H. Y.; Yakuphanoglu, F.; AlFaify, S. Organic semiconductor photodiode based on indigo carmine/n-Si for optoelectronic applications. *Appl. Phys. A* **2018**, *124(6),* 424.

[137] Salzillo, T.; d'Agostino, S.; Rivalta, A.; Giunchi, A.; Brillante, A.; Della Valle, R. G.; Venuti, E. Structural, Spectroscopic, and Computational Characterization of the Concomitant Polymorphs of the Natural Semiconductor Indigo carmine. *J. Phys. Chem. C* **2018**, *122(32),* 18422-18431.

[138] Sadauskas, M.; Vaitekūnas, J.; Gasparavičiūtė, R.; Meškys, R. Indole biodegradation in Acinetobacter sp. strain O153: genetic and biochemical characterization. *Appl. Environ. Microbiol.* **2017**, *83(19)*, e01453-17.

[139] Levin, L.; Melignani, E.; Ramos, A. M. Effect of nitrogen sources and vitamins on ligninolytic enzyme production by some white-rot fungi. Dye decolorization by selected culture filtrates. *Biores. Technol.* **2010**, *101(12)*, 4554-4563.

[140] Diwaniyan, S.; Kharb, D.; Raghukumar, C.; Kuhad, R. C. Decolorization of synthetic dyes and textile effluents by basidiomycetous fungi. *Water Air Soil Pollut.* **2010**, *210(1-4)*, 409-419.

[141] Qin, X.; Zhang, J.; Zhang, X.; & Yang, Y. Induction, purification and characterization of a novel manganese peroxidase from *Irpex lacteus* CD2 and its application in the decolorization of different types of dye. *PLoS One* **2014**, *9(11)*, e113282.

[142] Legerská, B.; Chmelová, D.; Ondrejovič, M. Degradation of synthetic dyes by laccases–a mini-review. *Nova Biotechnol. Chim.* **2016**, *15(1)*, 90-106.

[143] Papinutti, L.; Forchiassin, F. Adsorption and decolorization of dyes using solid residues from *Pleurotus ostreatus* mushroom production. *Biotechnol. Bioproc. Eng.* **2010**, *15(6)*, 1102-1109.

[144] Srinivasan, A.; Viraraghavan, T. Decolorization of dye wastewaters by biosorbents: a review. *J. Environ. Manag.* **2010**, *91(10),* 1915-1929.

[145] Zapata-Castillo, P.; Villalonga-Santana, L.; Islas-Flores, I.; Rivera-Muñoz, G.; Ancona-Escalante, W.; Solís-Pereira, S. Synergistic action of laccases from Trametes hirsuta Bm2 improves decolourization of indigo carmine. *Lett. Appl. Microbiol.* **2015**, *61(3)*, 252-258.

[146] Savinova, O. S.; Moiseenko, K. V.; Vavilova, E. A.; Tyazhelova, T. V.; Vasina, D. V. Properties of two laccases from the Trametes hirsuta o72 multigene family: Twins with different faces. *Biochimie* **2017**, *142*, 183-190.

[147] Grassi, E.; Scodeller, P.; Filiel, N.; Carballo, R.; Levin, L. Potential of *Trametes trogii* culture fluids and its purified laccase for the decolorization of different types of recalcitrant dyes without the addition of redox mediators. *Int. Biodet. Biodegr.* **2011**, *65(4)*, 635-643.

[148] Ancona-Escalante, W.; Tapia-Tussell, R.; Pool-Yam, L.; Can-Cauich, A.; Lizama-Uc, G.; Solís-Pereira, S. Laccase-mediator system produced by Trametes hirsuta Bm-2 on lignocellulosic substrate improves dye decolorization. *Biotech* **2018**, *8(7)*, 298.

[149] Cano, M.; Solis, M.; Diaz, J.; Solis, A.; Loera, O.; Teutli, M. M. Biotransformation of indigo carmine to isatin sulfonic acid by lyophilized mycelia from Trametes versicolor. *African J. Biotechnol.* **2011**, *10(57)*, 12224-12231.

[150] Pan, K.; Zhao, N.; Yin, Q.; Zhang, T.; Xu, X.; Fang, W.; Xiao, Y. Induction of a laccase Lcc9 from Coprinopsis cinerea by fungal coculture and its application on indigo dye decolorization. *Biores. Technol.* **2014**, *162*, 45-52.

[151] Younes, S. B.; Bouallagui, Z.; Gargoubi, A.; Sayadi, S. Investigation of dyes degradation intermediates with Scytalidium thermophilum laccase. *Eur. Food Res. Technol.* **2011**, *233(5)*, 751.

[152] Han, X.; Zhao, M.; Lu, L.; & Liu, Y. Purification, characterization and decolorization of bilirubin oxidase from Myrothecium verrucaria 3.2190. *Fungal Biol.* **2012**, *116(8)*, 863-871.

[153] Miranda, R. de C. M. de; Gomes, E. de B.; Pereira, N.; Marin-Morales, M. A.; Machado, K. M. G.; Gusmão, N. B. de. Biotreatment of Textile Effluent in Static Bioreactor by Curvularia Lunata URM 6179 and Phanerochaete Chrysosporium URM 6181. *Bioresour. Technol.* **2013**, *142*, 361–367.

[154] Bankole, P. O.; Adekunle, A. A.; Obidi, O. F.; Olukanni, O. D.; Govindwar, S. P. Degradation of indigo dye by a newly isolated yeast, Diutina rugosa from dye wastewater polluted soil. *J. Environ. Chem. Eng.* **2017**, *5(5)*, 4639-4648.

[155] Khelifi, E.; Touhami, Y.; Thabet, O. B. D.; Ayed, L.; Bouallagui, H.; Fardeau, M. L.; Hamdi, M. Exploring Bioaugmentation Strategies for the Decolourization of Textile Wastewater Using a Two Species Consortium (Bacillus Cereus and Bacillus Pumilus) and Characterization of Produced Metabolites. *Desalin. Water Treat.* **2012**, *45(1–3)*, 48–54.

[156] Sharma, P.; Goel, R.; Capalash, N. Bacterial laccases. *World J. Microbiol. Biotechnol.* **2007**, *23*, 823–832.

[157] Qu, Y.; Shen, E.; Ma, Q.; Zhang, Z.; Liu, Z.; Shen, W.; Wang, J.; Li, D.; Li, H.; Zhou, J. Biodegradation of Indole by a Newly Isolated Cupriavidus Sp. SHE. *J. Environ. Sci.* **2015**, *34*, 126–132.

[158] Fukuoka, K.; Tanaka, K.; Ozeki, Y.; Kanaly, R. A. Biotransformation of indole by Cupriavidus sp. strain KK10 proceeds through N-heterocyclic-and carbocyclic-aromatic ring cleavage and production of indigoids. *Int. Biodet. Biodegr.* **2015**, *97*, 13-24.

[159] Dong, X.; Wang, Y.; Zhang, P.; Tan, Z.; Jiao, Z.; Jin, Q. Degradation of isatin and anthranilic acid by Achromobacter xylosoxidans N4 isolated from denim-manufacturing mill sludge. *Fresen. Environ. Bull.* **2016**, *25(8)*, 2784-2794.

[160] Lu, L.; Zeng, G.; Fan, C.; Ren, X.; Wang, C.; Zhao, Q.; Jiang, M. Characterization of a laccase-like multicopper oxidase from newly isolated Streptomyces sp. C1 in agricultural waste compost and enzymatic decolorization of azo dyes. *Biochem. Eng. J.* **2013**, *72*, 70-76.

[161] Lu, L.; Zhao, M.; Wang, T. N.; Zhao, L. Y.; Du, M. H.; Li, T. L.; Li, D. B. Characterization and dye decolorization ability of an alkaline resistant and organic solvents tolerant laccase from Bacillus licheniformis LS04. *Biores. Technol.* **2012**, *115*, 35-40.

[162] Hadibarata, T.; Yusoff, A. R. M.; Kristanti, R. A. Decolorization and metabolism of anthraquinone-type dye by laccase of white-rot fungi Polyporus sp. S133. *Water Air Soil Pollut.* **2012**, *223(2)*, 933-941.

[163] Hadibarata, T.; Yusoff, A. R. M.; Aris, A.; Hidayat, T.; Kristanti, R. A. Decolorization of azo, triphenylmethane and anthraquinone dyes by laccase of a newly isolated Armillaria sp. F022. *Water Air Soil Pollut.* **2012**, *223(3)*, 1045-1054.

[164] Aubert, S.; Schwitzguébel, J. Screening of plant species for the phytotreatment of wastewater containing sulphonated anthraquinones. *Water Res.* **2004**, *38*, 3569–3575.

[165] Page, V.; Schwitzguébel, J. The role of cytochromes P450 and peroxidases in the detoxification of sulphonated anthraquinones by rhubarb and common sorrel plants cultivated under hydroponic conditions. *Environ. Sci. Pollut. Res.* **2009**, *16*, 805–816.

[166] Khandare, R. V.; Govindwar, S. P. Phytoremediation of textile dyes and effluents: Current scenario and future prospects. *Biotechnol. Adv.* **2015**, *33(8)*, 1697-1714.

[167] Molina, M.C.; White, J.F.; Kingsley, K.L. Gónzalez-Benítez, N. Seed endophytes of Jasione montana arsenic detoxification workers in an eco-friendly factory. In Seed Endophytes-Biology and Biotechnology; Verma, S.K. and White, J.F., Eds.; Springer Int. Pub.: Ney York, NY, 2019, DOI: 10.1007/978-3-030-10504-4 (in press).

[168] Rascio, N.; Navari-Izzo, F. Heavy Metal Hyperaccumulating Plants: How and Why Do They Do It? And What Makes Them so Interesting? *Plant Sci.* **2011**, *180(2)*, 169–181.

[169] Sinha, A.; Lulu, S.; Vino, S.; Osborne, W. J. Reactive green dye remediation by Alternanthera philoxeroides in association with plant growth promoting Klebsiella sp. VITAJ23: A pot culture study. *Microbiol. Res.* **2019**, *220*, 42-52.

[170] Chandanshive, V. V.; Kadam, S. K.; Khandare, R. V.; Kurade, M. B.; Jeon, B. H.; Jadhav, J. P.; Govindwar, S. P. In situ phytoremediation of dyes from textile wastewater using garden ornamental plants, effect on soil quality and plant growth. *Chemosphere* **2018**, *210*, 968-976.

[171] Mahajan, P.; Kaushal, J. Phytoremediation of carcinogenic diazo congo red dye by using Pistia stratiotes (water lettuce). *Res. J. Chem. Environ.* **2019**, *23(1)*, 65-73.

[172] Ekperusi, A. O.; Sikoki, F. D.; Nwachukwu, E. O. Application of Common Duckweed (Lemna minor) in Phytoremediation of Chemicals in the Environment: State and Future Perspective. *Chemosphere* **2019**, *223*, 285-309.

[173] Lobiuc, A.; Olaru, S.; Hancu, E. I.; Costica, N.; Fortuna, M. E.; Zamfirache, M. M.; Constantinescu, G. Toxicity and removal of Direct Red 28 diazo dye in living polymeric systems. *Rev. Chim.* **2018**, *69(7)*, 1628-1635.

[174] Shang, N.; Ding, M.; Dai, M.; Si, H.; Li, S.; Zhao, G. Biodegradation of malachite green by an endophytic bacterium Klebsiella aerogenes S27 involving a novel oxidoreductase. *Appl. Microbiol.Biotechnol.* **2019**, *103(5)*, 2141-2153.

[175] Hussain, Z.; Arslan, M.; Malik, M. H.; Mohsin, M.; Iqbal, S.; Afzal, M. Integrated perspectives on the use of bacterial endophytes in horizontal flow constructed wetlands for the treatment of liquid textile effluent: phytoremediation advances in the field. *J. Environ. Manag.* **2018**, *224*, 387-395.

[176] Hussain, Z.; Arslan, M.; Malik, M. H.; Mohsin, M.; Iqbal, S.; Afzal, M. Treatment of the textile industry effluent in a pilot-scale vertical flow constructed wetland system augmented with bacterial endophytes. *Sci. Total Environ.* **2018**, *645*, 966-973.

[177] Chen, Y.; Xie, X. G.; Ren, C. G.; Dai, C. C. Degradation of N-heterocyclic indole by a novel endophytic fungus Phomopsis liquidambari. *Biores. Technol.* **2013**, *129*, 568-574.

[178] Mora, S. L.; Cadavid, Y.; Ch, E. M. C.; Vélez, J. M.; Buitrago-Sierra, R.; Santa, J. F. Plantain fibers obtained from pseudostems residues for efficient color degradation of indigo carmine dye. *Ind. Crops Prod.* **2018**, *126*, 302-308.

[179] Yang, X. Q.; Zhao, X. X.; Liu, C. Y.; Zheng, Y.; Qian, S. J. Decolorization of azo, triphenylmethane and anthraquinone dyes by a newly isolated Trametes sp. SQ01 and its laccase. *Process Biochem.* **2009**, *44(10)*, 1185–1189.

[180] Zeng, X.; Cai, Y.; Liao, X.; Zeng, X.; Luo, S.; Zhang, D. Anthraquinone dye assisted the decolorization of azo dyes by a novel Trametes trogii laccase. *Process Biochem.* **2012**, *47(1)*, 160–163.

[181] Afreen, S.; Anwer, R.; Singh, R. K.; Fatma, T. Extracellular laccase production and its optimization from Arthrospira maxima catalyzed decolorization of synthetic dyes. *Saudi J. Biol. Sci.* **2018**, *25(7),* 1446–1453.

[182] Beggiato, G.; Casalboremiceli, G.; Geri, A.; Pietropaolo, D. Indigo carmine - An electrochemical study. *Ann. Chim.* **1993**, *83(7-8)*, 355-363.

[183] Campos, R.; Kandelbauer, A.; Robra, K. H.; Cavaco-Paulo, A.; Gübitz, G. M. Indigo degradation with purified laccases from Trametes hirsuta and Sclerotium rolfsii. *J. Biotechnol.* **2001**, *89(2)*, 131–139.

[184] Sakamoto, Y.; Uchida, M.; Ichihara, K. The bacterial decomposition of indole. I. Studies on its metabolic pathway by successive adaptation. *Med. J. Osaka Univ.* **1953**, *3*, 477-486.

[185] Fukuoka, K.; Tanaka, K.; Ozeki, Y.; Kanaly, R. A. Biotransformation of indole by Cupriavidus sp. strain KK10 proceeds through n-heterocyclic- and carbocyclic-aromatic ring cleavage and production of indigoids. *Int. Biodet. Biodegr.* **2015**, *97*, 13–24.

[186] Hadibarata, T.; Mohd Yusoff, A. R.; Ayu, R. Decolorization and metabolism of anthraquionone-type dye by laccase of white-rot fungi Polyporus sp. S133. *Water, Air, Soil Pollut.* **2012**, *223(2)*, 933–941.

[187] Osma, J. F.; Toca-Herrera, J. L.; Rodríguez-Couto, S. Transformation pathway of Remazol Brilliant Blue R by immobilised laccase. *Bioresour. Technol.* **2010**, *101(22)*, 8509–8514.

[188] Ma, Q., Liu, Z., Yang, B., Dai, C., & Qu, Y. Characterization and functional gene analysis of a newly isolated indole-degrading bacterium Burkholderia sp. IDO3. *J. Hazard. Mater.* **2019**, *367*, 144-151.

[189] Zhang, X.; Jing, J.; Zhang, L.; Song, Z.; Zhou, H.; Wu, M.; Qu, Y.; Liu, L. Biodegradation characteristics and genomic functional analysis of indole-degrading bacterial strain Acinetobacter sp. JW. *J. Chem. Technol. Biotechnol.* **2019**, *94 (4)*, 1114–1122.

[190] Regar, R. K.; Gaur, V. K.; Mishra, G.; Jadhao, S.; Kamthan, M.; Manickam, N. Draft genome sequence of Alcaligenes faecalis strain IITR89, an indole-oxidizing bacterium. *Genome Announc.* **2016**, *4(2)*, e00067-16.

[191] Khelifi, E.; Gannoun, H.; Touhami, Y.; Bouallagui, H.; Hamdi, M. Aerobic Decolourization of the Indigo Dye-Containing Textile Wastewater Using Continuous Combined Bioreactors. *J. Hazard. Mater.* **2008**, *152(2)*, 683–689.

[192] Garcia, L. F.; Marcuzzo, J. S.; Pessela, B. C.; Lobón, G. S.; Rodrigues Siqueira, A. C.; Garcia, T. A.; de Souza Gil, E.; Mendez, E. Bio-Electro Oxidation of Indigo Carmine by Using Microporous Activated Carbon Fiber Felt as Anode and Bioreactor Support. *Chemosphere* **2017**, *186*, 519–526.

[193] Rodríguez Couto, S.; Domínguez, A.; Sanromán, Á. Production of Manganese-Dependent Peroxidase in a New Solid-State Bioreactor by Phanerochœte Chrysosporium Grown on Wood Shavings. Application to the Decolorization of Synthetic Dyes. *Folia Microbiol.* **2002**, *47(4)*, 417–421.

[194] Das, P.; Banerjee, P.; Zaman, A.; Bhattacharya, P. Biodegradation of two azo dyes using Dietzia sp. PD1: process optimization using response surface methodology and artificial neural network. *Desal. Water Treat.* **2016**, *57(16)*, 7293-7301.

[195] Yang, Z.; Zhou, J.; Xu, Y.; Zhang, Y.; Luo, H.; Chang, K.; Wang, Y. Analysis of the metabolites of indole degraded by an isolated Acinetobacter pittii L1. *BioMed Res. Int.,* **2017**, 2564363.

[196] Younes, S. B.; Sayadi, S. Detoxification of Indigo carmine using a combined treatment via a novel trimeric thermostable laccase and microbial consortium. *J. Mol. Catal. B: Enz.* **2013**, *87*, 62-68.

[197] Fdhila, K.; Haddaji, N.; Chakroun, I.; Dhiaf, A.; Macherki, M. E. E.; Khouildi, B.; Khouadja, S. Culture conditions improvement of Crassostrea gigas using a potential probiotic Bacillus sp strain. *Microb. Pathogen.* **2017**, *110*, 654-658.

[198] Zhang, X.; Qu, Y.; Ma, Q.; Li, S.; Dai, C.; Lian, S.; Zhou, J. Performance and Microbial Community Analysis of Bioaugmented Activated Sludge System for Indigo Production from Indole. *Appl. Biochem. Biotechnol.* **2018**, 1-11.

[199] Chaudhari, A. U.; Paul, D.; Dhotre, D.; Kodam, K. M. Effective Biotransformation and Detoxification of Anthraquinone Dye Reactive Blue 4 by Using Aerobic Bacterial Granules. *Water Res.* **2017**, *122*, 603–613.

[200] Cho, E. A.; Seo, J.; Lee, D. W.; Pan, J. G. Decolorization of indigo carmine by laccase displayed on Bacillus subtilis spores. *Enzyme Microbiol. Technol.* **2011**, *49(1)*, 100-104.

[201] Teerapatsakul, C.; Parra, R.; Keshavarz, T.; Chitradon, L. Repeated Batch for Dye Degradation in an Airlift Bioreactor by Laccase Entrapped in Copper Alginate. *Int. Biodeterior. Biodegrad.* **2017**, *120*, 52–57.

[202] Jasińska, A.; Góralczyk, A.; Soboń, A.; Dlugoński, J. Novel Laccase-like Multicopper Oxidases from the Myrothecium roridum Fungus - Production Enhancement, Identification and Application in the Dye Removal Process. *Acta Biochim. Pol.* **2018**, *65(2),* 287–295.

[203] Navada, K. K.; Sanjeev, G.; Kulal, A. Enhanced Biodegradation and Kinetics of Anthraquinone Dye by Laccase from an Electron Beam Irradiated Endophytic Fungus. *Int. Biodeterior. Biodegrad.* **2018**, *132*, 241–250.

[204] Niimi, K.; Kang M. J.; Miyazaki, E.; Osaka, I.; Takimiya K. General Synthesis of Dinaphtho[2,3-b:2′,3′-f]thieno[3,2-b]thiophene (DNTT) Derivatives. *Org. Lett.* **2011**, *13(13)* 3430–3433.

[205] M.; Krammer, Borchert, J. W.; Petritz, A.; Karner-Petritz, E.; Schider, G.; Stadlober, B.; Klauk, H.; Zojer, K. Critical Evaluation of Organic Thin-Film Transistor Models. *Crystals* **2019**, *9*, 85; DOI:10.3390/cryst9020085.

[206] Dunst, S.; Karner, E.; Coppola, M. E.; Trimmel, G.; Irimia-Vladu, M. Comparison of the Solution and Vacuum Processed Quinacridones in Homojunction Photovoltaics. *Monatsh. Chem.* **2017**, *148(5)*, 863–870.

[207] Jung, M.; Ji, S.-G.; Kim, G.; Seok, S. I. Perovskite precursor solution chemistry: from fundamentals to photovoltaic applications. *Chem. Soc. Rev.* **2019**, *48*, 2011-2038.

[208] Boyd, C. C.; Cheacharoen, R.; Leijtens, T. ;McGehee M. D. Understanding Degradation Mechanisms and Improving Stability of Perovskite Photovoltaics. *Chem. Rev.* **2019**, *119 (5)*, 3418–3451.